

DEVELOPMENT OF RAPID IMMUNOASSAYS FOR IMPROVED POINT-OF-CARE
MALARIA DIAGNOSTICS

By

Keersten Michelle Davis

Dissertation

Submitted to the Faculty of the
Graduate School of Vanderbilt University
in partial fulfillment of the requirements

for the degree of

DOCTOR OF PHILOSOPHY

In

Chemistry

August, 2015

Nashville, TN

Approved:

David W. Wright, Ph.D.

John A. McLean, Ph.D.

Frederick R. Haselton, Ph.D.

Janet E. Macdonald, Ph.D.

To my parents.

Thank you for choosing me.

ACKNOWLEDGEMENTS

Several times in the Wright lab, we have joked about acknowledgement sections in dissertations being novel-ishly long. Now that I have reached the end of my PhD career, I now realize why these sections tend to be so long. As 22 years of school comes to a close, I would be remiss not to wholeheartedly thank all those who have contributed to the person I am today. In starting graduate school, I knew I did not want to come out on the other side of my PhD thinking, “I had a miserable time.” I can truly say I have had an amazing 5 years at Vanderbilt. With that said—brace yourselves.

To my PhD advisor, Dr. David Wright—thank you for being a major part of what I would consider a wonderful graduate career. I remember walking into your office after my first rotation and telling you, “Do not give the extraction project away. I want it.” Looking back now, I realized that was a tad demanding for a rotation student. Five years and many experiments (and meetings) later, I am so appreciative for your approach toward mentorship. You have taught me to take ownership of my science and to not shy away from speaking up for myself. As a woman in science, this is crucial. I remember this specific Gates meeting where I was getting prodded (pretty hard) about my results, and you did not say a word. I left the meeting fairly upset that you did not stick up for me in that moment. But I quickly realized—that was the point—you wanted me to stick up for myself. Thank you for allowing me to be demanding. I know that sounds weird, but you have given me so much freedom and space to do my research (and to travel), which has allowed me to get out of a graduate career exactly what I wanted. While I did not necessarily know that career would be in global health, I knew I wanted certain tangibility in knowing that my research was helping people. I am grateful that I can use what you have taught me in my future career as an independent scientist. Thank you for being supportive in all my life

changes. So much can happen in the years we are in graduate school, and I am very thankful for your understanding and support. I could go on forever, so from the bottom of my heart—Thank you. As a parting gift, here are my nicknames I have given you these past five years (Dubs, D. Dubs, DubWubs—you will probably notice a theme).

To my collaborator Dr. Rick Haselton—thank you for all your ideas and support in my graduate career. For the better part of my scientific career, I have had the chance to work with engineers, but none quite as special as you. I can say I have laughed more in our Gates meetings than any other meeting I have had. Thank you for pushing me to explain my research better and to be concise in those explanations. Thank you for your so very helpful comments on my manuscripts, as they have helped me become a better scientific writer (sorry if there is a “hence” here or there in my dissertation). Lastly, I would like to thank you for always asking me how I am doing when I stop by your office. While the science is important, it has always made me smile when you genuinely want to know if I, as a person, not a scientist, am doing ok.

To my committee members Dr. John McLean and Dr. Janet Macdonald—thank you for being such an integral part of my career at Vanderbilt. Your perspective in my exams has been so very welcomed. While the settings in which we usually meet can be a little stressful (at least for me because it is either a prelim, qual or IRP), I truly value your advice, outlook on my research, and pathway toward an independent career. Dr. McLean—the juxtaposition of your calm yet enthusiastic nature and outlook on science is amazing to me. One day we will put an RFID chip in David so we can more easily find him. But for now, keep popping by the lab, when you are unable find him, and telling us stories. Dr. Macdonald—your arrival at Vanderbilt was so exciting because, as a graduate student, you were the first faculty candidate seminar I had

attended. Thank you for always challenging me and for being a role model for women in science.

To the Wright Lab— Not every graduate student can call the people they work with friends, but I can truly say that each and every one of you are my friend. I do not know what it is about our lab that attracts such driven and fun people (and good looking, amiright), but I would not trade any second of it for the world. Even when Chris chains a hood shut!

To former Wright lab members (John Stone, Alex Rutledge, Josh Swartz, Rebecca Sandlin, Stephen Jackson, Phoebe Penamon, Matt Bryant, Holly Carrell) of whom I have had the privilege to know, thank you for accepting me into the lab as a first year graduate student and making the first couple years of graduate school such an amazing environment. Josh Swartz— You literally taught me everything I know and the majority of this dissertation is because of you. Your passion and drive for research was so inspiring during my rotation. I can only hope that I took your groundwork in a direction that makes you proud. I still miss the snack cabinet. Becca Sandlin—I really thought you did not like me the first year I was in graduate school, but I have since learned that you were just feeling me out (getting “Becca-ed” as we call it now). You blow me away...seriously. I brag about you every chance I get. Thank you for all your advice then and now, and I am fortunate to consider you one of my closest friends. Stephen (Stevie) Jackson—I blame Swartz for making it really hard to call you by your actual name. You are one of the most compassionate people I have ever met, and you have an incredibly brilliant mind. I will never forget ironing your tie on a hot plate before your defense because your “book press” method did not quite do the trick. Thank you for everything. Alex Rutledge—You are such an inspiring scientist and woman. How you take care of two kids, drive an hour to and from Vanderbilt to work, and manage to stay beautiful, sane, and on top of your science game is

astounding. Thanks for all the career advice and for all the stories! Thanks for introducing me to Ryan and Leila. Bonnaroo!

To current Wright lab members (Chris Gulka, Jenny Nesbitt, Kim Fong, Anna Bitting, Adam Ryan Travis, Wes Bauer, Lauren Gibson, Alexis Wong, Nicholas Wright, Christine Markwalter, Andrew “Bandrew” Kantor, Joseph Conrad, Danielle Kimmel), I could not dream of a better group of scientists and friends to work with on a daily basis. I am so appreciative of our relationships. In how we challenge each other to do better (or is it be better?) and strive for the best we can be. Chris Gulka—you are a brilliant materials scientist. I do not think I will ever meet anyone who loves surface plasmon resonance as much as you do. Sorry I gave you that Snickers that time you were angry. Thanks for being a sounding board for ideas and ways to make the lab atmosphere the best it can be. Jenny Nesbitt—My first memory of you is when you popped your tire riding your bike to orientation. You mean more to me than you know. I am so thankful we have spent the last 4 years together as baymates. Life has thrown us some loops lately but we are still killing it right? Thank you for your support and love, and I hope you always know I am here to offer the same. Kim Fong—You are the strongest person I know. Your gentle spirit is contagious. You have such a wonderful future ahead of you. Anna Bitting—You were my first rotation student to join the lab! Thanks for all the laughs and adventures the past 4 years. Adam Ryan Travis—Your Halloween costumes are ON POINT. Wes Bauer—I am sorry I do not remember showing you around the lab when you visited. Even though you are 4 days older than me, it has been fun watching you grow as a scientist. Lauren Gibson-- My second graduate student to join the lab! I loved every second of our European adventure, of course after going to the conference. Alexis Wong—Stay sassy! You will need it. But seriously, you are such a powerful and confident scientist. It is inspiring. Christine Markwalter—My third

graduate student to join! You are the most astounding graduate student I have ever seen. You blow me away daily. I could not dream of a better person to take over my research after I leave. Stick up for yourself. Do not let anyone walk all over you. It was something I had to learn, but I am glad I did. Andrew (Bandrew) Kantor—Thanks for letting us call you that ridiculous nickname. You fit so well with the lab, and I was honestly so pumped when you joined. I can already tell you are doing to do some great science. Keep drinking that water. Joseph Conrad—Mad props to you keeping VZNIGHT going. I really appreciate all your advice on how to deal with certain situations over the past couple years. Danielle Kimmel—Although most of my “dealings” with you have been as a Cliffel lab member, you are officially ours now. I could thank you for a million things, but in the interest of time, just thank you. You have been such a strong person for me when I have needed it most.

To current and former Haselton lab members (Ash Jayagopal, Nick Adams, Tom Scherr, Bill Gabella, Megan Pask, Andrew Doyle, Francesca Solinas, Josh Trantum, Hali Bordelon, Amy Creecy, Alex Short, Tricia Russ), thanks for all the support, laughs and brainstorming sessions over the past few years. So much of the work I have done has been in collaboration with engineers, and I have been fortunate to work with some wonderful engineers. Josh Trantum—I will never look at a coffee ring the same again. Tom Scherr—Keep those gifs coming. They are hilarious and always so appropriate! Nick Adams—Thanks for the design advice along the crazy journey that is the RDT garage. You are so innovative, and I know that you will be so successful. Ash Jayagopal—So many memories from the House of J’s. Thank you for all your life and career advice. I am somewhat still upset Roche took you away from us, but we will come visit you in Switzerland. Thank you for trusting me with Jack. If two dogs could be best friends, Andy and Jack were. 100%. I miss him dearly.

To all the amazing staff in the Chemistry Department (Sandra Ford, Rachel Harrell, Magda Paszewska, Heather Watkins, Robert Hayes, Paulette Lynch, Robert Padgett, Jackie Brown)-- Thank you for all of your support. So much of grad school does not involve the actual benchwork, and you all have helped me navigate forms and administrative things tremendously.

To my first year graduate class, if someone would have told me an entering graduate class of 40 students would still be as close now as the first day of orientation, I probably would have been a tad skeptical. 5 years later I am so grateful for every single one of you. Graduate school is NOT easy, and it has its ups and downs. Thank you all for so much support. Festivus, Semestivus, Pontoon Days, Chemistry Picnic after parties, jaunts to Midtown. We really do like hanging out with each other! Jeremy, Dave, and Bobby—what would I have done without you guys? Sadly we cannot all live within walking distance of each other for the rest of our lives, but I will cherish every memory we have made at Vanderbilt. Marta—I have so enjoyed getting to spend time with you and James over the years. You two are so inspiring. Bobby—We have known each other the longest!!! Seeing you walk into orientation, after visiting together, was such a relief. I know someone! Thanks for all the crippling laughs and an ear to listen when I am frustrated or just need someone to talk to. I am thrilled we get to spend the next phase of our career together.

A host of people supported me on my journey to graduate school. I would like to thank all of my college professors and high school teachers for giving me such a strong foundation. Mrs. Hester and Mr. Holloman—I cannot begin to thank you for all you have done for me. If it were not for you I would not be where I am today. Mrs. Hester—Yes you were technically my English teacher, but you are so much more than that. Your spirit and passion for all life is in me. I love you. Mr. Holloman—you sparked my love of chemistry, and for that I thank you. Ken

Johnson—Thank you for helping me discover who I am outside of being a scientist. I owe a lot of my outlook on life to the Scholars Program and your guidance. I admire all you do. Cathy Reed—Never would I have guessed that my organic lab TA would be one of my closest friends 7 years later. I have laughed more this year because you have been in it. Thanks for your support and friendship. Gail Blakley—Someone asked me the other day if you and I talk on the phone all the time. I said, “Um no. We just text each other all day, every day.” That person said, “Y’all sound like a pair of bros.” I guess we are somewhat bro-like. You have been a constant presence in my life for the past 9 years, and I can truly say you are my best friend. Thank you for all the support from Sullivan 204 to University Woods 204. From Maryland to Tennessee. From Louisiana to Tennessee. And wherever else life takes us.

To my family—I consider myself so incredibly blessed. I would like to think that not many people could say they were chosen to have the life that they have. I can though. Mom and Dad—Thank you for choosing to adopt me. I do not often think about the life that I may have had if you had not chosen me, because the life that I do have swamps all of those thoughts. I owe everything I am to you, Mom and Dad. You raised me to love God and have faith. That faith has carried me so far in this life, and I cannot thank you enough. Thank you for telling me I could be whoever I wanted to be. Thank you for supporting me in everything I have attempted in life. Thank you for telling me when I am wrong and still being there for me when I make wrong choices. I can never express in words to you how much I love you and how much I thank you for giving me the life I have now. Just know that I am so thankful that God picked me to be your daughter and you chose to follow that calling. Richard—I love you. Thanks for being the big brother I need. I brag about our childhood all the time, because it was the best. Although we have not been able to see each other as much in the past few years, I love that we can always

pick up right where we left off. Joanna—I am so thrilled you are a part of our family and that you have been able to share in this journey with me. I could not have picked a better wife for Richard (and sister in law for me). Your joy is infectious. Thank you for supporting Richard in all he strives to do. Andy—Thanks for being literally the best dog child I could ever imagine. I wouldd like to think you know what I am saying to you when I speak to you like a human (which makes me sound really creepy), but you are such a special dog. Thanks for always being excited to see me when I come home and being that constant source of unconditional love in my life when things are going crazy.

“This is the way. Walk in it.”

TABLE OF CONTENTS

	Page	
DEDICATION	ii	
ACKNOWLEDGEMENTS	iii	
LIST OF TABLES	xv	
LIST OF FIGURES	xvi	
 Chapter		
I. INTRODUCTION	1	
A Brief History of an Ancient Disease	1	
The Biology of the Malaria Parasite	3	
Malaria in the Modern World	4	
Diagnostic Strategies for Malaria Detection	7	
Scope of this Work	12	
 II. A METAL BASED PLATFORM FOR EXTRACTION OF <i>PLASMODIUM FALCIPARUM</i> HISTIDINE RICH PROTEIN II FROM BIOLOGICAL SAMPLES		15
Introduction	15	
Materials	17	
Experimental	18	
Spiked Plasma Sample Preparation	18	
Spiked Whole Blood Sample Preparation	18	
pfHRP II Extraction from Plasma and Whole Blood using the Self- Contained Extraction Device	19	
ELISA Quantification of pfHRP II	20	
ELISA Quantification of HRG	21	
Quantification of Hemoglobin Content in Samples Extracted from Whole Blood	21	
Whole Protein Gel Analysis	22	
Bradford Protein Assay for Whole Protein Quantification	22	
Carryover Volume Determination	22	
Determination of the Elution Profile of pfHRP II with Imidazole	23	
Determination of the Elution Profile of HRG with Imidazole	23	
Malaria Rapid Diagnostic Test Enhancement	24	
Results and Discussion	24	
Design of the pfHRP II Extraction Cassette	24	
Optimization of the pfHRP II Extraction Cassette	25	
Efficiency of pfHRP II Extraction Using the Self-Contained Cassette	30	
Purification of pfHRP II from Spiked Human Plasma and Whole Blood	32	
Effect of pfHRP II Concentration on Malaria Rapid Diagnostic Test Performance	35	

Conclusion	36
Acknowledgements.....	37

III. DEVELOPMENT OF A “SWITCH-ON” IRIDIUM (III) PROBE FOR THE DETECTION OF THE MALARIAL BIOMARKER HISTIDINE RICH PROTEIN II.....38

Introduction.....	38
Materials	41
Instrumentation	41
Experimental.....	42
Synthesis of Iridium (III) Complex Ir1	42
Activity of Ir1 against Amino Acids and Biomolecules.....	42
Amino Acid Selectivity of Ir1.....	42
Optimization of In-Solution Assay Parameters	43
Real-Time Kinetic Analysis of Ir1 with BNT-II.....	43
In-Solution Limit of Detection of 6-His, BNT-II and rcHRP II	43
On-Particle Limit of Detection of BNT-II and rcHRP II.....	44
Results and Discussion	44
Physical and Spectroscopic Characteristics of Ir1	44
Optimization of Ir1 Signal with L-Histidine.....	45
Development of Optimized Ir1 Assay with a pfHRP II Mimic.....	50
Ir1 Assay for the On-Bead Detection of pfHRP II	52
Conclusion	55
Acknowledgements.....	57

IV. DEVELOPMENT OF A RAPID IMMUNOMAGNETIC ELISA FOR DETECTION OF PLASMODIUM FALCIPARUM HISTIDINE RICH PROTEIN II.....59

Introduction.....	59
Materials	63
Experimental.....	63
M(II)NTA On-Bead ELISA General Protocol	63
α -HRP II On-Bead ELISA General Protocol	64
Surface Functionalization of Streptavidin Dynabead Particles with α -HRP II-Ab.....	65
Spiked Whole Blood Sample Preparation.....	66
Results and Discussion	66
On-Bead ELISA using Ni(II)NTA Magnetic Particles as the Capture Reagent	66
Optimization of the Co(II)NTA On-Bead ELISA	70
All-in-One On-Bead ELISA with α -HRP II Protein-G Magnetic Particles	72
Optimization of the All-in-One On-Bead ELISA for pfHRP II	75
Conclusion	79
Acknowledgements.....	81

V. MALARIA RAPID DIAGNOSTIC TESTS: UNCOVERING HOW THEY WORK AND HOW THEY CAN BE IMPROVED	82
A History of Rapid Diagnostic Tests	82
Principle of Lateral Flow Assays	82
Components of a Lateral Flow Assay	83
Rapid Diagnostic Tests for Malaria	86
Malaria RDT Landscape	89
VI. SIMPLE SAMPLE PROCESSING ENHANCES MALARIA RAPID DIAGNOSTIC TEST PERFORMANCE	91
Introduction	91
Materials	93
Experimental	94
Blood Sample Preparation	94
Extraction and Analysis with RDTs	95
Image Analysis	96
Results and Discussion	97
Enhancement in RDT Performance	97
Limit of Detection of Enhanced RDT Signal	101
Effect of Individual Donor Samples on RDT Performance	103
Conclusion	106
Acknowledgements	107
VII. FUTURE DIRECTIONS: TOWARD DEVELOPMENT OF A NEW RAPID DIAGNOSTIC PLATFORM FOR MALARIA DETECTION	108
Introduction	108
Materials	110
Methods	110
Proof of Concept RDT Enhancement via Elution Off-Beads	110
Proof of Concept RDT Enhancement via Elution Off-Beads without Purification	111
RDT Enhancement using the RDT Garage	111
Haiti Field Trial Workflow	113
Results and Discussion	114
On-RDT Elution of pfHRPII for RDT Signal Generation	114
RDT Enhancement without Purification Steps	115
Design and Evaluation of a User-Enabled Device for RDT Enhancement	116
Enhancement with the RDT Garage	121
Prototype Field Trial in Gobert, Haiti	122

Conclusions.....	125
Future Directions and Perspectives.....	125
Acknowledgements.....	129
REFERENCES	130
Appendix	
A. SUPPORTING INFORMATION: CHAPTER II.....	140
B. SUPPORTING INFORMATION: CHAPTER III.....	146
C. AUTOMATED EXTRACTION OF <i>PFHRPII</i> FROM BIOLOGICAL SAMPLES.....	158

LIST OF TABLES

Table	Page
1. Summary of diagnostic tools for malaria detection.	8
2. Checkerboard on-bead ELISA assay to determine effect of BSA and detection antibody concentration on signal at 650nm.	67
3. On-bead ELISA signal, at 650nm, over a range of HRPII concentrations with increasing detection antibody concentration.	69
4. Malaria RDT specifications for RDT enhancement.	92
5. Specifications of individual blood donor samples.	94
6. Calculated limit of detection (in parasites/ μ L) for all brands tested.	102

LIST OF FIGURES

Figure	Page
1. Pamphlet illustrated by Dr. Seuss for malaria transmission education.[8]	2
2. Life cycle of the malaria parasite.[2]	3
3. Ongoing malaria transmission in 2013 (top); Percentage of countries living under \$2 a day (bottom). [1]	5
4. Target use settings for malaria diagnostics.[6]	7
5. Microscopic differentiation of malaria parasites by Giemsa staining.[3]	9
6. Purification and identification of <i>pfHRP2</i> from culture, by Pantou et.al.[9]	10
7. Protein sequences of <i>Plasmodium falciparum</i> protein biomarkers.....	11
8. Malaria rapid diagnostic test processed at the point of care. (USAID Kenya ©. All rights reserved.)	12
9. Generalized schematic of the self-contained <i>pfHRP2</i> extraction cassette	16
10. Interaction between histidine side chains of <i>pfHRP2</i> and the Ni(II)NTA magnetic particle	25
11. A) Incubation and B) Elution time profiles of <i>pfHRP2</i> with Ni(II)NTA magnetic particles	26
12. Effect of imidazole on <i>pfHRP2</i> and HRG binding to Ni(II)NTA particles	27
13. Post-extraction distribution of <i>pfHRP2</i> in the extraction cassette. WI-III refer to the sequential wash chambers in the cassette.....	29
14. Silver-stained SDS-page gel pre- and post- extraction from A) plasma and B) blood.....	32
15. Comparison of recovery of non-specific protein interferents and <i>pfHRP2</i> from A) plasma and B) whole blood using our extraction device and a commercially available HisPur Ni(II)NTA spin column	33
16. Recovery of <i>pfHRP2</i> below the WHO recommended limit of detection for rapid diagnostic tests.....	34
17. Improvement in the visual limit of detection of the SD BIOLINE malaria RDT after extraction from either plasma (middle) or whole blood (bottom)	

for 50 (left), 100 (middle) and 200 (right) parasites/ μ L as compared to mimic patient samples (top).	35
18. Examples of organic fluorophores (left) and quantum dots (right) in solution. Images adapted from the Anzenbacher Research Group and Sigma Aldrich, respectively.	38
19. Synthesis of Ir1.	44
20. Fluorescent response of amino acids with Ir1.....	45
21. Effect of signal response of Ir1 with L-Histidine as a function of A) buffer type and B) ionic strength.	46
22. Reaction kinetics of Ir1 with L-histidine in various buffers.	47
23. Effect of varying A) pH and B) temperature on the relative fluorescence signal of L-Histidine with Ir1	48
24. Structure of the <i>pf</i> HRP _{II} peptide mimic, BNT-II.	49
25. A) Relative fluorescence signal intensity (RFU) of micromolar concentrations and B) correlation between signal intensity and concentration of total histidine in L-Histidine versus BNT-II.....	50
26. Titration of nanomolar concentrations of BNT-II and rc-HRP _{II} with Ir1.....	52
27. A) Comparison of a standard sandwich ELISA format for the detection of <i>pf</i> HRP _{II} to the Ir1 on-particle assay. B) Titration of nanomolar concentrations of rcHRP _{II} bound to 50 μ m Ni(II)NTA magnetic agarose particles.	53
28. Phosphorescence of Ir1 bound to BNT-II on the surface of Ni(II)NTA magnetic particles, under broadband UV light.	54
29. Background signal from Ir1 with plasma and Ni(II)NTA particles after sequential PBS washes.....	56
30. Number of papers published on ELISAs since 1971.....	59
31. Diagram of common ELISA formats. Image adapted from Life Technologies.	60
32. General diagram of an on-bead ELISA format.....	62
33. Diagram of Co(II)NTA on-bead ELISA.....	68
34. On-bead ELISA response to increasing detection antibody concentrations, where B) focuses on the 0-200 parasites/ μ L range represented in A).....	70

35. Effect of increasing BSA in blocking buffer on signal response, where B) focuses on the 0-200 parasites/ μ L range represented in A).....	71
36. Effect of decreased time and increased detection antibody on on-bead ELISA signal	72
37. All in one on-bead ELISA proof of concept with Protein-G magnetic particles.....	73
38. General diagram of the all-in-one on-bead ELISA.....	74
39. Limit of detection of <i>pf</i> HRP II using the proof of concept on-bead ELISA.....	75
40. Comparison of <i>pf</i> HRP II depletion, using NiNTA particles or antibody particles, from a blood sample as a function of time.	76
41. Effect of A) detection antibody concentration and B) particle volume added on on-bead ELISA signal and background noise.	77
42. On-bead ELISA signal at various incubation times using optimized reagent concentrations.	78
43. Effect of TMB incubation time on on-bead ELISA signal.	79
44. Limit of detection of <i>pf</i> HRP II, using optimized on-bead ELISA reagents, at 1, 5 and 10 minute sample incubation times.....	80
45. Diagram of capillary action. Image adapted from Physics Stack Exchange.	83
46. Basic components of a lateral flow immunoassay.[4]	83
47. Interaction of sample with AuNPs on lateral flow conjugate pad.[5].....	84
49. Trapping of excess reagents by the wicking pad. [5].....	85
48. Wicking of antigen bound AuNPs down the nitrocellulose strip. [5].....	85
50. Generalized diagram of a <i>Plasmodium</i> RDT.[1]	86
51. Panel detection scores of malaria RDT brands tested by the WHO.	87
52. Example of panel detection score calculation. [1]	88
53. Number of malaria RDTs (<i>Pf</i> and Combo tests) purchased between 2008-2012.[7]	89
54. Workflow for RDT processing.	96
55. RDT enhancement curves before and after sample processing.	98

56. Example of a missing control line (right image). Both RDTs were from the same manufacturer.	99
57. Faulty sample clearance across the nitrocellulose strip of the RDT.	100
58. Calculated enhancement factors at 200 parasites/ μ L.	100
59. Comparison of enhancement curves of three different RDTs.	101
60. Effect of donor sample on RDT signal. Donor 1 (red), Donor 2 (green), Donor 3 (yellow), Donor 4 (black), Donor 5 (blue).	104
61. Plots of the average peak areas from the RDT test lines for each mimic donor sample, extracted and unextracted, at all parasitemias. Donor 1 (red), Donor 2 (green), Donor 3 (yellow), Donor 4 (black), Donor 5 (blue).	105
62. Prototype RDT garage.	112
63. On-RDT enhancement from a negative (0 parasites/ μ L) and positive (200 parasites/ μ L) lysed blood sample.	114
64. Proof of concept RDT enhancement without sample purification.	115
65. General schematic of the RDT garage. Image graciously provided by Dr. Nick Adams.	116
66. Comparison of Paracheck RDT unenhanced (top) and enhanced using the RDT garage (bottom) at 200 parasites/ μ L.	117
67. Flow of Co(II)NTA Dynabeads across the nitrocellulose (top strip). In the presence of a magnetic field this flow is prevented (bottom strip).	119
68. Effect of mixing mode on enhanced RDT signal.	120
69. Comparison of Chapter VI and Chapter VII enhancement methods.	121
70. Processing candidate patient samples for the RDT garage field trial in Gobert, Haiti.	122
71. Lysed candidate patient blood samples processed using the handheld mixer designed by Dr. Nick Adams.	123
72. Ideal workflow using the RDT garage.	126

CHAPTER I

INTRODUCTION

A Brief History of an Ancient Disease

The modern malaria epidemic is commonly associated with developing nations, where healthcare workers dispatched from centralized facilities face difficult terrain, intermittent/lack of electricity, poorly equipped facilities, unskilled workforce, and limited financial resources. In the past, however, malaria was a global problem. Only as recently as 1951 has malaria been considered completely eradicated from the United States. Some of the earliest documented symptoms of malaria date back to ancient Chinese medical writings from 2700BCE.[10] Many Greek and Roman writings around the 4th century BCE attributed population decline and symptoms in swampy regions to malaria infection. As early as 340 CE, the Chinese documented the antifever properties of the Qinghao plant (*Artemisia annua*). It was not until the late 1800s that Charles Alphonse, a French Army surgeon, discovered the malaria parasite in a patient's blood. After this observation, there was a flood of research between 1880-1900 to identify and name the parasite species, understand the differentiation of the parasite, and discover parasite transmission through a mosquito vector.

In the Americas, the construction of the Panama Canal spearheaded efforts towards tropical infectious disease awareness and control. Not until malaria and yellow fever were controlled, due to vector control and disease treatment strategies, was the Panama Canal completed in 1914. Between 1914 and 1942, the United States Public Health Service (USPHS)

THIS IS Ann..

*Her full name is Anopheles Mosquito
and she's dying to meet you!*



... *she drinks blood!*

Her trade is dishing out
MALARIA. She's at home in
Africa, the Caribbean, India, the
South and Southwest Pacific
and other hot spots.



Ann moves around at
night (a real party gal)
and she's got a thirst.
No whiskey, gin, beer
or rum coke for Ann . . .
she drinks G. I. blood. She jabs
that beak of hers in like
a drill and sucks
up the juice . . . then
the poor G. I. is going
to feel awful in about
eight or fourteen days . .
because he is going to
have **ma/aria**

Dr. Seuss



Turn the page

Figure 1. Pamphlet illustrated by Dr. Seuss for malaria transmission education.[8]

boosted efforts to investigate and combat malaria in the United States. While the creation of the Tennessee Valley Authority (TVA) in 1933 under the New Deal was focused on development in the southeastern region of the US, malaria was essentially eliminated by 1947 under the TVA and the USPHS programs. As this era also coincided with war time, the Malaria Control in War Areas (MCWA) was implemented on military bases stateside and overseas to help control and eliminate malaria in the US and protect soldiers from infection overseas. Dr. Theodor Geisel, also known as Dr. Seuss, was a captain in the US Army during World War II. He illustrated a pamphlet to disseminate information to the troops about malaria transmission and treatment (Figure 1).[8] Further, with the creation of the CDC, malaria was considered fully eliminated

from the US in 1951 via extensive surveillance and prevention efforts for treatment of suspected malaria patients and vector control. Despite, its eradication in the United States, the malaria epidemic is still a significant global issue.

The Biology of the Malaria Parasite

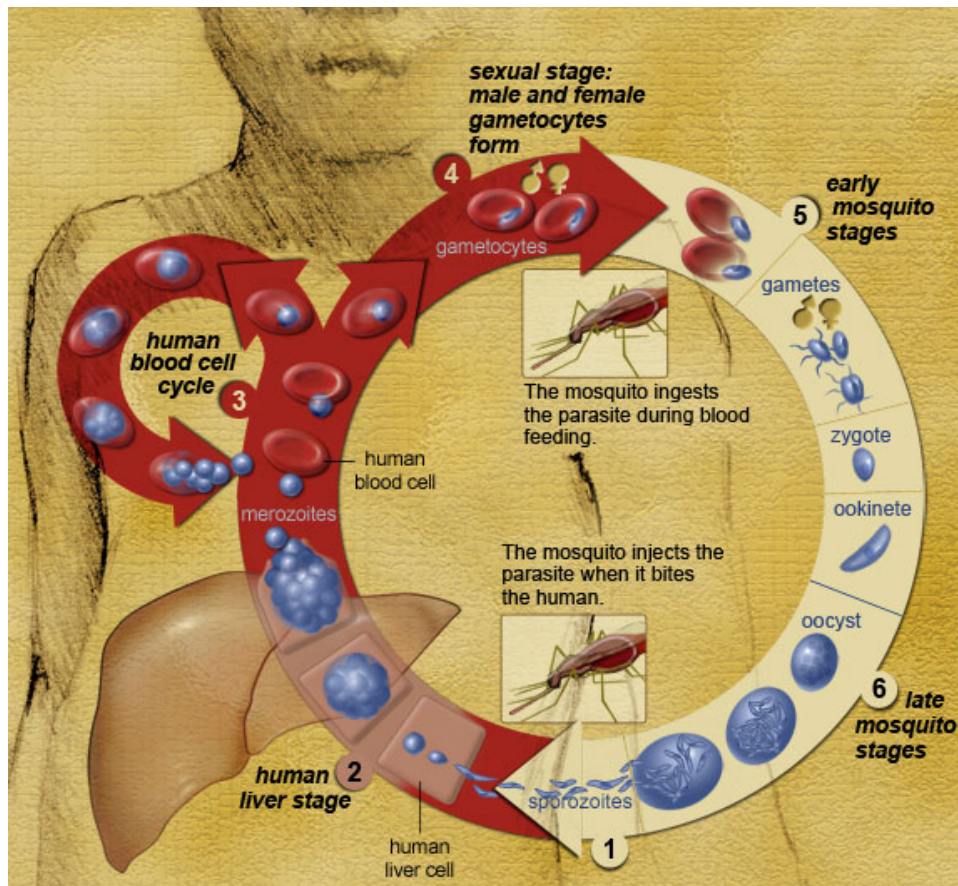


Figure 2. Life cycle of the malaria parasite.[2]

Malaria is a tropical infectious disease caused by parasites of the *Plasmodium* genus.[2] Five species of the *Plasmodium* parasite, *falciparum*, *vivax*, *malariae*, *ovale*, and *knowlesi*, are known to be infectious to humans, where *P. falciparum* is the most prevalent and virulent species. *P. knowlesi* predominantly infects primates, but the first documented case of human infection was found in 1956. The disease is spread through the bite of an *Anopholes* mosquito. The parasite can undergo two life cycles, one in the midgut of the mosquito and another in the

human host (Figure 2).[11] Upon biting a human host, sporozoites, the late stage form of the parasite, are injected into the blood stream, where they first travel to the liver. The parasite resides in the liver for a period of time (Note: This varies by species. Some species can lay dormant for weeks to months before signs of infection.) before the liver cells release a haploid form of the parasite, called merozoites, into the blood stream. These merozoites invade healthy red blood cells (RBCs) and asexually reproduce within this infected red blood cell (iRBC). After a full life cycle has elapsed within the iRBCs, the iRBC ruptures, releasing next generation merozoites into the blood stream to infect new RBCs. This intraerythrocytic life cycle of the parasite is what causes symptoms of malaria (fever, chills, nausea, headache, fatigue). Although a single iRBC releases 10-36 merozoites into the blood stream upon RBC rupture, the iRBC from which the merozoites were released is considered a singly parasitized RBC.[12] Physiological iRBC concentrations can vary from single parasites/ μL to thousands of parasites/ μL ., When considering implications on symptoms, most patients exhibiting symptoms of malaria infection have parasite densities greater than 200 parasites/ μL . Asymptomatic patients can still host and transmit the parasite, but do not show signs of infection.[13; 14] Exact cut offs for asymptomatic patients have not been distinguished yet, but it is widely accepted by the community that these patients have parasite densities less than 200 parasites/ μL . Identifying and treating these patient communities poses a significant challenge for the malaria community.

Malaria in the Modern World

In 2014, 97 countries and territories were documented to still have ongoing malaria transmission, and 3.3 million people are estimated to be at risk of infection.[1] 198 million cases of malaria and 584,000 deaths were estimated in 2013, 90% of which were in Africa (Figure 3; top).[1] In the past decade, malaria aid has helped to reduce global incidence and mortality by

30% and 47%, respectively. This comes in lieu of a 43% population increase in affected areas

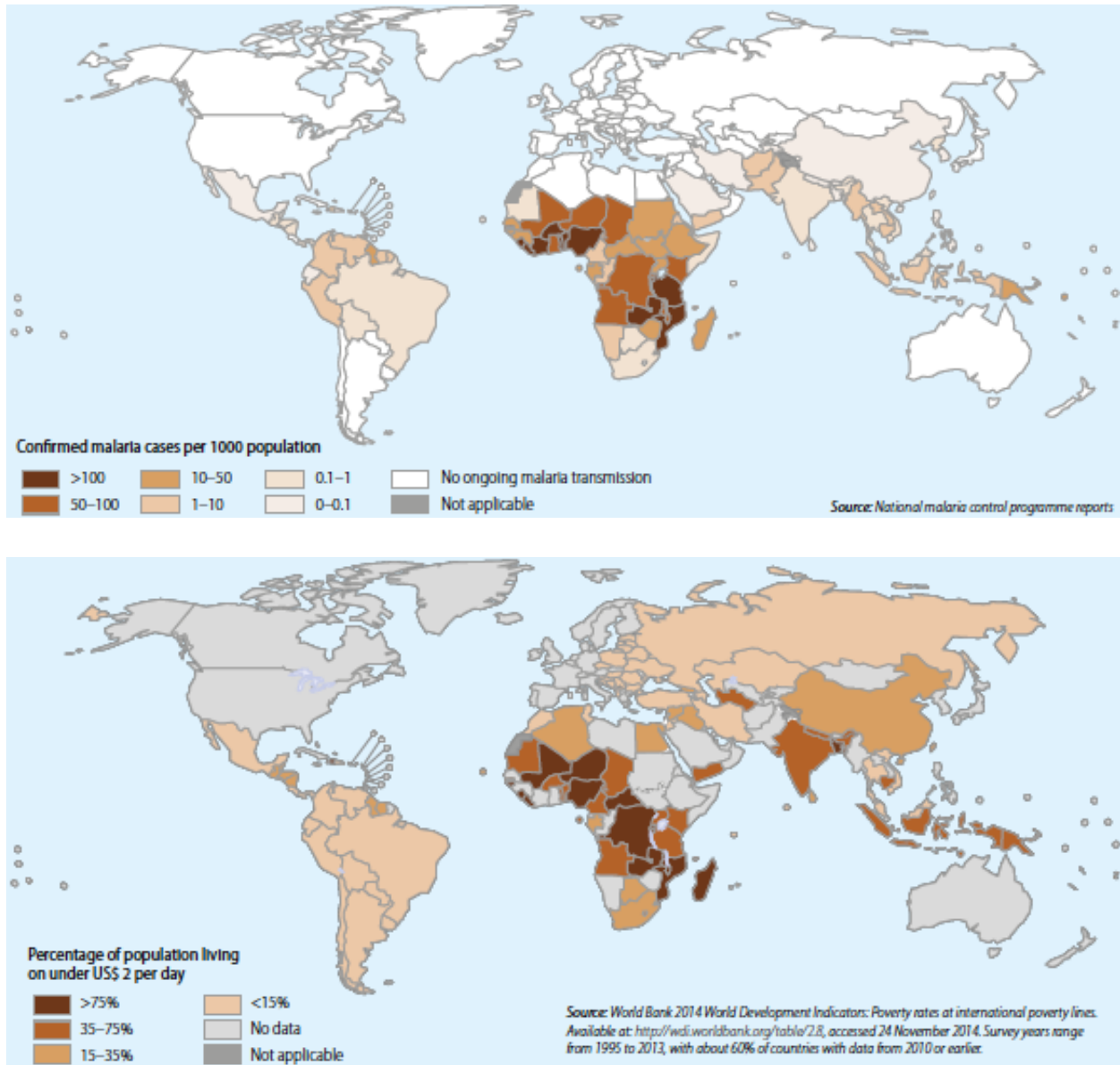


Figure 3. Ongoing malaria transmission in 2013 (top); Percentage of countries living under \$2 a day (bottom). [1]

in Africa. Populations most at risk of malaria infection include children, pregnant women, and immunocompromised persons. For countries that have eliminated malaria outbreaks, border control proves difficult to prevent residents of neighboring endemic countries from bringing malaria back into these countries. The US was able to control and ultimately eliminate malaria by implementation of government programs and agencies, insecticides, vector control, diagnosis, and treatment. Similar interventions are currently being implemented in developing nations affected by malaria in the form of insecticide bed nets, household spraying, and active surveillance, but there is a strong correlation between areas of ongoing transmission and poverty (Figure 3; bottom).[1] In the United States, an employee pays between \$4000-5000 annually toward cost of health insurance, with upwards of \$1000 out of pocket. In many developing nations, most families only make \$2 a day and cannot afford to spend 10% of their annual wages on healthcare and preventative measures. Corrupt governments, poor infrastructure, and lack of a skilled healthcare workforce at the point of care can significantly impede progress toward malaria elimination, as getting supplies, diagnostic tools, and treatments to these affected areas must go through the government first. The degree of diagnostic capability can vary depending on the region of the country to which the tools will be deployed. The Gates Foundation has defined target support areas in terms of level (Figure 4).[6] These areas vary in location, quality of instruments and technicians/scientists, access to equipment, and funding. Level 1 to Level 0 (not shown on the pyramid but often indicative of diagnosis “under the tree” in a village setting) are the areas where active malaria surveillance and treatment is needed most. Recent decades have seen great improvement in reducing malaria transmission in affected areas, as the push for elimination campaigns grows. To reach an elimination state, three major issues must be

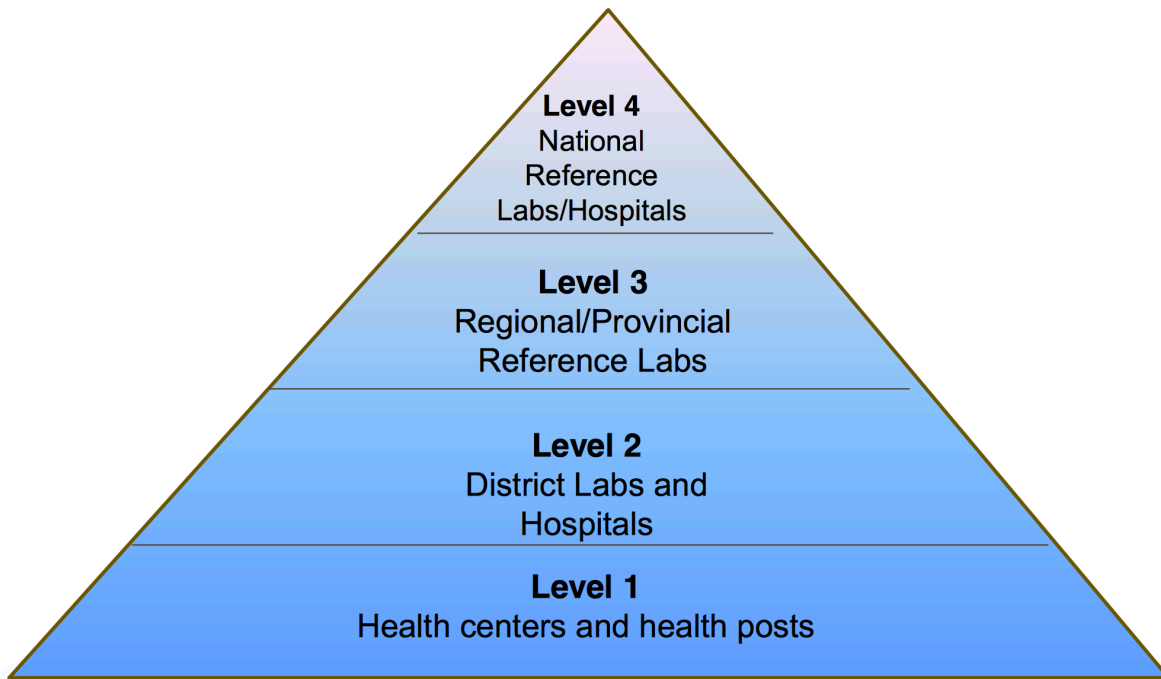


Figure 4. Target use settings for malaria diagnostics.[6]

addressed: 1) increased diagnostic sensitivity, 2) vector control, and 3) drug and insecticide resistance.

Diagnostic Strategies for Malaria Detection

There is a two sided approach for detection and diagnosis of infectious disease: 1) detecting the infectious agent itself and/or 2) detecting a biological or chemical marker of infection. Examples of these diagnostic approaches, their level of expertise required, cost, and sensitivity can be seen in Table 1. The current gold standard for malaria diagnosis, light microscopy, falls under the former category. Upon receiving a patient blood sample, a blood smear is analyzed via the light microscope to determine the level of infection and species of parasite (Figure 5).[3] While this technique is inexpensive and rapid, the requirements of a highly skilled technician and a clean workspace is vital to proper diagnosis. Ohrt and coworkers cited a 20% difference in sensitivity and specificity of interpreting a malaria blood smear

Technique	Special Instruments Needed	Expertise Needed	Cost	Time Needed (mins)	Limit of Detection (parasites/ μ L)
Microscopy	Yes	Yes	Moderate	30-60	5-100
ELISA	Yes	Yes	Expensive	300+	<1
RDT	No	No	Cheap	10-15	100

Table 1. Summary of diagnostic tools for malaria detection.

between an expert and a basic microscopist.[15] The limit of detection for malaria using microscopy in field conditions has been shown to be between 50-100 parasites/ μ L. This limit may be even higher in situations with poor equipment, poorly trained microscopists, and variable blood smearing techniques.

Aside from using microscopy to detect the parasite in a patient blood sample, other diagnostic tools have been developed to identify biomarkers of infection. *Plasmodium falciparum* expresses several protein biomarkers during the course of infection. The most common, Histidine Rich Protein II (*pfHRP*II), is from a series of histidine rich proteins (HRP I, HRP II, and HRP III).[9] *PfHRP*I is associated with the knoblike protrusions on cytoskeleton of iRBCs, as these infected cells exhibit morphological changes upon infection. *PfHRP*III is similar in amino acid structure to *pfHRP*II, but in lower abundance.[16; 17] *pfHRP*II is a 67kDa dimer comprised of 34% histidine with tandem repeats of AHH and AHHAAD (Figure 6).[9] Its function is still not established, but it has been shown to be an efficient heme binder, which protects the parasite from heme toxicity upon rupture of the iRBCs. Physiological concentrations of *pfHRP*II can range from low picomolar to high nanomolar, in an infected blood sample. Diagnostic assays for *P.falciparum* malaria heavily rely on *pfHRP*II detection; however, there are reported instances of gene deletion in some *Pf* isolates. This could potentially lead to

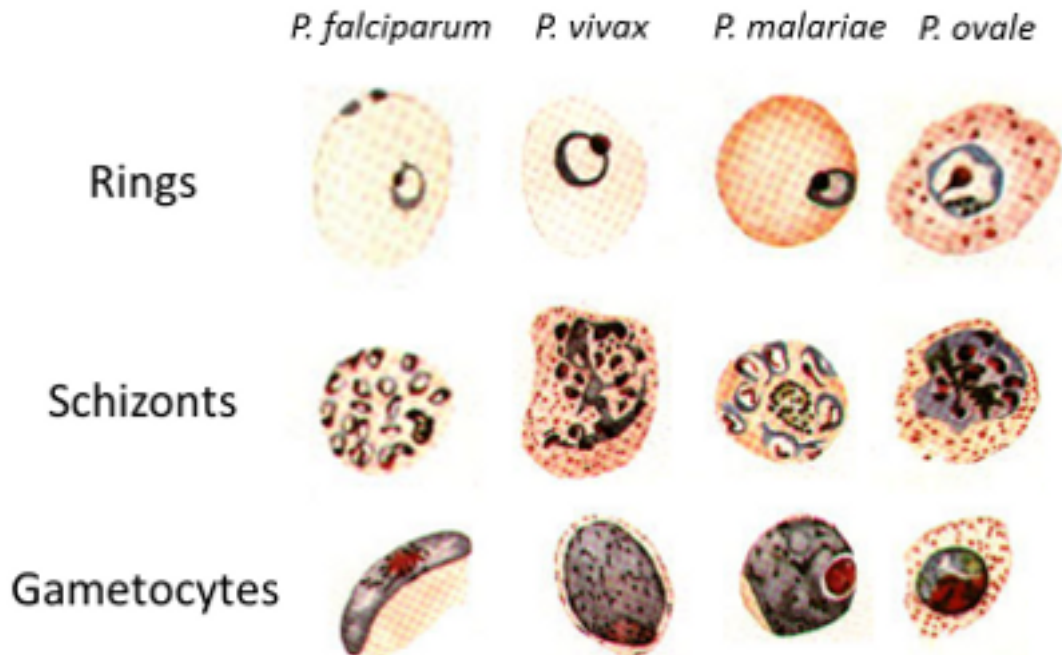


Figure 5. Microscopic differentiation of malaria parasites by Giemsa staining.[3]

false negatives. Furthermore, *pfHRP2* is not a good measure of treatment efficacy, as it can persist in circulation for weeks after parasite clearance. Despite these instances, *pfHRP2* informed diagnosis is still quite powerful for *P.falciparum* infections.

Plasmodium lactate dehydrogenase (*pLDH*) is a second class of biomarker for malaria detection and is essential to the anaerobic lifestyle of the parasite. Like *pfHRP2*, it is expressed during the blood stage of the parasite life cycle, but in smaller quantities than *pfHRP2*. [18] It has a high affinity for 3-acetyl pyridine adenine dinucleotide (APAD) as a cofactor, which distinguishes it from the human LDH counterpart (using NAD). Unlike *pfHRP2*, *pLDH* is a pan-malarial biomarker, in that all plasmodia express the enzyme, with 87% sequence homology to *pLDH*. Additionally, the enzyme is cleared from the body in a few days, and thus can be used as an effective marker of successful treatment. *Plasmodium* aldolase, another protein in the

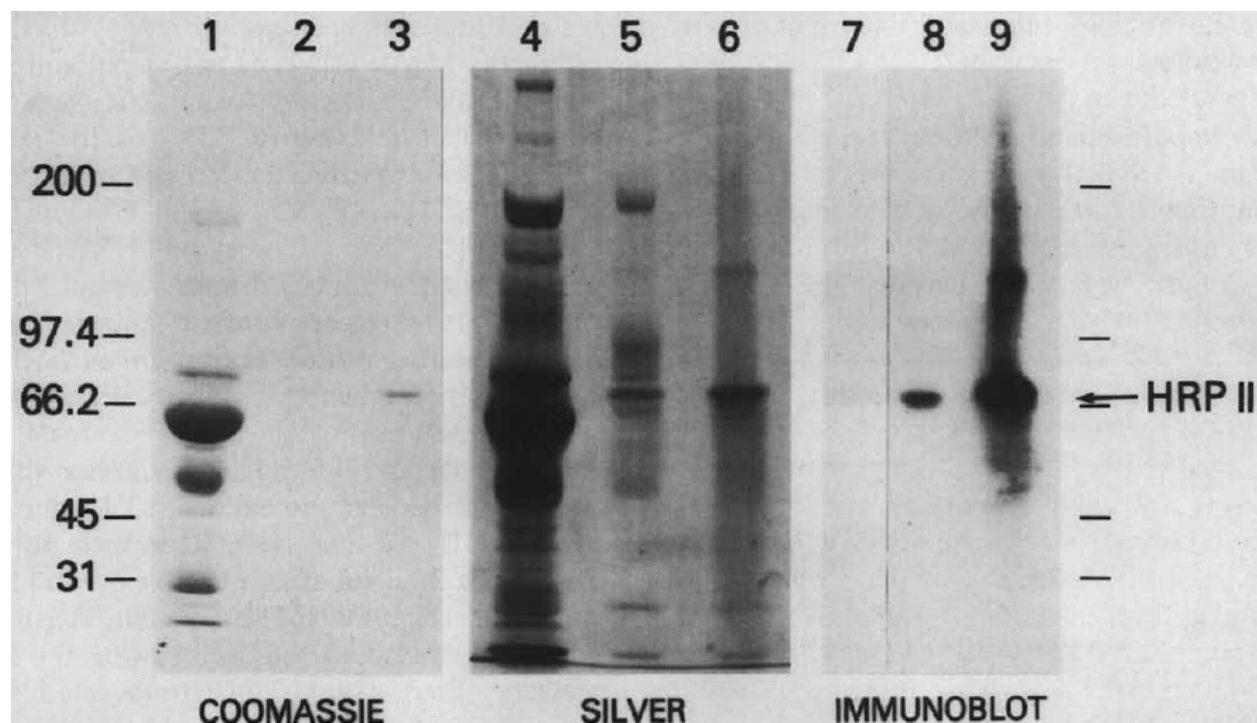


Figure 6. Purification and identification of *pf*HRP II from culture, by Panton et.al.[9]

parasite's glycolytic pathway, is a third biomarker of pan-malarial infection. The protein sequences of these three malaria biomarkers can be seen in Figure 7.

In order to detect these biomarkers in a patient sample, immunoassays have been developed and utilized at various settings within malaria endemic countries. Enzyme linked sandwich immunoassays (ELISAs) have long been used to quantitate protein concentrations from a complex sample matrix, with remarkable sensitivity for asymptomatic patient samples. There are reports of using ELISAs to identify malaria infected biological samples, but the complexity, cost, experience and infrastructure needed, and time to result limit these tests from being run at level 0 and level 1 facilities.[19] The development of the rapid immunochromatographic diagnostic test (RDT) has revolutionized point of care detection of malaria.[20; 21] These rapid, disposable tests, shown in Figure 8, detect malarial antigens by sandwiching the biomarker between a capture antibody on a nitrocellulose strip and a gold

nanoparticle. After processing a blood sample from a fingerprick, the immobilized gold nanoparticles on the test strip indicate infection. As these tests are complete in 20 minutes, easy to use, disposable, and cheap, they have been widely used for surveillance and treatment

pfHRPII

```
mvsfsknkvl saavfasvll ldnnnsafnn nlcsknakgl nlnkrllhet
qahvddahha hhvadahhah hvadahhahh vadahhahha adahhahhaa
dahhahhaad ahhahhahha adahhahhaa dahhahhaad ahhahhaada
hhahhaadah hahasdahh ahhaayahha hhasdahhaa dahhaayahh
ahhaadahha adahhatdah haadahhaad ahhaadahha tdahhahhaa
dahhatdahh ahhaadahha aahhatdahh aaahhatdah haaahheat
hclrh
```

pfLDH

```
mapkaktivlv gsgmiggvma tlivqknlgd vvlfdivknm phgkaldtsh
tnvmaysnck vsgsntyddl agadvvivta gftkapgksd kewnrddllp
lnnkimieig ghikkncpna fiiivvtnpvd vmvqllhghs gvpknkiigl
ggvldtsrlk yyisqklnvc prdvnahivg ahgnkmvllk ryitvvgipl
qefinnklis daeleaifdr tvntaleivn lhaspyvapa aaiiemaesy
lkdlkkvlic stlleggygh sdifggtpvv lgangveqvi elqlnseeka
kfdeaiaetk rmkala
```

pfAldo

```
mnapkklpad vaeelattag klvqagkgil aadestqtik krfdniklen
tienrasyrd llfgtkglgk fisgailfee tlfqkneagv pmvnllhnen
iipgikvdkg lvnipctdee kstqgldgla erckeyyag arfakwrtvl
vidtakgkpt dlsnhetawg laryasicqq nrlvpivepe iladgphsie
vcavvtqkvl scvfkalqen gvllegallk pnmvtagyec taktttqdvq
fltvrtlrrt vppalpgvvf lsggqseee svnlnsinal gphpwalfts
ygralqasvl ntwqgkknv akarevllqr aeanslatyg kykkggaggen
agaslyekky
vy
```

Figure 7. Protein sequences of *Plasmodium falciparum* protein biomarkers.

programs in level 0 and level 1 areas. They can be designed to detect single species infection (ie. Pf only infection) or multiplexed to determine the course of treatment in areas with multiple species of Plasmodium transmission. Despite these advantages, RDTs are unable to detect asymptomatic infections below 200 parasites/ μ L. It is common practice to microscopically



Figure 8. Malaria rapid diagnostic test processed at the point of care. (USAID Kenya ©. All rights reserved.)

examine the sample from a negative RDT to validate the negative result. Any genetic variation in the biomarker will also not be recognized by the RDT and show up as a false negative. The utility of RDTs for malaria control is still very apparent, as the volume of sales increased from 46 million to 319 million between 2008 to 2013.

Scope of this Work

When considering a diagnostic test for areas with high transmission rates of malaria and other infectious diseases, the World Health Organization recommends that new point of care diagnostic tests be characterized by the acronym ASSURED.[22] These tests should be Affordable, Sensitive, Specific, User friendly, Rapid and robust, Equipment free, and

Deliverable. Of all the outlined detection methods for malaria (light microscopy, ELISA, RDT), only the RDT stands out as meeting most of the ASSURED criteria. As the landscape of malaria testing changes from symptomatic patient surveillance and control to a total malaria elimination campaign, finding and treating the asymptomatic carriers of the parasite will be critical. It is easy to envision designing an ELISA for improved sensitivity at a level 4 or level 5 facility, but the greatest malaria burden is found at the point of care—at these level 0 and level 1 facilities. This dissertation will outline a platform for development of new diagnostic formats in addition to enhanced sensitivity of currently existing RDTs—sample preparation and concentration. Chapters II-IV discuss how surface functionalized magnetic particles can be used to rapidly isolate *pfHRP*II from a blood sample and how that bound protein can be detected by two classes of reagents: metal phosphorescent probes and enzyme conjugated antibodies. **Chapter II** discusses the development of a self-contained extraction device for the selective isolation, purification and concentration of *pfHRP*II from human whole blood, by exploiting the high affinity of Ni^{2+} toward histidine. The extraction cassette consists of a small diameter tube containing a series of pre-loaded processing solutions separated by mineral oil valves. Ni(II)NTA functionalized magnetic beads are processed through the device in the presence of an external magnetic field in order to 1) capture *pfHRP*II from whole blood, 2) wash away any contaminating proteins and 3) release a 1000-fold purified *pfHRP*II sample for subsequent analysis. **Chapter III** discusses the synthesis and optimization of a non-emissive, cyclometalated Ir(III) complex, $\text{Ir}(\text{ppy})_2(\text{H}_2\text{O})_2^+$ (Ir1), which upon binding histidine/histidine containing peptides, elicits a rapid, long-lived phosphorescent signal in aqueous buffer. Only the addition of histidine results in a signal response, while other amino acids with coordinating side chains have no effect. After optimization, this probe was explored as a robust detection reagent for *pfHRP*II

in solution and on the surface of the magnetic particles employed in Chapter II. **Chapter IV** outlines the development of an on-bead ELISA assay that is complete in under 20 minutes, on the surface of a magnetic particle, with single parasite/ μ L limits of detection. These three chapters outline progress toward new assay formats for more sensitive detection of *pfHRP2* for *Plasmodium falciparum* identification. **Chapter V** further unravels malarial rapid diagnostic tests—how they work, their successes, and their failures. Using what was developed in Chapter II, **Chapter VI** outlines how currently manufactured malaria RDTs can be enhanced to achieve asymptomatic limits of detection. Finally, **Chapter VII** details the streamlining of this enhancement process and what a total device for RDT enhancement could potentially look like. In looking at the history of malaria, it is very clear that it takes action from all factions of society to work toward malaria eradication. Full understanding of the disease, its transmission, and the end user will be vital in assuring that new diagnostics for point of care malaria detection will continue to push toward achieving this goal.

CHAPTER II

A METAL BASED PLATFORM FOR EXTRACTION OF *PLASMODIUM FALCIPARUM* HISTIDINE RICH PROTEIN II FROM BIOLOGICAL SAMPLES

Introduction

When considering analysis of biomarkers from a complex matrix, sample preparation is a key component to ensure detection of the biomarker of interest above the background noise from the sample itself. While there are many differences between techniques used to distinguish proteins from nucleic acids from small molecules, common to all of these is often a form of sample preparation. Solid phase extraction techniques, where the biomarker is separated from contaminants and unwanted materials by immobilization on a solid phase, have been streamlined by marketing of disposable spin columns and size exclusion filters. Using a centrifuge, proteins and nucleic acids can be rapidly purified and concentrated for downstream detection. However, access to these materials and instruments in low-resource areas is not guaranteed. Thus, there is a need for designing sample preparation techniques that can be applied at the point-of-care.

Current fluidic approaches for the concentration and purification of protein biomarkers include microfluidic and paper devices.[23; 24; 25] Microfluidic devices aim to provide multi-step sample-processing and detection procedures in a small, disposable all-in-one device.[26; 27] Incorporation of sample preparation and detection into micron-sized channels allows for smaller sample and reagent volumes as well as shorter test times,[28; 29] but mechanical failure of valves and pumps and cost of manufacturing and materials imposes limitations on the availability of such devices in low-resources areas.[30] Paper based diagnostics circumvent the cost and need for valves and pumps in microfluidic cassettes by directing lateral flow of liquids

across two and three dimensional paper strips and pads.[31; 32] However, inconsistencies associated with retention factors of different fluids and samples, non-specific interferences, and susceptibility of paper to environmental conditions can yield failed matrix clearance and poor diagnostic readout.

As an alternative to the valve complexity of traditional microfluidic devices, researchers have developed a rapid purification method based on immiscible phase filtration in which a barrier is created using oil, wax or organic solvent to separate two aqueous solutions on either the macro- or microscale. This approach utilizes a magnet to transport analyte-bound magnetic beads across the barrier from one solution to the next. This technique has been effective in the rapid isolation of nucleic acids,[33; 34] proteins[35; 36] and cells.[37; 38] Similarly, Haselton and coworkers demonstrated the creation of effective air gap barriers in a filament-based design for the detection of viruses.[39] Based on these principles, a self-contained, extraction cassette for the isolation of a viral RNA biomarker from nasal washes was developed.[40]

This chapter outlines the modification of this self-contained design to demonstrate its

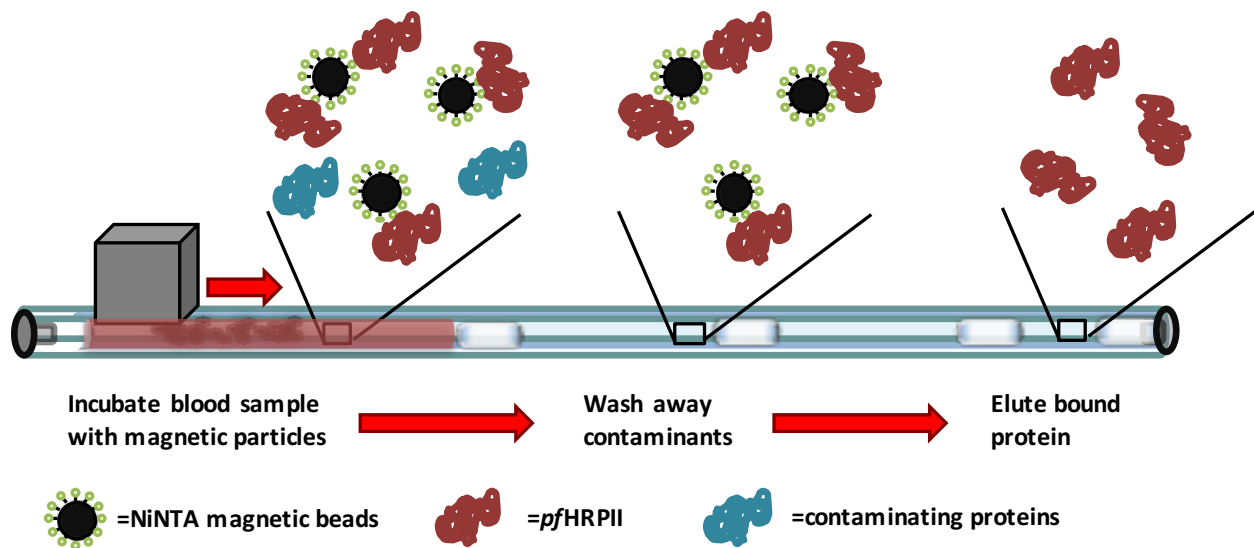


Figure 9. Generalized schematic of the self-contained *pfHRP* II extraction cassette

utility for the extraction of a protein biomarker from a more complex sample matrix, e.g. whole blood (Figure 9). The extraction cassette incorporates preloaded buffer solutions separated by small volumes of mineral oil, deemed surface tension valves, into a single length of tubing. By confining immiscible materials, such as buffers and oil, into a small tube, the interfacial tension at their surface creates a valve, which regulates the transport of materials. Due to the high affinity of histidine toward metal(II) chelation, Ni(II)NTA magnetic particles are used to extract the malarial protein biomarker *Plasmodium falciparum* Histidine Rich Protein II (*pfHRP*II) from spiked whole blood. These magnetic beads are processed through the device in the presence of an external magnetic field in order to 1) capture *pfHRP*II from whole blood, 2) wash away any contaminating proteins and 3) release *pfHRP*II for subsequent analysis. The presence of oil valves stabilizes the device and prevents the chambers from intermixing. By optimizing the components and assessing the efficiency of the cassette, the device was demonstrated to extract, purify and concentrate *pfHRP*II in under 30 minutes, using a hand held magnet. The unique design of this device will enable low-resource extraction without the restraints of antibodies or costly equipment.

Materials

Ni-NTA Magnetic Agarose Beads (Cat # 36111) were purchased from Qiagen Inc. Human Plasma (A+) collected in citrate phosphate dextrose (CPD) (Cat # HP1013) was purchased from Valley Biomedical Inc. Human A+ Whole Blood collected in CPD (Cat# HMWBCPD) was purchased from Bioreclamation LLC. (Note: A+ biologicals are used as this was the blood type utilized by Walter Reed Army Medical Center during malaria parasite culture training.) Human Histidine Rich Glycoprotein ELISA kit (Cat # SEK10836) was purchased from Sino Biological Inc. Antibodies for the *pfHRP*-II ELISA (Cat # ab9206 and ab30384) were purchased from

Abcam Inc. 3,3',5,5'-tetramethylbenzidine (TMB) One solution (Cat # G7431) was purchased from Promega Corporation. Micro Spin Desalting Columns (Cat # PI89877) were purchased from Fisher Scientific Inc. Recombinant HRP-II (Cat # AGPF-55) was purchased from Immunology Consultants Laboratory Inc. HisPur NiNTA agarose spin columns (Cat # 88227) were purchased from ThermoScientific Inc. SD Bioline Malaria Ag P.f Rapid Diagnostic Tests (Cat # 05FK50) were purchased from Standard Diagnostics Inc. The donut shaped magnet used in this study was purchased from Emovendo LLC. All other reagents were purchased from Sigma Aldrich Inc. or Fisher Scientific Inc.

Experimental

Spiked Plasma Sample Preparation

Human A+ plasma was mixed 1:1 (v:v) with 2X lysis buffer (100mM potassium phosphate pH 8.0, 600mM NaCl, 250mM imidazole, 2% Triton X-100) to make a stock of lysed plasma for dilution. *P. falciparum* culture (at ~51500 parasites/ μ L) was diluted into a lower concentration stock of 200 parasites/ μ L in the above lysed human plasma. This second stock was serially diluted by half using lysed plasma to 12.5 parasites/ μ L giving a range of parasite protein concentrations for extraction. To do this, 500 μ L of 200 parasites/ μ L was pipetted into an eppendorf tube containing 500 μ L of unspiked lysed plasma to yield 1mL of 100 parasites/ μ L. After mixing, 500 μ L of 100 parasites/ μ L was pipetted into an eppendorf tube containing 500 μ L of unspiked plasma to yield 1mL of 50 parasites/ μ L. This process was repeated until 12.5 parasites/ μ L was reached. Lysed plasma without parasite was used as a control.

Spiked Whole Blood Sample Preparation

Human A+ Whole Blood collected in CPD was mixed 1:1 (v:v) with 2X lysis buffer and allowed to lyse until the blood became translucent. *P. falciparum* culture (at ~51500

parasites/ μL) was diluted into a lower concentration stock of 200 parasites/ μL in the above lysed whole blood. The bottom of a 10mL syringe was fitted with a small layer (\sim 1-2mm thick) of glass wool. The lysed, spiked whole blood was filtered through the syringe by gravity filtration and collected into a new vial. A second volume of whole blood was lysed and filtered. The 200 parasites/ μL stock was serially diluted by half using the second volume of filtered whole blood to 12.5 parasites/ μL . Lysed and filtered whole blood without parasite was used as a control.

pfHRP II Extraction from Plasma and Whole Blood using the Self-Contained Extraction Device

The design and chamber contents of the extraction device was prepared by preloading four processing solutions and four mineral oil valves within Tygon[®] R-3603 tubing \sim 24cm in length (1.6mm inner diameter). The rounded end of a 200 μL PCR eppendorf tube was cut, and the top of the cap was punctured with a 27 $\frac{1}{2}$ gauge needle to serve as an air release valve, prior to insertion into one end of the tubing. 10 μL of elution buffer (50mM potassium phosphate (PB) pH 8.0, 300mM NaCl, 500mM imidazole, 0.05% Tween-20) was pipetted into the end of the tubing opposite the PCR tube using a gel tip pipette tip. The elution end of the tube was sealed with the rounded end of a MelTemp capillary tube. Using a 27 $\frac{1}{2}$ gauge syringe, mineral oil (25 μL of mineral oil, \sim 2mm length) was added in front of the elution chamber prior to the sequential addition of three wash chambers (100 μL of 50mM PB, pH 8.0, 300 mM NaCl, 125mM imidazole, and 0.05% Tween 20) separated by mineral oil valves. Mineral oil was also added between the first wash chamber and the end of the PCR tube to seal off the tubing to air. 200 μL of the prepared plasma or whole blood samples was pipetted into the PCR tube, followed by a 10 μL suspension of magnetic Qiagen Ni(II)NTA agarose beads (concentration, 152.8 beads/ μL). Four extraction tubes were prepared for each concentration of parasite spiked into plasma or whole blood. The tubes were incubated on a bench-top rotisserie for 10 minutes to ensure mixing

of the agarose beads throughout the sample. After the incubation period, by threading the tube through the center of a donut magnet (2.5mm OD, 1.4mm ID, 0.6mm thickness, 250-300mT from center), the beads were collected, pulled across the oil valve and transferred into the first wash chamber. The beads were mixed with the magnet throughout the first wash chamber for 30 seconds using a back and forth movement. After mixing, the beads were collected at the end of the wash chamber and pulled across the oil valve into the second wash chamber. Likewise, the beads were mixed within the second and third wash chambers until reaching the final 10 μ L elution chamber. In the elution chamber, the beads were dispersed for 10 minutes to ensure total release of the protein from the surface of the beads. After the elution period, the beads were transferred back into the previous oil valve.

ELISA Quantification of pfHRP II

A 100 μ L solution of 1 μ g/mL IgM anti HRPII in 1X PBS was added to each well of a Immulon 2 HB 96-well plate, sealed with Parafilm and allowed to incubate for 1 hour on an orbital shaker. After incubation, the plate was washed 3 times with 300 μ L of 1X PBS containing 0.1% Tween-20 (PBST). Next, 300 μ L of a solution of PBST with 5% BSA (by weight) was added to each well and incubated for 2 hours. The plate was then washed three times with PBST before adding the standard curve, controls and samples. Note: The working range of this ELISA assay is 0-25pM *pfHRP II*, so the samples were diluted into the range using a dilution buffer of PBST with 0.1% BSA. After the 2-hour sample incubation period, the plate was washed four times with PBST. Next, a 100 μ L solution of 0.5 μ g/mL IgG anti HRPII with HRP in PBST containing 0.5% BSA was added to each well and incubated for 1 hour while protected from light. The plate was then washed five times prior to development. 100 μ L of TMB One solution was added to each well and developed for 5-10 minutes in low light. The reaction was quenched

with 100 μ L of 2M H₂SO₄. The absorbance at 450nm was measured using a BioTek Synergy H4 microplate reader.

ELISA Quantification of HRG

A 100 μ L solution of 2 μ g/mL of mouse anti-HPRG in CBS was added to each well of a Immulon 2 HB 96-well plate, sealed with Parafilm and allowed to incubate for 1 hour on an orbital shaker. After incubation, the plate was washed 3 times with 300 μ L of 1X TBS containing 0.05% Tween-20 (TBST). Next, 300 μ L of a solution of TBST with 2% BSA (by weight) was added to each well and incubated for 2 hours. The plate was then washed three times with TBST before adding the standard curve, controls and samples. Note: the working range of this ELISA assay is 0-600 pg/mL, so the samples were serially diluted in dilution buffer of TBST with 0.1% BSA 10-fold from 10x-10,000x to ensure the samples would fall into the range of the assay. After the 2-hour sample incubation period, the plate was washed four times with TBST. Next, a 100 μ L solution of 1 μ g/mL rabbit anti-HPRG with HRP in PBST containing 0.5% BSA was added to each well and incubated for 1 hour while protected from light. The plate was then washed five times prior to development. 100 μ L of TMB One solution was added to each well and developed for 5-10 minutes in low light. The reaction was quenched with 100 μ L of 2M H₂SO₄. The absorbance at 450nm was measured using a BioTek Synergy H4 microplate reader.

Quantification of Hemoglobin Content in Samples Extracted from Whole Blood

Samples of whole blood spiked to 200 parasites/ μ L were extracted as described in the materials and methods section (n=3). Each chamber (supernatant through elution) was diluted in water and analyzed spectrophotometrically at 414nm ($\epsilon_{\text{hemoglobin}} = 524280 \text{ M}^{-1} \text{ cm}^{-1}$) using a BioTek Synergy H4 microplate reader. Recovery of hemoglobin was normalized to the concentration of hemoglobin in the supernatant.

Whole Protein Gel Analysis

Each of the chambers within the extraction cassette was analyzed for whole protein content using standard denaturing SDS-PAGE gel protocols. The bands were stained with either Coomassie Blue or silver staining for qualitative analysis of protein content. For silver staining, the gel was removed from its cassette and soaked 1 hr in fixing solution (50% MeOH, 12% acetic acid, and 0.0185% formaldehyde). Next, the gel was washed three times for 8 minutes with 50% MeOH. After washing, the gel was soaked for 1 min in pretreatment solution (0.02% $\text{Na}_2\text{S}_2\text{O}_3$) and washed three times for 20 seconds in water. The water was decanted, and the silver stain solution (0.2% AgNO_3) was added and incubated with the gel for 20 min. After incubation, the silver stain was removed and the gel was washed three times for 20 seconds in water. Next, the development solution (6% Na_2CO_3 , 0.0004% $\text{Na}_2\text{S}_2\text{O}_3$, 0.0135% formaldehyde) was added and mixed with the gel until proper resolution was achieved (~ 5 minutes). The development solution was then removed and the stop solution (50% MeOH and 12% acetic acid) was added. The gel was washed with water and photographed.

Bradford Protein Assay for Whole Protein Quantification

Prior to quantitating the concentration of total protein, the spiked plasma and whole blood (200 parasites/ μL) elution samples to be analyzed were desalted using the protocol outlined in the Zeba Spin Desalting Column kit. Salts and surfactants must be removed so as to not interfere with the Bradford reagent. Once desalted, elution samples were assayed using the standard microtiter plate Bradford assay protocol as detailed through Bio-Rad Laboratories.

Carryover Volume Determination

To a ~15mm piece of Tygon tubing, sealed on one end with a glass capillary tube, 100 μL of wash buffer followed by 25 μL of mineral oil was added to the sealed end using a 27 ½ gauge

syringe. Then, a 100 μ L solution of 1x lysis buffer spiked with 100nM fluorescein was added in front of the oil valve. Under reduced light conditions, 10 μ L of Ni(II)NTA magnetic particles were added to the fluorescein containing solution at the open end of the tubing. The particles were magnetically processed through the chamber, pulled across the valve and into the second chamber with a total processing time of ~20 seconds. The second chamber was cut out and stored in an eppendorf tube in reduced light conditions. Fluorescence (ex 494/em 521) of the second chamber was measured using a BioTek Synergy H4 microplate reader against a standard curve of fluorescein to determine the concentration of fluorescein carried over from the first chamber. This concentration was then converted to a volume measurement. Carryover experiments (n=5) were conducted on the following chamber variations: 1) lysis to wash, 2) wash to wash and 3) wash to elution.

Determination of the Elution Profile of pfHRPII with Imidazole

100 μ L of 1nM *pfHRPII* in an eppendorf tube was diluted with 100 μ L of 2x lysis buffer containing various amounts of imidazole (0-800mM imidazole in 100mM increments) to bring the final concentration of *pfHRPII* to 0.5nM in 1x lysis buffer conditions (n=3 for each concentration of imidazole). 10 μ L of Ni(II)NTA agarose beads (bead concentration of 76.4 beads/ μ L) was added to each sample and incubated for 30 minutes on a benchtop rotisserie. After incubation, the beads were pulled down magnetically, and the supernatant was measured using *pfHRPII* ELISA.

Determination of the Elution Profile of HRG with Imidazole

500 μ L of human serum was diluted with 500 μ L of 2x lysis buffer containing various amounts of imidazole (0-800mM imidazole in 100mM increments). 10 μ L of Ni(II)NTA agarose beads (bead concentration of 76.4 beads/ μ L) was added to 200 μ L of each sample (n=3) and

incubated for 30 minutes on a benchtop rotisserie. After incubation, the beads were washed five times with wash buffer containing the appropriate amount of imidazole (0-400mM in 50mM increments) to remove any residual HRG unbound by the beads. 100 μ L of elution buffer was added to the samples and incubated for 10 minutes on the benchtop rotisserie. After incubation, the beads were pulled down magnetically, and the elution sample was measured using HRG ELISA.

Malaria Rapid Diagnostic Test Enhancement

For each concentration of parasite extracted from plasma and whole blood, the 10 μ L elution chamber, from a previously prepared extraction tube, was excised and spotted onto an RDT, allowed to develop for 20 minutes (per manufacturer's specifications) and photographed.

Results and Discussion

Design of the pfHRP II Extraction Cassette

In transition from extraction of nucleic acids by Haselton and coworkers to protein targets, several parameters of the device were redesigned to make this approach suitable for targeting *pfHRP II*, including selective binding of *pfHRP II*, incorporation of mineral oil valves, arrangement and composition of the processing chambers, and optimization of incubation and elution parameters. The cassette consists of five sequential aqueous buffer chambers separated by mineral oil valves contained within a single length of flexible Tygon® tubing: a binding chamber, three wash chambers, and a final elution chamber. As the 50 μ m Ni(II)NTA agarose particles in this design are significantly larger than the one-micron beads previously used and are unable to traverse air efficiently, mineral oil was substituted for air. It has been shown that immiscible oil barriers are resistant to deformation within a microfluidic device, due to the interfacial energy at their contact region, which enhances the stability of the chamber

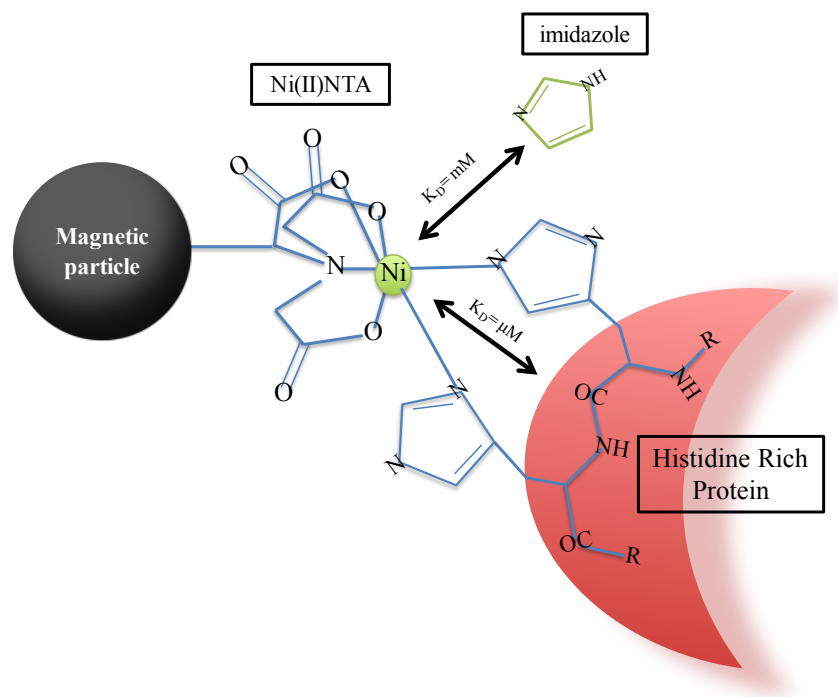


Figure 10. Interaction between histidine side chains of *pfHRPII* and the Ni(II)NTA magnetic particle

configuration.[34] We have recently shown that mineral oil valves are the most stable, when compared to air valves, over a wide range of processing buffer compositions.[41] Thus mineral oil valves were selected for this cassette design. During the extraction process, the microparticles are magnetically entrained at the end of a chamber, where they are collectively passed through the barrier. Once the particles traverse the oil into the next chamber, the mineral oil valve returns to its resting state, leaving the valve and flanking chambers intact.

Optimization of the pfHRPII Extraction Cassette

Ni(II)NTA technology has been widely used to bind and purify histidine rich proteins from complex matrices due to selective coordination of the imidazole side chains of histidine to the metal center (ie. purification of His-tagged recombinant proteins from the expression media). Given this, 50 μ m magnetic Ni(II)NTA agarose microparticles were selected as the motive solid phase

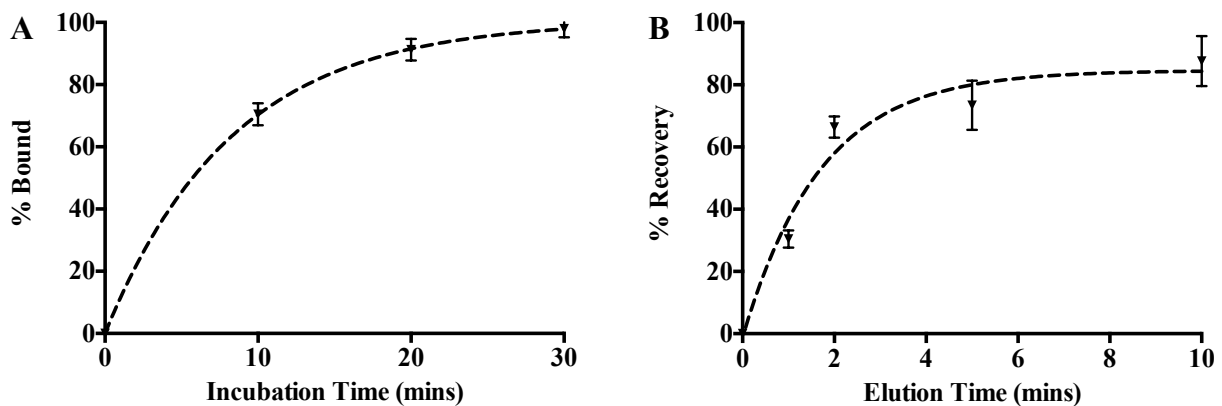


Figure 11. A) Incubation and B) Elution time profiles of *pfHRPII* with Ni(II)NTA magnetic particles

for biomarker capture (Figure 10).[9; 42],[43] Multiple coordination interactions to the nickel metal center are more robust than surface adsorption and ensure that the biomarker is not leached from the surface of the particle. Considering the end goal of a rapid sample preparation technique for low-resource areas, finding a balance between time required to capture and release maximum biomarker versus total extraction time was necessary for creation of a rapid and efficient cassette. Optimal target binding and elution profiles, from a plasma sample, were determined from kinetic studies. After 10 minutes, more than 70% of the biomarker was bound to the beads (Figure 11A). At 30 minutes, greater than 90% recovery was achieved. While incubation time was ultimately optimized at 10 minutes, this does not negate the future possibility of increasing biomarker-binding time to achieve higher yields. Similarly, elution time was optimized at 10 minutes (Figure 11B). Both curves were fit to a one-phase association model, and the rate constants were calculated to be 0.1160 and 0.5860 min^{-1} , respectively.

Given the principle of solid phase extraction, immobilization of *pfHRPII* on the surface of the Ni(II)NTA magnetic particles provides a means for easy removal of contaminating proteins and other biomolecules. However, manipulation of the bound protein for enhanced

purification can be achieved by sequential wash steps and/or adding reagents to the sample to aid in purification. Both of these approaches were incorporated into the extraction design. It is known that several small volumes are usually more effective at partitioning the analyte of interest into the extraction phase rather than a single large volume.[44] Consequently, three wash chambers were incorporated into the cassette design to serve as isolated purification reservoirs. A consequence of these transfer steps is the carryover of fluid with the bead packet upon leaving

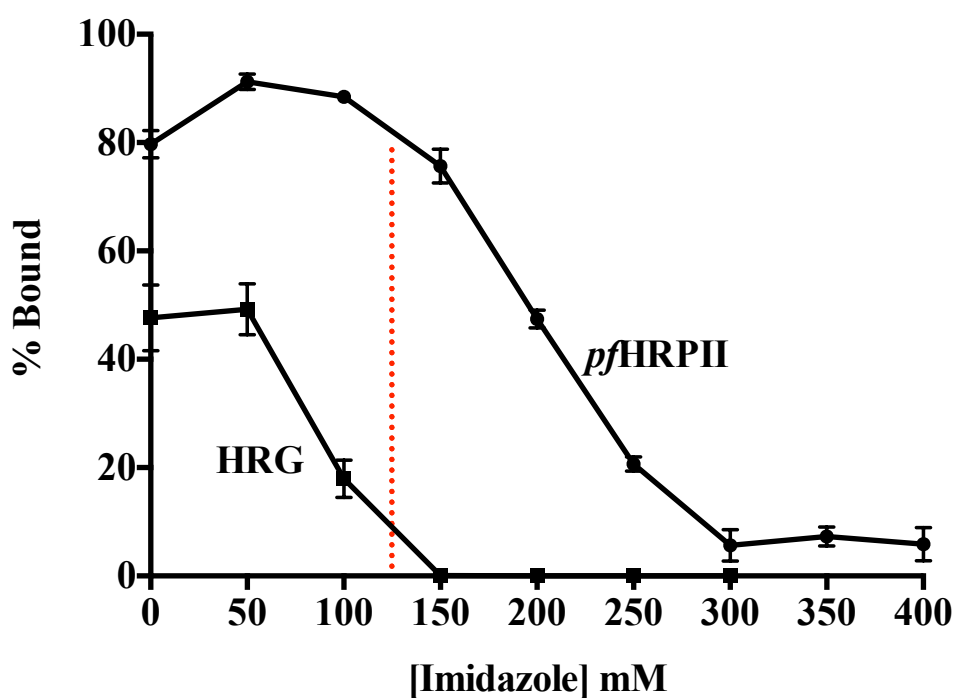


Figure 12. Effect of imidazole on *p/HRP II* and HRG binding to Ni(II)NTA particles

one aqueous phase to the next. This carry over volume was determined to be $1.24 \pm 0.56 \mu\text{L}$, regardless of the chamber environments (i.e. moving from binding to wash, wash to wash, or wash to elution). Thus, any amount of plasma or whole blood carried over from the loading chamber in this volume will be sequentially diluted 100-fold in each of the subsequent wash chambers, prior to elution.

While isolation of the wash chambers from the binding chamber via mineral oil limits the effect of carryover of contaminating proteins, introducing imidazole to the aqueous phase enhances the level of purification by blocking undesired metal binding proteins. Patient blood samples contain a host of potential contaminating proteins, such as histidine rich glycoprotein (HRG) and human serum albumin (HSA), that can interact with the Ni(II)NTA particles by either specific coordination to Ni(II)NTA or non-specific association to the bead. HRG, a globular protein with a physiological concentration of 1.5 μ M, is characterized by a centralized histidine rich region with 5 tandem repeats of GHHPH amino acid motifs and has been shown to chelate free metal ions such as Zn²⁺. [45];[46];[47] Although HRG can coordinate to the metal center, the coordination is weaker than that of *pf*HRP_{II} due to fewer number of metal binding sites. Therefore, imidazole can be used to competitively block HRG from binding Ni(II)NTA without disrupting bound *pf*HRP_{II}. Aside from blocking potential metal-coordinating contaminants, imidazole also mediates non-specific protein interactions (e.g. electrostatic interactions of HSA and hemoglobin, and other non-metal coordinating proteins) by charge neutralization of the particle surface. To observe the effect of imidazole on binding efficiency of *pf*HRP_{II} and HRG to Ni(II)NTA particles, increasing concentrations of imidazole was titrated into lysis buffer prior to incubating a *pf*HRP_{II} spiked sample with the particles (Figure 12). At an imidazole concentration of 300mM, *pf*HRP_{II} was completely eluted from the particles, while HRG was released with 150mM imidazole. Similar observations in the elution profile of *pf*HRP_{II} and HRG were previously noted in purification of *pf*HRP_{II} by Panton et al. using Zn²⁺ affinity chromatography.[9] An overlay of the titration curves of *pf*HRP_{II} and HRG identifies a region between 100-200mM imidazole where the yield and purity of the final sample is maximized. For the sake of maintaining high yields of biomarker and minimizing the presence

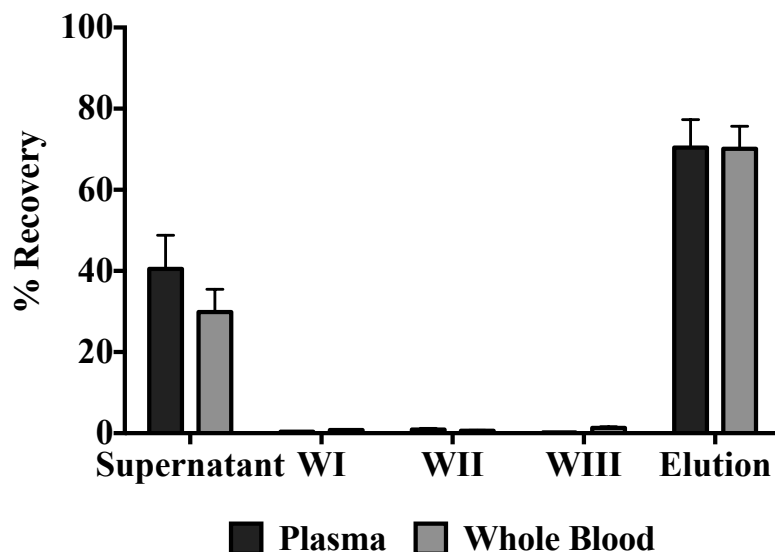


Figure 13. Post-extraction distribution of *pfHRP* II in the extraction cassette. WI-III refer to the sequential wash chambers in the cassette.

of contaminants, the blocking conditions were set at 125mM imidazole. Global analysis of the purification of target was qualitatively monitored by Coomassie stained SDS-PAGE gels (Figure SI II.1).

After processing the biomarker bound particles through the wash chambers, *pfHRP* II is released from the surface of the particles into an elution chamber containing 500mM imidazole. If the volume of this chamber can be reduced from the initial sample volume, then the purified protein can be concentrated for downstream detection. Considering the concentration of *pfHRP* II in the patient reservoir we are interested in is in the picomolar range, concentration is a vital aspect to achieve sensitivity and reducing false negatives in a downstream detection format. It was determined that a 10 μ L elution volume was the minimum convenient volume for protein release and (Figure SI II.2), resulting in a 10-fold concentration of target.

Specific capture of the malarial protein *pfHRP* II by Ni(II)NTA magnetic particles and purification of the biomarker from whole blood in a low-resource format distinguishes this

device from other protein extraction methods. Separation of the binding and elution chambers by three wash chambers limits the carryover of small volumes of contaminants from the original sample, while the composition of the aqueous wash solutions facilitates the removal of interferences from the biomarker bound particles. The binding and release kinetics of the protein from Ni(II)NTA ensured that total extraction time took approximately 25 minutes, compared to commercial kits, which can take 1.5 hours and require several centrifugation and transfer steps. These optimized conditions were subsequently used for the extraction of target biomarker from the complex biological matrices of plasma and whole blood.

Efficiency of pfHRP II Extraction Using the Self-Contained Cassette

The optimized cassette was utilized to extract *pfHRP II* from complex matrices, such as plasma and whole blood. Initial studies were conducted on plasma samples spiked to 200 parasites/ μL using a concentrated *Pf* culture. ELISA analysis of all of the chambers (and subsequent propagation of error within the measurement of each chamber) demonstrated total recovery ($112.4 \pm 10.8\%$) of *pfHRP II* within the cassette. Under these conditions, $74.0 \pm 9.1\%$ of the protein was recovered in the elution, with the wash chambers having minimal *pfHRP II* protein content (Figure 13- black bars). The mass balance remained unbound in the initial binding chamber. While high yields were achieved from a plasma sample, blood remains an attractive choice for biomarker detection at the point-of-care, as plasma separation from a blood sample is not a trivial task. Many plasma separation protocols require centrifugation or application of the sample to a plasma separation membrane. These processing steps require additional equipment, additional processing time, and a potential loss in sample volume.[48]

Lysed whole blood samples were similarly spiked and processed through the extraction cassette. Preprocessing the lysed blood sample through glass wool eliminated excess cellular

debris, which was observed to aggregate the particles. As seen with plasma, all ($102.7 \pm 7.9\%$) of the *pfHRP*II was accounted for among the chambers of the extraction cassette (Figure 13- gray bars). $70.1 \pm 5.6\%$ of the protein was recovered in the elution. Analysis of the results by an unpaired t-test showed that there was no significant difference ($p \geq 0.05$) between the recovery of *pfHRP*II from plasma or whole blood. Additionally, there was no statistical difference ($p \geq 0.05$) in *pfHRP*II recovery from plasma between extractions using a HisPur Spin Column commercial kit ($68.8 \pm 5.4\%$). While the spin kit is faster than traditional solid phase extraction techniques (1-2 hours vs. 3-4 hours, respectively), it requires a centrifuge and several liquid transfer steps. Recovery of *pfHRP*II from whole blood using the spin kit ($45.3 \pm 2.1\%$) versus the extraction cassette was determined to be statistically different (Figure SI II.3). The extraction cassette represents an attractive design for low-resource applications, since it achieves the same or better protein recovery as laboratory-based methods that require multiple centrifugation/transfer steps without extensive processing times.

The extraction cassette design offers several advantages over recently developed approaches. For example, Stayton and coworkers used stimuli responsive antibody-polymer conjugates and membranes to isolate and concentrate *pfHRP*II from spiked plasma. The efficiencies of their system ranged from 7-35%.[49] The antibody-antigen complex was captured on the membrane at elevated temperatures and released for detection upon cooling. Another assay reported 100% recoveries of *pfHRP*II from 1/5 diluted serum with antibody conjugated magnetic nanoparticles, but took no steps to remove contaminants.[50] Neither of these systems attempted isolation from whole blood. While both of these approaches are intriguing, the use of antibodies for *pfHRP*II capture and purification limits ease of release for offline downstream detection.

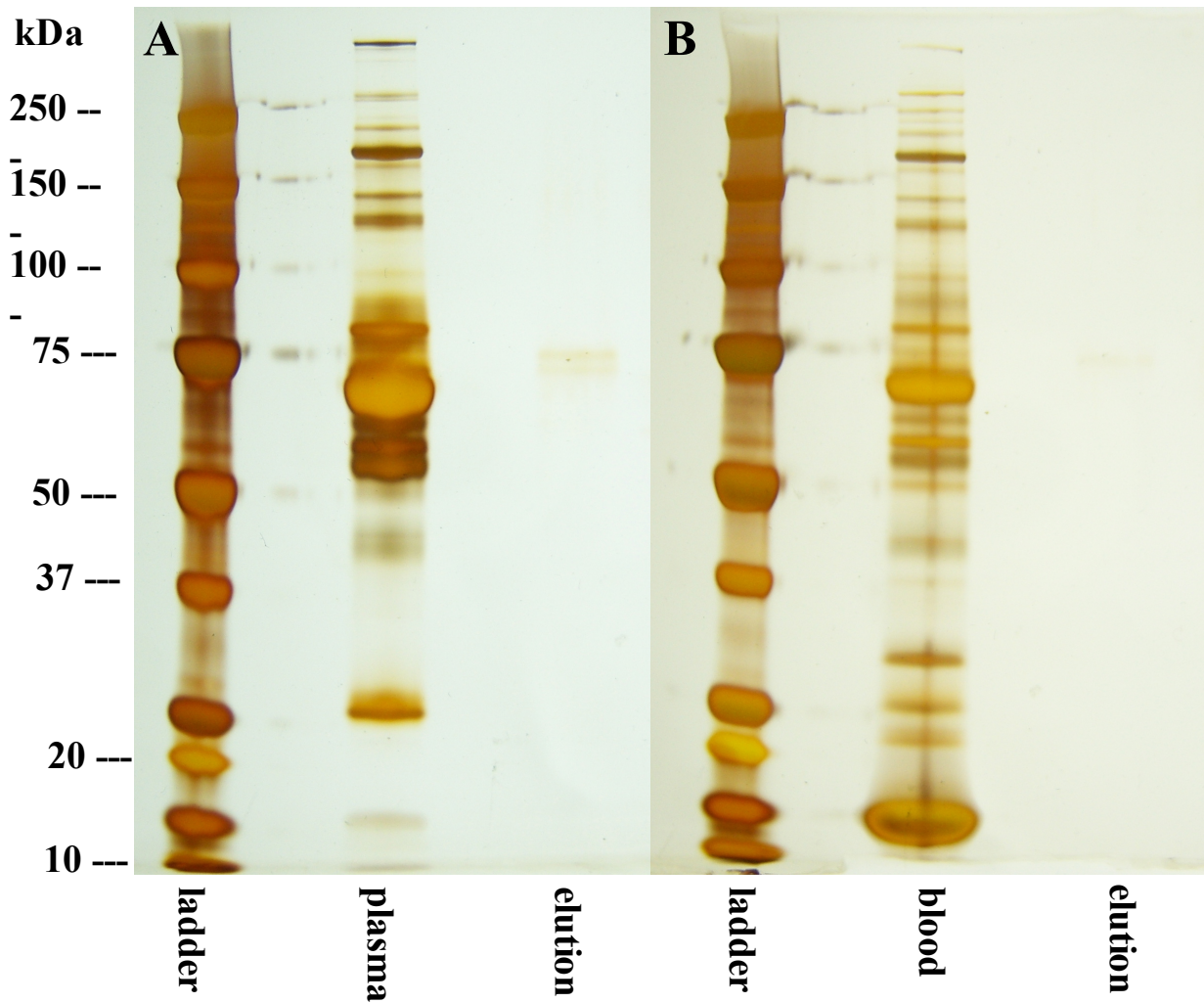


Figure 14. Silver-stained SDS-page gel pre- and post- extraction from A) plasma and B) blood.

Purification of pfHRP_{II} from Spiked Human Plasma and Whole Blood

In conjunction with analyzing the efficiency of *pfHRP_{II}* extraction, the degree of purification post-extraction of *pfHRP_{II}* was also investigated. While the Ni(II)NTA ligand on the surface of the particles acts to selectively capture the malarial biomarker, other metal chelating proteins can compete for binding to the metal center. Because of its propensity toward chelating metal centers, HRG content was quantified across the extraction cassette by ELISA

(Figure SI II.4). The presence of imidazole in the incubation and wash chambers, as previously optimized, serves to displace these proteins from binding to the Ni(II)NTA particles prior to reaching the elution chamber. There was a decrease in HRG concentrations across the wash chambers (132nM to 70nM, respectively). Similar trends were also observed in samples extracted from whole blood (505nM to 26nM, respectively). As previously noted, 150mM imidazole served to elute HRG completely from the surface of the particles, but the binding and

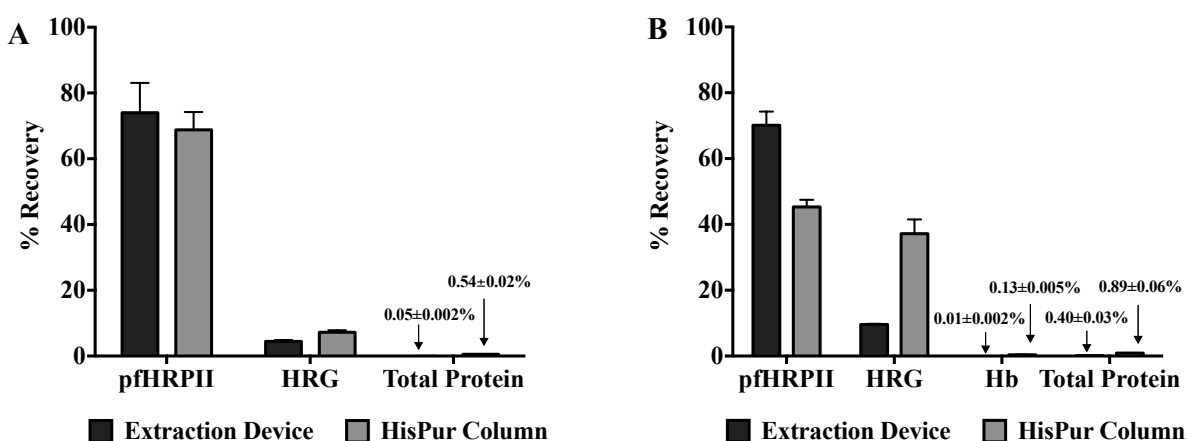


Figure 15. Comparison of recovery of non-specific protein interferents and *pfHRP II* from A) plasma and B) whole blood using our extraction device and a commercially available

HisPur Ni(II)NTA spin column

wash chambers contain slightly less imidazole (125mM). During the wash steps, imidazole slowly displaces HRG from Ni(II)NTA which accounts for the general decrease in HRG concentration across the wash chambers. Less than 10% of the physiological concentration of HRG was present in the final extracted sample.

For non-specific protein interferents (e.g. α -2-macroglobulin, HSA, lipoproteins), which may adsorb to the surface of the agarose particles, imidazole forms a salt barrier to prevent non-specific carryover of these proteins. The oxygen transport protein, hemoglobin, is present in red blood cells at concentrations of 2-3mM and represents an easily measured surrogate for non-

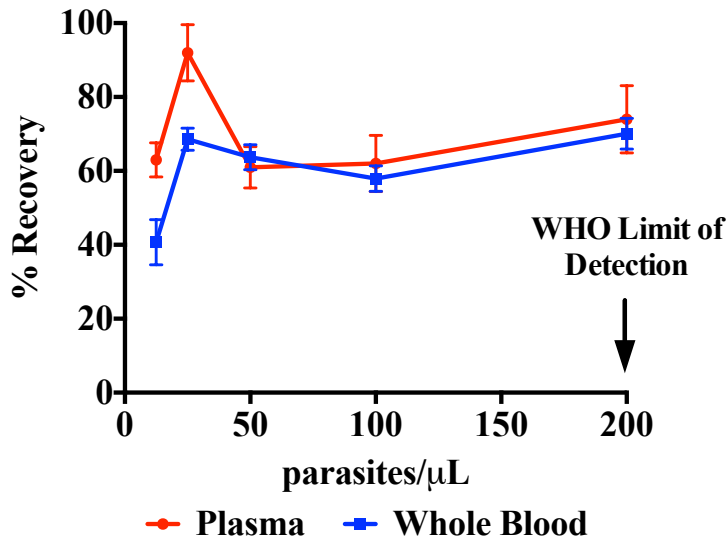


Figure 16. Recovery of *pf*HRPII below the WHO recommended limit of detection for rapid diagnostic tests

specific protein binding.[51] Presence of hemoglobin in a biological sample may occlude a colorimetric measurement, due to the deep red color of the protein. Analysis of the processing chambers for hemoglobin content showed that its concentration was reduced after the first wash chamber. The final eluate contained less than 0.1% hemoglobin (Figure SI II.5).

Finally, the samples were further analyzed by silver stained SDS-PAGE gels and Bradford assay to determine total protein content post-extraction. A very faint band is visible at approximately 67kDa on a silver stained SDS-PAGE gel (Figure 14). This band likely corresponds to HSA, as the limits of detection of silver staining limit *pf*HRPII detection. (Note: presence of *pf*HRPII in the final sample was validated by ELISA.) The Bradford assay was used to determine the total protein content in the eluted sample. Recovery of HRG from spiked plasma was reduced by two orders of magnitude, while a one order of magnitude reduction in HRG out of spiked blood was observed (Figure 15). Further, the total amount of protein present in the final elution from either plasma or whole blood was three to four orders of magnitude less

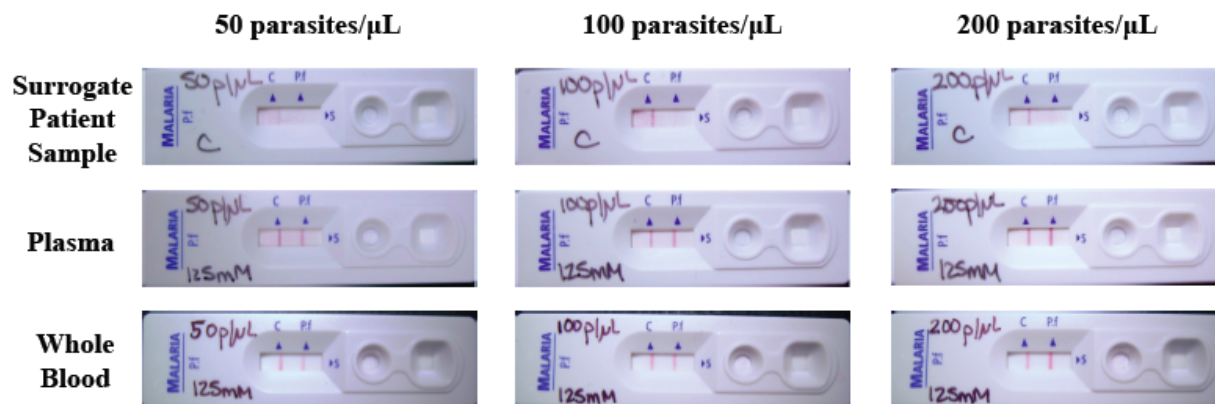


Figure 17. Improvement in the visual limit of detection of the SD BIOLINE malaria RDT after extraction from either plasma (middle) or whole blood (bottom) for 50 (left), 100 (middle) and 200 (right) parasites/ μL as compared to mimic patient samples (top).

than the original sample. Recovery of *pfHRP2* was three to four orders of magnitude greater than the amount of non-specific contaminants. Our cassette yielded a final sample one order of magnitude purer than the sample obtained using the spin kit (Figure 15). More strikingly, the spin kit appeared to co-purify HRG with *pfHRP2* when extracting from whole blood, with recoveries of HRG at 37%, versus 9% using the extraction cassette. Supporting Information Figure II.6 presents the recovery data in Figure 15 in terms of concentration of each protein recovered.

Effect of pfHRP2 Concentration on Malaria Rapid Diagnostic Test Performance

While the described cassette was designed for sample preparation, it is important to understand how this preparation can affect a given detection method. As *pfHRP2* is a biomarker of malarial infection, use of rapid lateral flow diagnostic tests as a readout was a logical choice for testing our sample preparation device. According to the World Health Organization, commercially manufactured immunochromatographic rapid diagnostic malaria tests (RDTs) should have a limit of detection of 200 parasites/ μL . Detection of parasite loads below this level have

major implications for the push toward malaria elimination. The extraction cassette functioned to both isolate *pfHRP*II in high yields, while simultaneously concentrating the biomarker 10-fold at clinically relevant concentrations of the parasite at and below the WHO limit of detection (Figure 16). In samples spiked to contain 12.5 parasites/ μ L, the yield of *pfHRP*II was $63.0 \pm 4.6\%$ from plasma and $40.7 \pm 6.1\%$ from blood. Further, the release of purified biomarker into a 10 μ L volume greatly enhanced the visual limit of detection of the commercially available SD BioLine malaria RDT (Figure SI II.7). Without processing through the cassette, no detectable signal was observed for any surrogate patient blood sample at or below 200 parasites/ μ L (Figure 17; top row). In contrast, for the extracted samples, positive test results were visualized reproducibly for samples with parasitemias as low as 25 parasites/ μ L (Figure 17; middle and bottom rows). The surrogate sample used for either direct application to the diagnostic test or for extraction was identical. Combination of this low-resource extraction cassette with readily available RDTs serves as a potential strategy for improving the diagnostic capabilities of these tests as well as extending into detection of clinically relevant parasitemias.

Conclusion

This chapter outlines the design and optimization of a self-contained sample preparation method for the selective isolation of *pfHRP*II from biological samples. This method extracts *pfHRP*II from human plasma and whole blood samples with $> 50\%$ percent yield. In addition, processing of the sample results in a thousand-fold improvement in *pfHRP*II purification. The device concentrates the biomarker, which was validated by enhanced the performance of a commercially available RDTs. This technology can be adapted for a wide range of sample platforms and biomarkers given the ease of modularity in the device components. By changing the surface chemistry on the magnetic bead, other proteins and biological biomarkers can be

targeted for extraction (eg. silica surface to capture nucleic acids, aptamer surface to capture small molecules, AgSO₃ surface to capture fatty acids). Incorporation of a detection method (colorimetric or fluorescent) within the cassette will allow for a complete diagnostic device. A potential candidate for in-line detection will be discussed in Chapter III.

Acknowledgements

“Reprinted with permission from K.M. Davis, J.D. Swartz, F.R. Haselton, and D.W. Wright, Low-Resource Method for Extracting the Malarial Biomarker Histidine-Rich Protein II To Enhance Diagnostic Test Performance. *Analytical Chemistry* 84 (2012) 6136-6142. Copyright 2012 American Chemical Society.”

Support for this work was provided by the Bill and Melinda Gates Foundation Grand Challenges in Global Health: Develop Technologies that Allow Assessment of Multiple Conditions and Pathogens at Point-of-Care. We thank Nick Adams and Catherine Majors for experimental design suggestions. We thank M.F. Richards for critical comments concerning this manuscript.

CHAPTER III

DEVELOPMENT OF A “SWITCH-ON” IRIDIUM (III) PROBE FOR THE DETECTION OF THE MALARIAL BIOMARKER HISTIDINE RICH PROTEIN II

Introduction

Biomarker detection via colorimetric and fluorescent signaling is important for a wide range of biochemical applications from molecular tracking to diagnostics.[23; 52] Low-molecular weight organic dyes are the most commonly used reagents in biological studies.[53],[54] Unfortunately, these organic fluorophores are subject to photobleaching, typically show small stokes shifts, and have broad, often overlapping, emission spectra. Enzymatic labels are widely used in immunoassays and western blots for quantification of a specific antigen.[55] Despite production of an amplified, highly detectable colorimetric signal, the enzymes and their substrates can be sensitive to light, environmental conditions and non-specific protein interferents. Further, many cofactors or co-reagents, such as hydrogen peroxide, used in these reactions do not have long shelf lives.

As an alternative, inorganic fluorescent probes, including quantum dots and metal-based



Figure 18. Examples of organic fluorophores (left) and quantum dots (right) in solution.

Images adapted from the Anzenbacher Research Group and Sigma Aldrich, respectively.

emissive complexes have been developed as diagnostic probes. Quantum dots are semiconducting nanocrystals that emit visible light based on their composition and size. Electron-hole pairs, known as excitons, formed during excitation recombine and release photons in narrow, long-lived symmetric energy bands.[56] Tuning the size and surface functionalization of quantum dots allows them to be used for multiplexed detection of biomolecules. However, surface defects can trap excitons and prevent light emission, which can lead to reduced quantum yield. Additionally, the “blinking” phenomena, common to quantum dots, can yield inconsistent measurements. Originally developed as nuclear magnetic resonance (NMR) and magnetic resonance imaging (MRI) reagents, metal lanthanide complexes have recently been employed for immunoassays and cellular imaging. These probes are marked by long lifetimes and large Stokes shifts, but the intricate synthetic pathways necessary for probe stability limit their use in biological settings.[57; 58]

An alternative class of signaling probes is based on emissive transition-metal complexes. The light emitting properties of cyclometalated Ir(III) have been studied in various applications, including organic light emitting diodes (OLEDs),[59; 60; 61] oxygen sensing,[62] catalysis[63] and cell staining.[64] Cyclometalated Ir (III) complexes are characterized by thermal and chemical stability, large Stokes shifts, long lifetimes, high quantum efficiency and photostability.[65] [66] Recently, Ma and coworkers demonstrated that cyclometalated Ir(III) complexes of the form $[\text{Ir}(\text{C}^{\wedge}\text{N})_2(\text{solv})_2]^+$, where $\text{C}^{\wedge}\text{N}$ represents cyclometalating ligands such as 2-phenylpyridine, selectively bind histidine and histidine containing peptides.[64; 67] When irradiated with long wave UV light, these complexes are non-emissive in their solvato state. In the presence of histidine, the associated solvent molecules are displaced as the histidine binds the metal center. Due to this ligand substitution, metal ligand charge transfer (MLCT) and ligand

centered transfer (LC) pathways are activated resulting in an intense blue-green phosphorescent signal is released as the triplet excited state electron relaxes to the ground singlet state. [60] [65] Previous research in these classes of compounds suggest that binding of the imidazole side chain to the iridium metal center serves to lower the HOMO energy to a similar energy as the occupied 5d orbitals of the iridium metal. This energy level coupling leads to strong $^3\text{MLCT}$, and thus strong emission characteristics from the Ir(III) complex.[68]

Enzyme linked immunosorbent assay (ELISA) is the most common methods for sensitive detection of biomarkers. Regulation of histidine rich proteins have been associated with several diseases including liver cirrhosis, cancer and thrombic disorders.[45] For malaria, *Plasmodium falciparum* Histidine Rich Protein II (*pfHRP*II) has long been validated as a major biomarker of malarial infection. The primary amino acid structure of this protein is marked by characteristic AHHAHHAAD motifs, which have been shown to bind free metal ions[9] as well as heme complexes.[69] Thus, a cyclometalated iridium (III) complex proves an attractive candidate as a probe for *pfHRP*II detection, due to its selective, stable and efficient emission properties. This chapter outlines the development of optimal assay conditions (e.g. buffer, temperature, pH) and assesses the detection limits of $[\text{Ir}(\text{ppy})_2(\text{H}_2\text{O})_2]^+$ (Ir1) toward BNT-II, a branched peptide mimic of *pfHRP*II.[70] The assay is then translated toward detection of recombinant HRP II (rcHRP II), bound to the surface of the 50 μm magnetic Ni(II)NTA agarose particles, introduced in Chapter II, in a solution based ELISA format. Incorporation of such a probe into the extraction cassette outlined in Chapter II would provide an excellent means to create an all-in-one detection device.

Materials

Dichlorotetrakis(2-(2-pyridinyl)phenyl)diiridium(III) (diIr1), silver trifluoromethanesulfonate (AgOTf), L-alanine (Ala), L-Histidine (His), L-Cystine (Cys), L-Tryptophan (Try), L-Valine (Val), L-Lysine (Lys), L-Isoleucine (Ile), L-Aspartic Acid (Asp), L-Phenylalanine (Phe), L-serine (Ser), bovine serum albumin (BSA), phosphate buffered saline (PBS) and 4-(2-hydroxyethyl)-1-piperazineethanesulfonic acid (HEPES) were purchased from Sigma-Aldrich. BNT-II was synthesized in the laboratory according to previously published methods.[70] Recombinant HRP-II (rcHRPII) was purchased from Immunology Consultants Laboratory Inc. Costar black and white polypropylene 96-well plates were purchased from Fisher Scientific. 50 μ m Ni(II)NTA magnetic agarose particles were purchased from Qiagen. Grenier black 96-well polystyrene plates for the Octet experiments were purchased from Fisher Scientific. The Ni(II)NTA biosensors were purchased from Pall ForteBio. All other reagents or buffers were purchased from either Sigma-Aldrich or Fisher Scientific.

Instrumentation

^1H NMR spectra of Ir1 in CDCl_3 were recorded using a Bruker AV-400 instrument at 400MHz. Electrospray ionization mass spectra (ESI-MS) of Ir1 in MeOH were measured with a Finnigan LCQ ion trap LC-MS with ESI ionization. UV-visible spectra were recorded with an Agilent 8453 UV-Visible spectrophotometer. Phosphorescence measurements were recorded using a BioTek Synergy H4 microplate reader. Cyclic voltammetry (CV) measurements of 200 μ M Ir1 in degassed acetonitrile were recorded on a CHI1030 potentiostat (5 V/s scan rate). Glassy carbon was used as the working electrode and platinum wire as the counter electrode. Ag/AgCl was used as the reference electrode with ferrocene as the internal standard. Real time kinetic data was collected using a ForteBio Octet Red96 Biolayer Interferometry instrument.

Experimental

Synthesis of Iridium (III) Complex Ir1

The complex $\text{Ir}(\text{ppy})_2(\text{H}_2\text{O})_2^+$, Ir1, was synthesized using a previously published method.[71] 50 μM diIr1 was dissolved in 5mL of methylene chloride before the addition of 100 μM solution of AgOTf in methanol. The slurry was stirred for 1hr at room temperature. Afterwards, the slurry was filtered through Celite, and the filtrate was evaporated until 1-2mL of filtrate remained. The remaining filtrate was lyophilized overnight yielding a bright yellow powder. ^1H NMR (400MHz, CDCl_3 , δ =ppm)--- 6.1047(H3A,doublet) 6.7061(H4A,triplet) 6.8631(H5A,triplet) 7.3657(H5B,doublet) 7.5236(H6A,doublet) 7.8926(H3B, H4B, overlapping resonances) 9.015(H6B,doublet); CV--- E_p (1.64V vs NHE) E_h (1.569V vs NHE)

Activity of Ir1 against Amino Acids and Biomolecules

Interactions between Ir1 and various amino acids, peptides and proteins were elucidated by observing changes in the phosphorescent emission upon reacting 50 μM Ir1 with these molecules. All reactions and titrations were done in black 96-well plates at a total volume of 100 μL . 2.5 μL of 2mM Ir1 in methanol was added to 100 μL solutions of a given molecule to bring the final concentration of Ir1 in each well to 50 μM .

Amino Acid Selectivity of Ir1

50 μM of Ir1 was incubated for 10 minutes with individual 100 μL solutions of the following amino acids: Ala, Asp, Cys, His, Ile, Lys, Ser, Try, and Val (n=3 for each amino acid). After the 10-minute incubation period, emission spectra of all amino acids were taken using the BioTek Synergy H4 plate reader (365ex/400-700em).

Optimization of In-Solution Assay Parameters

In order to optimize the reaction conditions for the assay, 50 μ M Ir1 was incubated with L-Histidine under various conditions (e.g. buffer type, pH, temperature, incubation time). Spectral scans (365ex/400-700em) and endpoint measurements (365ex/ 510em) were taken using the BioTek Synergy H4 plate reader.

Real-Time Kinetic Analysis of Ir1 with BNT-II

200 μ L of PBS was added to 8 wells in the first column of a black 96-well plate and inserted into a plastic sensor holder. 8 Ni(II)NTA biosensors were carefully transferred to the first column in the plastic holder such that the tips were suspended in the wells of buffer. This plastic holder was placed in the leftmost platform in the Octet Red96 instrument. 2mL of 0.5 μ M BNT-II was prepared in PBS and pipetted into column B of a new black 96-well plate. 200 μ L of PBS was added to each well in columns A and C of that plate. 500 μ L of a 10 μ M solution of Ir1 was prepared in PBS. This stock was serially diluted by half (7 dilutions in total). 200 μ L of each dilution was added to column D of the aforementioned black 96 well plate. This plate was then placed in the rightmost platform in the instrument. A basic kinetic experiment was set up with the following parameters: Equilibration (Custom), 60 seconds, Column A; Loading, 120 seconds, Column B; Baseline, 60 seconds, Column C; Association, 120 seconds, Column D; and Dissociation, 300 seconds, Column C. After the experiment was complete, the data was processed in the provided software to determine the K_D .

In-Solution Limit of Detection of 6-His, BNT-II and rcHRPII

50 μ M of Ir1 was titrated with varying nanomolar concentrations of BNT-II and rcHRPII in order to determine the limit of detection for each biomolecule. After a 10-minute incubation period, spectral scans (365ex/400-700em) and endpoint measurements (365ex/ 510em) were

taken using the BioTek Synergy H4 plate reader. Limit of detection was defined as the value of x when $y=3\sigma_{\text{blank}}$.

On-Particle Limit of Detection of BNT-II and rcHRPII

1 μM BNT-II and rcHRPII were serially diluted by half in Hepes Buffered Saline with Tween (HBST; 100mM HEPES, 137mM NaCl, pH 7.4, 0.25% Tween-20) and incubated with 10 μL of 50 μm Ni(II)NTA magnetic agarose particles for 15 minutes in a white 96 well plate ($n=6$; 100 μL for each concentration of BNT-II and rcHRPII). After the incubation period, the particles were washed 3 times with 250 μL of HBST using a 96 well plate magnetic rack. After washing, the particles were resuspended in 100 μL HBST and 2.5 μL of 2mM Ir1 was added to each well. The biomarker bound particles were incubated with Ir1 for 60 minutes before endpoint measurements (365ex/ 510em) were taken using the BioTek Synergy H4 plate reader. Limit of detection was defined as the value of x when $y=3\sigma_{\text{blank}}$. The statistical significance of the limit of detection of the on-bead assay to the in-solution assay was determined by an unpaired t-test using the Prism 5.0 graphing software.

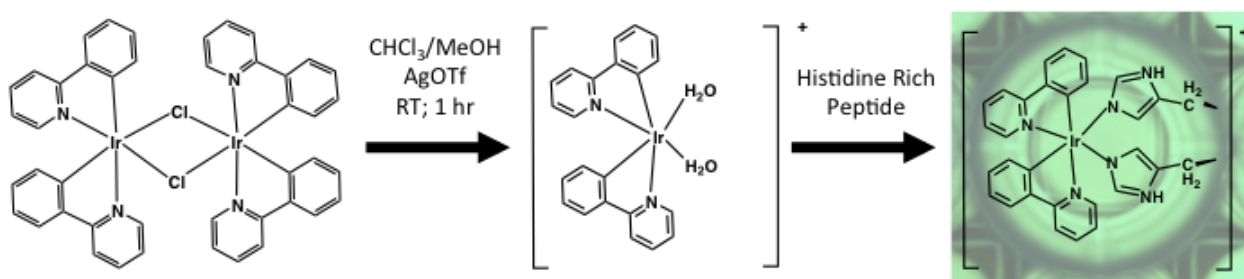


Figure 19. Synthesis of Ir1.

Results and Discussion

Physical and Spectroscopic Characteristics of Ir1

Synthesis and characterization of cyclometallated Ir(III) complexes have previously been studied for a wide range of applications. Following the synthetic route outlined in Figure 19,[71]

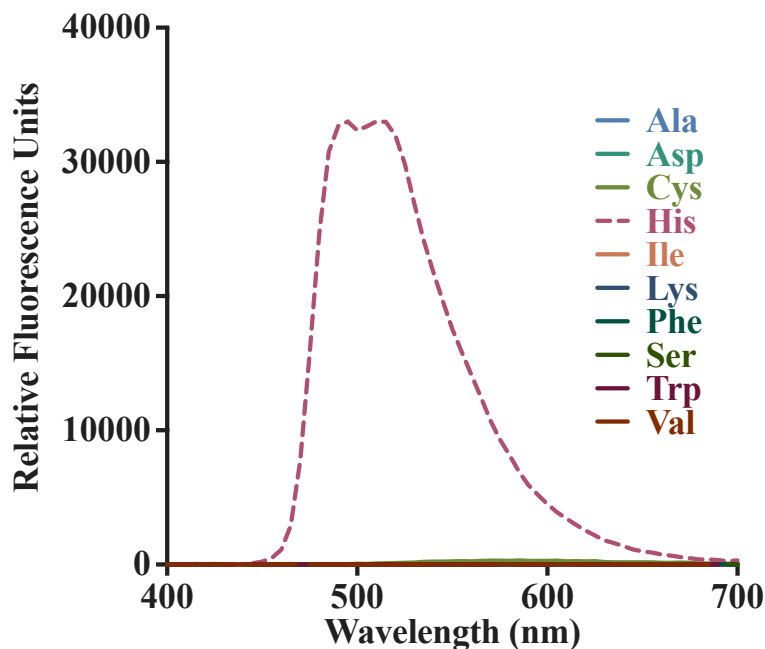


Figure 20. Fluorescent response of amino acids with Ir1.

a bright yellow powder was obtained and characterized to be $[\text{Ir}(\text{ppy})_2(\text{H}_2\text{O})_2]^+$ (Ir1). The solvento-complex was synthesized by first splitting the chloride bridge in the $[\text{Ir}(\text{ppy})_2(\text{Cl})_2]_2$ dimer by precipitation of the chloride in the form of an insoluble silver salt. Water molecules associate to the metal center to form a stable cationic complex. ^1H NMR,[71] ESI and CV[63] confirmed formation of Ir1 (Figure SI III.1 to III.3). High energy absorption bands were found in 200-300nm region of the UV-Visible spectrum of 200 μM Ir1 in methanol, while weaker bands in the 350-500nm region were assigned to metal-ligand charge transfer ($^1\text{MLCT}$ and $^3\text{MLCT}$) and intraligand transitions ($\pi\text{-}\pi^*$)[67] (Figure SI III.4). In solution, Ir1 exhibited no emissive properties upon excitation at 365nm.

Optimization of Ir1 Signal with L-Histidine

Given previously published work on the specificity of classes of Ir(III) probes toward histidine, the specificity of Ir1 toward L-Histidine (L-His) was first investigated. After reacting

Ir1 each of the 20 amino acids, only L-His coordination elicited a phosphorescent response at 510nm (Figure 20). This is consistent with previously published results.[67] The water molecules are displaced from the Ir(III) metal center by ligand substitution with L-His to create an emissive bioconjugate. The strong σ_{donor} nature of the C^N ligands pushes electron density to the metal center. Upon binding histidine and excitation with 365nm UV light, the singlet excited state (¹MLCT/¹LC) of the Ir(III) bioconjugate undergoes intersystem crossing to the triplet excited state (³MLCT) and “switches on” the phosphorescent signal at 510nm.

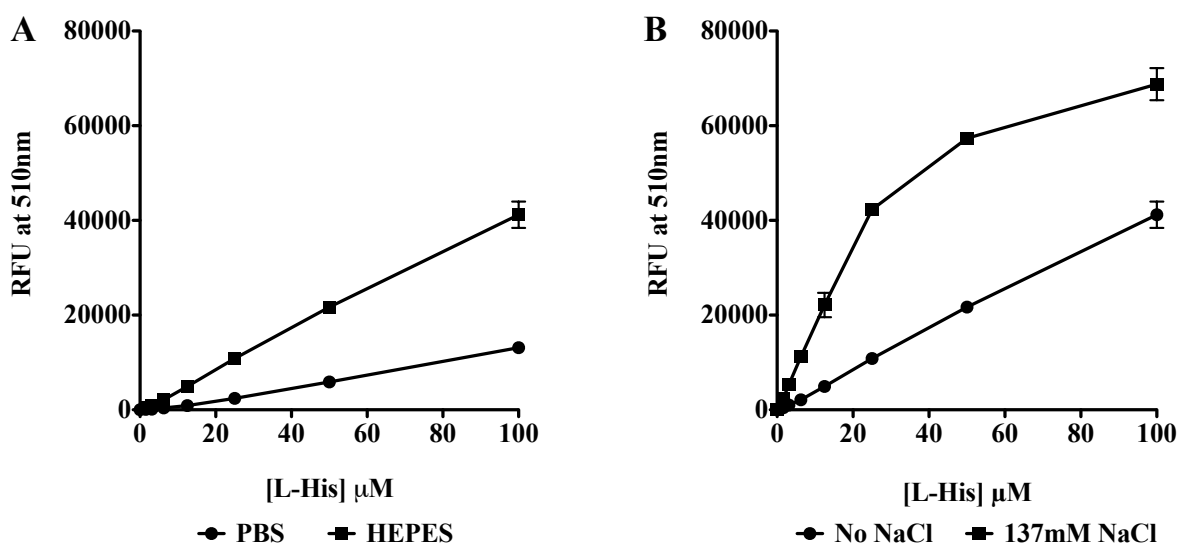


Figure 21. Effect of signal response of Ir1 with L-Histidine as a function of A) buffer type and B) ionic strength.

It is well known that the solution environment can change the photophysical properties of an emitting compound.[72] Additionally, coordinating buffers, such as phosphate buffer, can complex with metal ions, leading to insoluble precipitates. Although previously published methods used similar iridium probes in phosphate buffer, it was noted that Ir1, if stored in phosphate buffered saline (PBS), gradually precipitated as a yellow solid. The bidentate phosphate anion was likely displacing the water molecules and deactivating the Ir(III) complex

via the formation of an insoluble salt. By switching to HEPES, a non-coordinating zwitterionic buffer, the signal response of Ir1 to L-His increased 3-fold (Figure 21A). 137mM NaCl was added to the HEPES buffer (HBS) to closer mimic the salt concentration found in PBS solutions. This addition of salt increased the sensitivity of Ir1 toward L-His by a factor of four (Figure 21B).

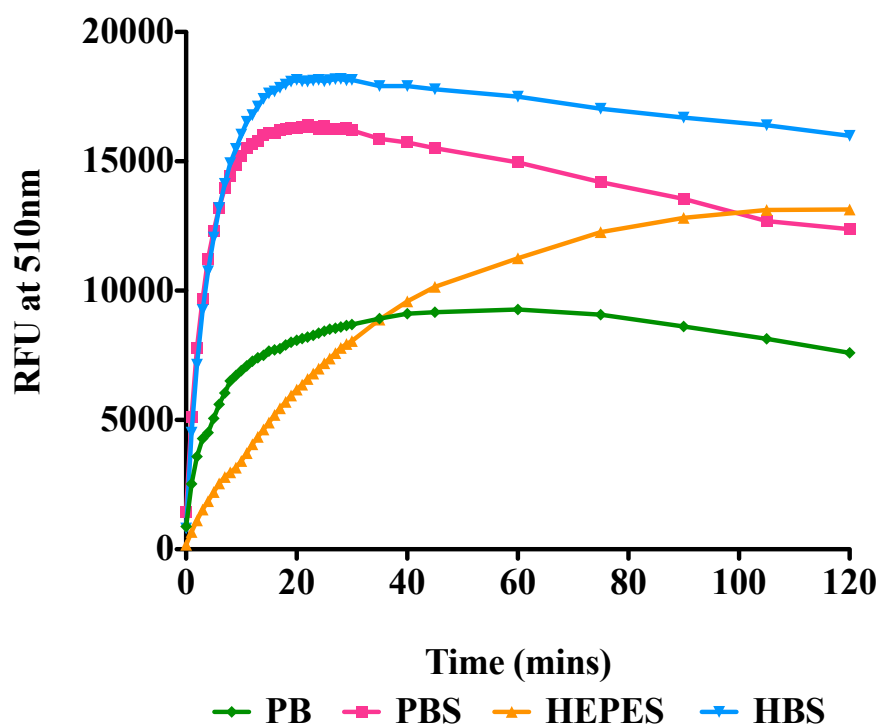


Figure 22. Reaction kinetics of Ir1 with L-histidine in various buffers.

To further explore this shift toward signal saturation of Ir1/L-His conjugate in the presence of salt, the reaction kinetics of 10 μ M L-His with Ir1 in phosphate buffer (PB), PBS, HEPES, and HBS was monitored at 510nm over the course of 2 hours (Figure 22). Both PBS and HBS showed a rapid increase in signal during the first 20 minutes of the reaction; however signal began to stabilize after 30 minutes. A similar trend was seen in PB, but the saturated signal was approximately half of that from PBS. The reaction coordinate in HEPES deviated

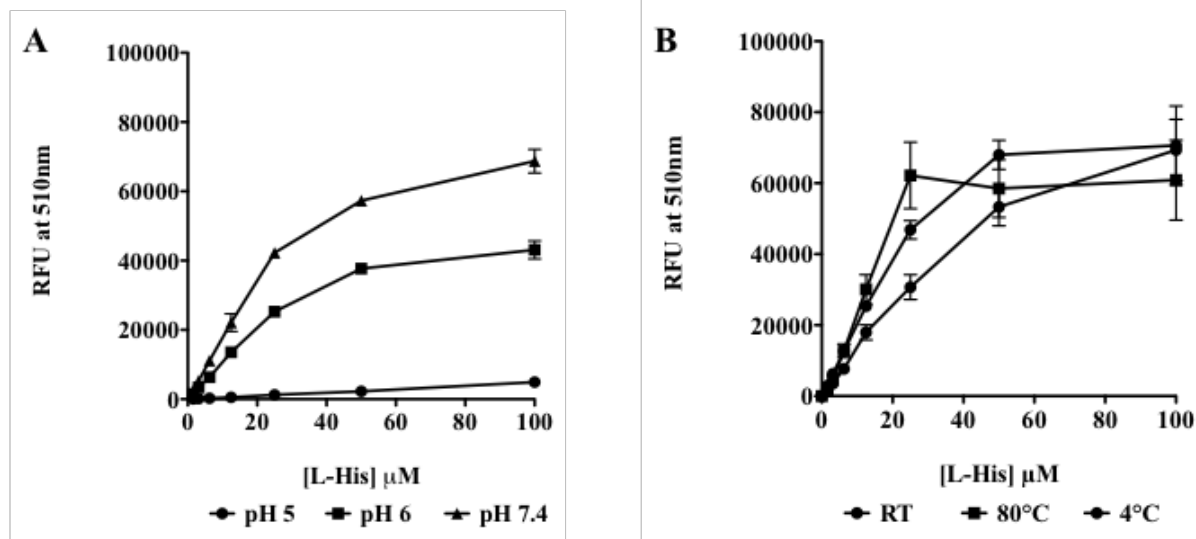


Figure 23. Effect of varying A) pH and B) temperature on the relative fluorescence signal of L-Histidine with Ir1

from the previous buffer systems in that the signal steadily increased over the course of 100 minutes. The effect of the coordinating phosphate anion on the loss of signal is apparent in the reaction of L-His with Ir1 in PB alone versus HEPES.

The presence of NaCl in both phosphate and HEPES buffers appeared to increase target complexation to Ir1 when compared with their salt deficient counterparts. This is likely due to a kinetic salt effect that the addition of NaCl to the buffer has the on the interaction between the probe and histidine.[73] In neutral buffer conditions, both Ir1 and L-Histidine are positively charged and thus are slightly repelled from each other in solution. This is evidenced in the slow generation of signal in PB and HEPES buffer systems. The addition of negatively charged chloride ions forms a charge screen around the reactants, as governed by the Debye-Huckel theory,[74] which in turn lowers the energy of the reactants and enhances the interaction between the two species as seen by the rapid increase in signal in the first 10 minutes in PBS and HBS.

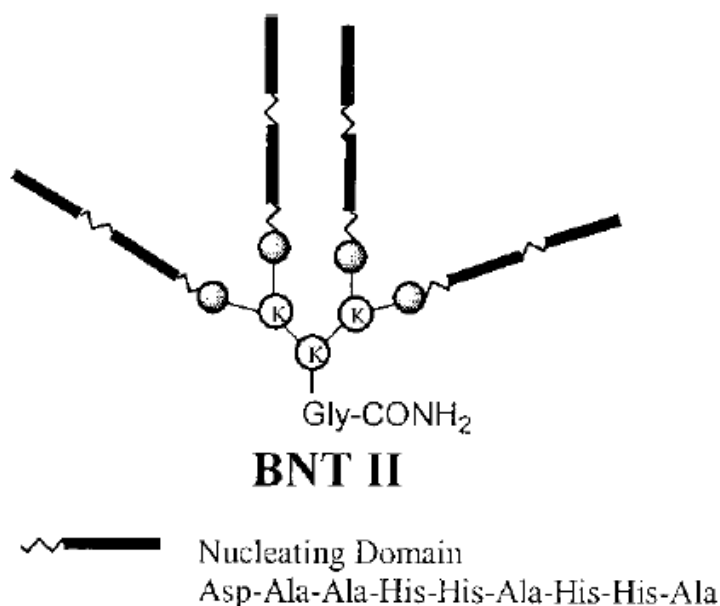


Figure 24. Structure of the *pf*HRPII peptide mimic, BNT-II.

Given these results, the amino acid specificity of Ir1 was then reanalyzed in HBS to confirm specificity to L-His alone was maintained.

The effect of pH and temperature on signal generation was also investigated (Figure 23A). Below pH 6, very little signal was observed. However, above pH 6, signal from the Ir1/L-His conjugate reached saturation around 50 μ M L-His. This correlation between intensity of signal and pH is related to the pKa of histidine. In order for histidine to bind to the Ir(III) metal center, the nitrogen on the imidazole ring must be deprotonated. It was observed that signal intensity correlated directly to this “working” concentration of deprotonated histidine (Figure SI III.5), calculated from the Henderson-Hasselbach equation. Below pH 6, there were fewer histidine molecules available for binding, which in turn reduced signal. Therefore, pH 7.4 was selected as the pH for HBS in the assay. When creating a diagnostic probe for possible use in a wide range of climates and conditions, operational temperature must be taken into account to ensure the diagnostic result will be consistent and independent of the environment. The signal

response at room temperature (RT) and 80°C was not statistically different over a range of histidine concentrations ($p < 0.05$), but at 4°C the signal response decreased two-fold (Figure 23B). At lower temperatures, the complexation of L-His is likely slower than at temperatures above 25°C, resulting in less signal. The optimized assay conditions for use of the Ir1 probe was standardized to be 100mM HEPES buffer, pH 7.4 with 137mM NaCl at temperatures at or above room temperature. With these assay conditions, the quantum yield of the Ir1/L-His conjugate agreed with previously published data (Figure SI III.6).[67]

Development of Optimized Ir1 Assay with a pfHRP II Mimic

With optimized reaction conditions against L-His, the probe was extended to detection of the malaria biomarker *pfHRP II*. Optimization of the assay with L-His as opposed to the whole protein allowed for fine-tuning of the basic buffer components prior to introducing the probe to a more complex spatial environment. Initial experiments utilized BNT-II, a branched peptide

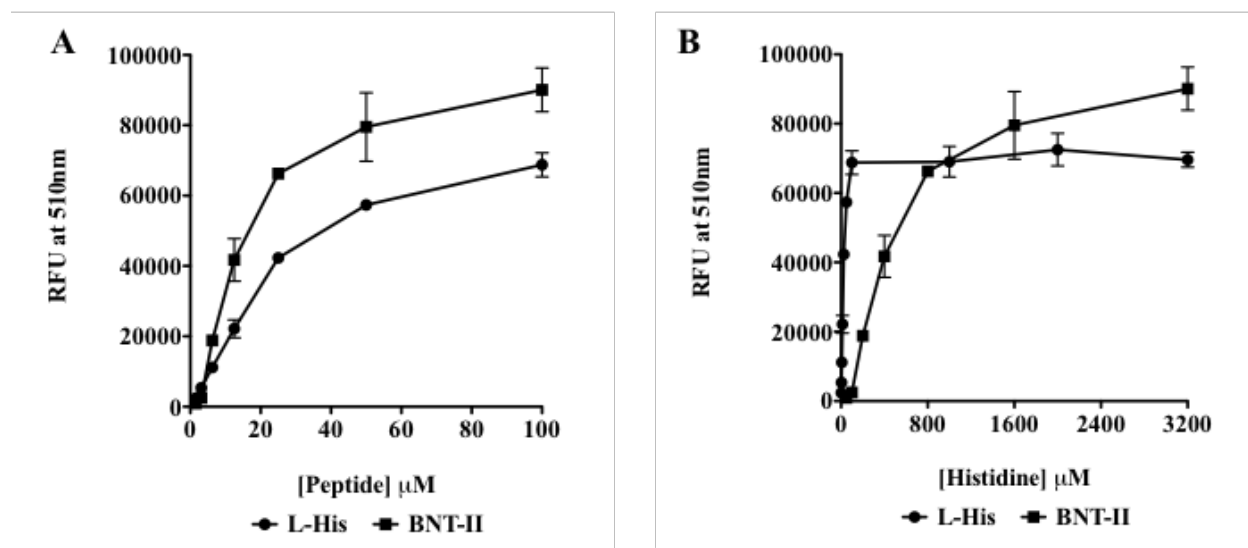


Figure 25. A) Relative fluorescence signal intensity (RFU) of micromolar concentrations and B) correlation between signal intensity and concentration of total histidine in L-Histidine versus BNT-II.

synthesized to mimic the primary repeating AHH/AHHAAD units characteristic of *p/HRP*II,[70] as the target (Figure 24). Using biolayer interferometry, the K_D of Ir1 binding to BNT-II was found to be 2.05 μ M. Comparing absolute signal generated on a molar basis, BNT-II yielded higher signal response than L-His upon incubation with Ir1 (Figure 25A). However, it was also noted that upon comparing signal response versus concentration of total histidine, the concentration of histidine necessary for signal saturation was reduced 16-fold from L-His (Figure 25B). Beyond 100 μ M L-His, the signal leveled off as Ir1 became the limiting reagent. If all of the imidazole side chains (32 per molecule) in BNT-II were available to bind Ir1, the two curves would overlap. Since this trend is not observed, stoichiometric signal generation is not achieved in the BNT-II system. This could be the result of either non-stoichiometric binding of Ir1 to BNT-II or quenching of the bound probes. While the assumption is Ir1 would preferentially bind adjacent histidines in the AHH motif, the probe could bind across the alanine in the HAH region, effectively reducing the signal by a factor of 2 (Figure SI III.7). Additionally, steric bulk around the lysine linker core of the peptide may prevent iridium from assuming the correct coordination geometry for binding.[70] Aside from non-stoichiometric binding of the probe to the target, photophysical quenching could be occurring in the system. Because of the structure of BNT-II, any bound Ir(III) probes would be in close proximity in chemical space and triplet-triplet annihilation could occur.[75] This annihilation effect would cancel two excited triplet states in the Ir(III) bioconjugate and relax the energy back to the ground state. While quantum yield of BNT-II with Ir1 was determined to be 8.3% (Figure SI III.6), the above analysis points to potential quenching within the system. Exploration of this effect would be important for future studies with this probe.

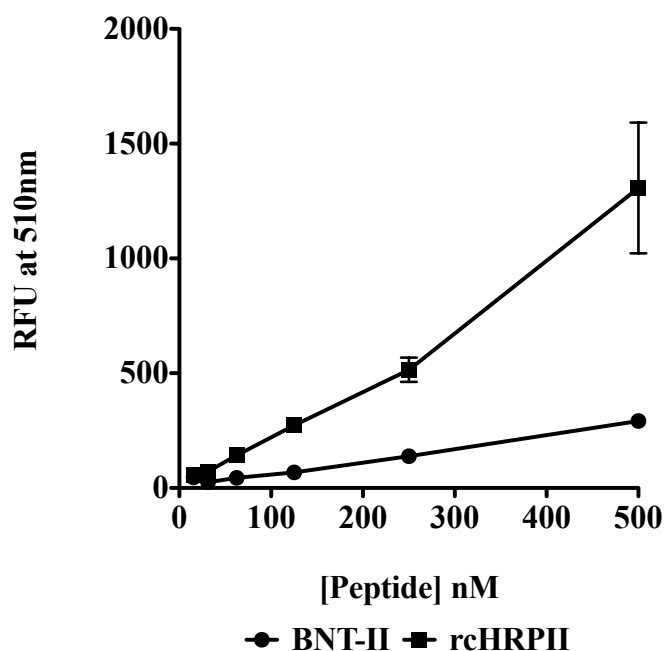


Figure 26. Titration of nanomolar concentrations of BNT-II and rc-HRP II with Ir1.

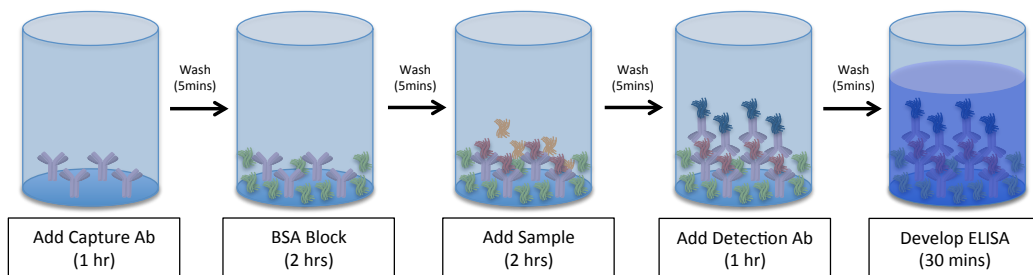
Using the optimized assay conditions, detection of the clinically relevant biomarker recombinant HRP II (rcHRP II) was assessed with the probe (Figure 26). When concentration of the protein was converted to concentration of total histidine, the titration curve was very similar to that of BNT-II, indicating that a similar loading/quenching effect is likely occurring in the rcHRP II/Ir1 system (Figure SI III.8). Regardless of these effects, the limit of detection in solution was determined to be 54.8nM and 12.8nM for BNT-II and rcHRP II, respectively.

Ir1 Assay for the On-Bead Detection of pfHRP II

With the advent of particle-based diagnostic tools, the ability to detect a target biomolecule on the surface of the particle becomes increasingly advantageous. Current methods for the detection of disease protein biomarkers rely heavily on antibody-based techniques such as enzyme linked immunosorbent assays (ELISAs).[76] ELISAs can achieve low picomolar limits of detection, but the entire assay takes 4-5 hours, relies on temperature and time-sensitive

reagents, and requires specialized equipment. Chapter II outlined the use of 50 μ m Ni(II)NTA magnetic agarose particles to bind *pfHRP*II through the imidazole side chains to facilitate the purification of the biomarker away from contaminating blood proteins and cellular debris.[77]

A) Standard Sandwich ELISA: Total Time 6+ hours



Ir1 On-Particle Assay: Total Time 1-2 hours

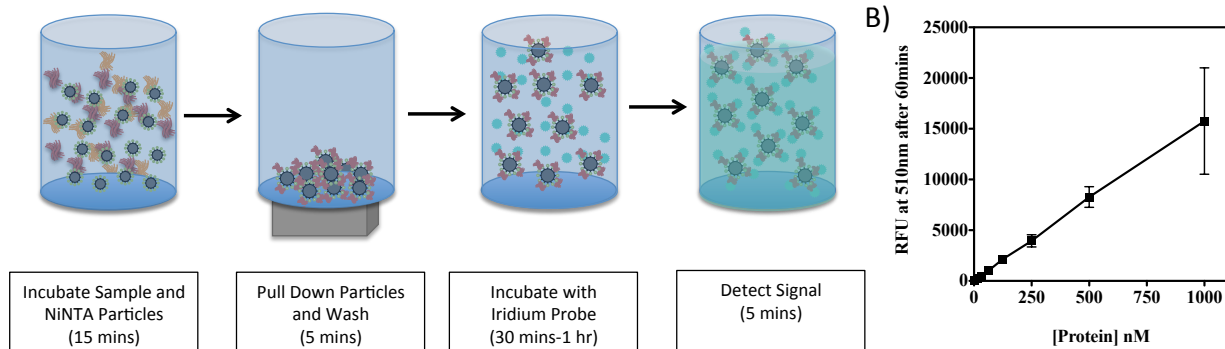


Figure 27. A) Comparison of a standard sandwich ELISA format for the detection of *pfHRP*II to the Ir1 on-particle assay. B) Titration of nanomolar concentrations of rCHRP^{II} bound to 50 μ m Ni(II)NTA magnetic agarose particles.

Many histidines would still be available for coordination to the iridium probe when the protein is bound to the surface of the particle. Labeling the bound histidine rich biomarker effectively creates a solution-based sandwich ELISA assay that is complete in 1.5 hours without needing several hours of processing time and environmentally sensitive antibody reagents (Figure 27A).

Use of magnetic particles for immobilization of target biomarker for processing is the key component for the reduction of assay time. In a traditional ELISA format, each reagent is incubated in the well plate in 1-2 hour steps to allow for passive diffusion and immobilization of the reagent to the walls of the well. The plate must be washed extensively in between these steps to remove any unbound reagents. A modified, on-particle ELISA assay has fewer overall steps

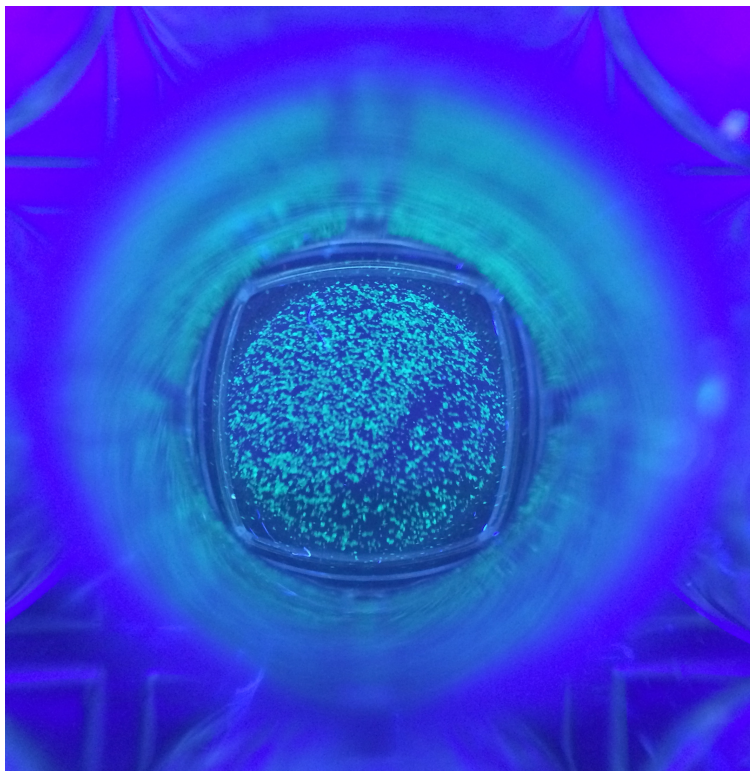


Figure 28. Phosphorescence of Ir1 bound to BNT-II on the surface of Ni(II)NTA magnetic particles, under broadband UV light.

than a traditional ELISA format, as the magnetic particles can be intermixed with the sample for more efficient binding, and the particles can be pulled down to the bottom of the reaction chamber for fast washing.

Qualitatively, the iridium probe was visualized on the surface of BNT-II bound particles under long-wave UV light (Figure 28). Optimal probe binding time was increased from 10

minutes, in the case of free protein in solution, to 45 minutes for bead bound target (Figure SI III.9). This is likely due to decreasing degrees of freedom of Ir1 to react with the protein upon binding to the surface of the particle. Using the previously optimized assay conditions, the limit of detection for rHRP_{II} on-particle was 14.5nM (0.972 μg/mL), with no signal generated from the blank (Figure 27B). The linear range of the assay spans three orders of magnitude in the nanomolar regime. Beyond this range, the signal becomes saturated, likely due to quenching effects and/or the probe being the limiting reagent at increasing concentrations of target. The limit of detection for rHRP_{II} in-solution and on-bead were statistically the same based on an unpaired t-test (p=0.731), thus validating both the binding capacity of the magnetic particle as well as the flexibility of the probe to detect the biomarker free in solution or immobilized on a surface.

Conclusion

This chapter describes the utility of a cyclometallated Ir(III) probe for the selective labeling and detection of the malarial biomarker *pf*HRP_{II} on the surface of a magnetic particle. By first optimizing several assay parameters, the Ir1 probe was applied to the particle platform outlined in Chapter II for the detection of low nanomolar amounts of rHRP_{II} bound to the surface of the particles. This type of on-particle assay mimics that of a traditional ELISA design performed in a 96-well plate, but the assay is complete in under two hours, due to the use of magnetic particles for biomarker immobilization, processing and detection. While this probe is promising for protein detection, the absolute sensitivity and specificity of this probe for *pf*HRP_{II} must be discussed. While the limit of detection fell within what is considered physiologically relevant concentrations of *pf*HRP_{II}, detection of increasingly low picomolar levels of *pf*HRP_{II} has become necessary for the identification of asymptomatic patients, who serve as transmission

reservoirs for the disease. Additionally, these patients must be identifiable for malaria elimination campaigns. This is seen in comparing the curve of the presented on-bead assay to a traditional ELISA for *pf*HRP II (Figure SI III.10). Ir1 is indeed specific for histidine but not necessarily for *pf*HRP II. The presence of additional histidine containing proteins, such as human serum albumin or histidine rich glycoprotein, could give false positives for the proposed assay design. This was evidenced by needing upwards of five washes to make signal from HRP II

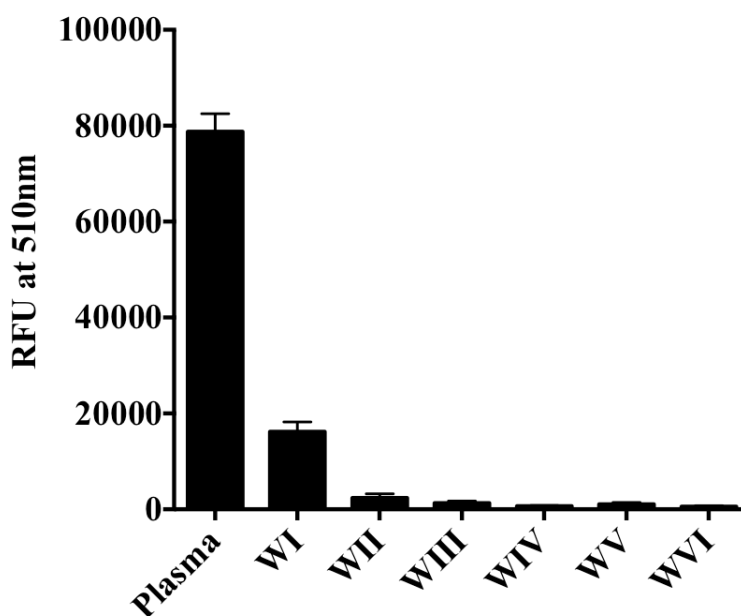


Figure 29. Background signal from Ir1 with plasma and Ni(II)NTA particles after sequential PBS washes.

distinguishable from the background signal generated from the surface of particles that were incubated with un-spiked diluted plasma so that signal (Figure 29). While the extraction device outlined in Chapter II is effective at reducing the total amount of protein in the final concentrated sample by three orders of magnitude, the presence of HRG and HSA in this extracted sample is still much higher (upper nM) than the final concentration of *pf*HRP II (mid to upper pM). Nonetheless, this probe can be modified to ensure high signal to noise values and reduce false

positives. To take advantage of Ir1's singular specificity to histidine, conjugation of a histidine rich peptide to a molecular recognition element (MRE), specific for the biomarker of interest, could potentially provide a solution to the issue of target specificity previously presented. By coupling this peptide to target specific MREs, a dual-functional probe can be created, which greatly mimics the enzyme-conjugated antibodies used in traditional ELISAs for detection. If this histidine rich peptide is branched, much like the structure of BNT-II, instead of single chain, like common hexa-histidine tags, there is the potential for greater signal enhancement per recognition event. Antibodies are the most common reagents for protein biomarker detection, and certainly a histidine rich peptide can be conjugated to an antibody for a new class of iridium probes (preliminary work outlined in Appendix B). However, antibodies could reduce the robustness of the system outlined in this chapter in conjunction with that of Chapter II. Aptamers, single strand DNA fragments, have recently gained attention, due to their stability, relative to antibodies, and specificity (K_D on the order of high pM to low nM) to a given target. Incorporating this technology into the design of a second generation iridium probe could prove powerful for creating new robust reagents for low-resource biomarker detection.

Acknowledgements

“Reprinted with permission from K.M. Davis, A.L. Bitting, and D.W. Wright, On-particle detection of *Plasmodium falciparum* histidine rich-protein II by a “switch-on” iridium (III) probe. *Analytical Biochemistry* 445(7) (2014). Copyright 2014 Elsevier.”

Support for this work was provided by the Bill and Melinda Gates Foundation Grand Challenges in Global Health: Develop Technologies That Allow Assessment of Multiple Conditions and Pathogens at Point-of-Care. K.M.D. was supported by an NSF Graduate Research Fellowship (2012095464). We would like to thank E. Gizzie for assistance with the

CV measurement of **Ir1**, A. Balinski for ESI, and M.F. Richards for critical comments in the preparation of the manuscript.

CHAPTER IV

DEVELOPMENT OF A RAPID IMMUNOMAGNETIC ELISA FOR DETECTION OF PLASMODIUM FALCIPARUM HISTIDINE RICH PROTEIN II

Introduction

Enzyme immunoassays (EIA) and enzyme linked immunoassays (ELISA) have been powerful research tools for sensitive and selective measurement of analytes. In the early 60's, the idea of using bulky enzymes as labels on antigens (Ag) or antibodies (Ab) was met with great skepticism. However, during the late 60's and early 70's, two groups (Perlmann and Engvall of Stockholm University and Schuurs and van Weemen of The Netherlands) simultaneously, but independently published quantitative assays for detection of IgG in rabbit serum and human chorionic gonadotropic in urine,

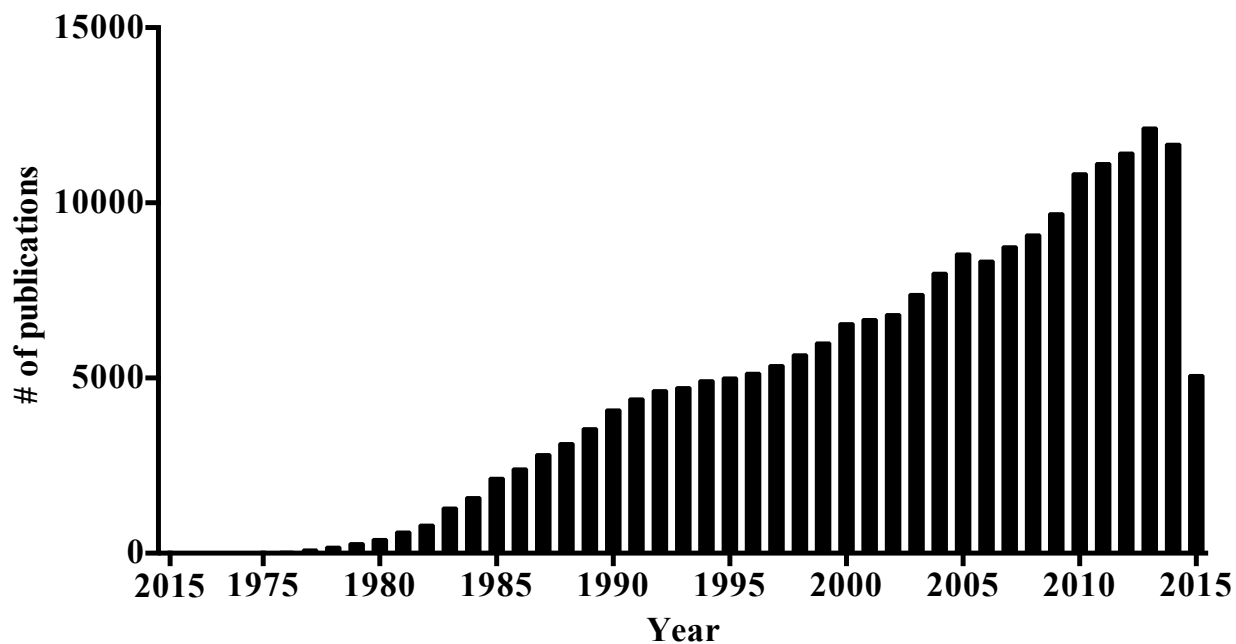


Figure 30. Number of papers published on ELISAs since 1971.

respectively.[78] Perlmann and Schuurs created one of the most critical diagnostic tools used worldwide. A quick Pubmed search reveals over 200,000 papers have been published on ELISA since the early 1970s. As seen in Figure 30, the number of papers published each year is on an upward trend, with over 5000 publications already published in the first half of 2015.

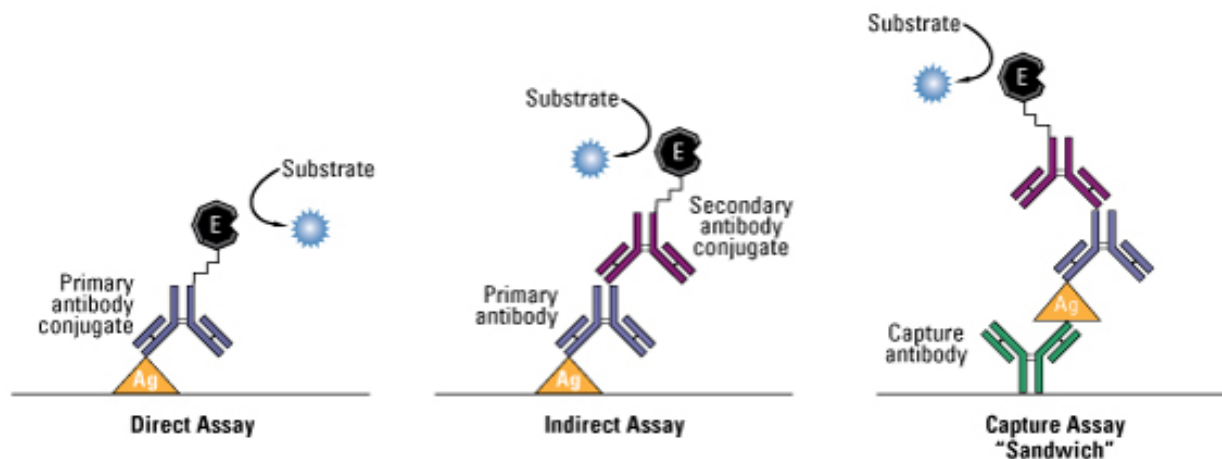


Figure 31. Diagram of common ELISA formats. Image adapted from Life Technologies.

The working principle of ELISA is founded on detection of analytes in a matrix by using enzymatically labeled reagents that are specific for the analyte of interest. In order to perform this assay, the analyte must be able to be immobilized on a surface prior to labeling for detection. This allows for washing away of any unwanted molecules during the assay. Various ELISA formats, as seen in Figure 31,[79] have been developed over the years, from direct (enzyme labeled Ab directly detects an Ag) to indirect (primary Ab binds the Ag, then an enzyme labeled secondary Ab labels the primary Ab); however, one of the most common forms of this assay is the sandwich-ELISA. A capture Ab is first laid down on a high-binding surface, such as a 96-well plate. After immobilization of the capture Ab, the surface of the plate is blocked to prevent any non-specific interactions. This blocking agent can be proteins (bovine serum albumin,

casein), nucleic acids (salmon sperm DNA), surfactants (Tween, SDS), or a combination of molecules. After blocking, the sample is added to the plate to allow the Ag to bind irreversibly the capture Ab. After extensive washing, the Ag must be labeled for detection. This can be done in a direct or indirect format, where the detection Ab, specific for the antigen, is labeled with an enzyme. Two common enzymatic labels are horseradish peroxidase and alkaline phosphatase. Finally, the appropriate substrate is added to the well to generate a concentration dependent response. This response can be colorimetric or fluorescent product, depending on the class of substrate chosen for the enzyme. While the average detection limit for ELISA is 100 pg mL^{-1} , this value can vary depending on the affinity of the Ag-Ab complexes used.[80] If an ELISA is to be made quantitative, an appropriate standard must be validated for the assay so that unknown samples can be quantitated against the standard curve. Additionally, optimizing the concentration of reagents and blocking conditions are necessary for a successful assay. As such, development of an ELISA for a given analyte can be a time consuming process.

Use of micro- and nanoparticles for sample preparation and analyte detection has become a hallmark of modern assay development.[81] Various techniques, such as flow cytometry, surface plasmon resonance, and piezoelectric balances among many others, have been utilized to measure binding events, as a particle detection event often correlates to the presence of an analyte molecule.[82; 83] Researchers have also begun to use particles as platforms on which to perform assays in solution, as opposed to using the particle as the detection moiety. Consequently, immunomagnetic ELISAs on the surface of magnetic particles have emerged as an alternative to a traditional 96-well plate ELISA.[84; 85] While the basic assay steps and reagents are the same, the entirety of the assay is performed on the surface of the particle, as diagramed in Figure 32. In a traditional ELISA, the working surface area on the 96-well plate is

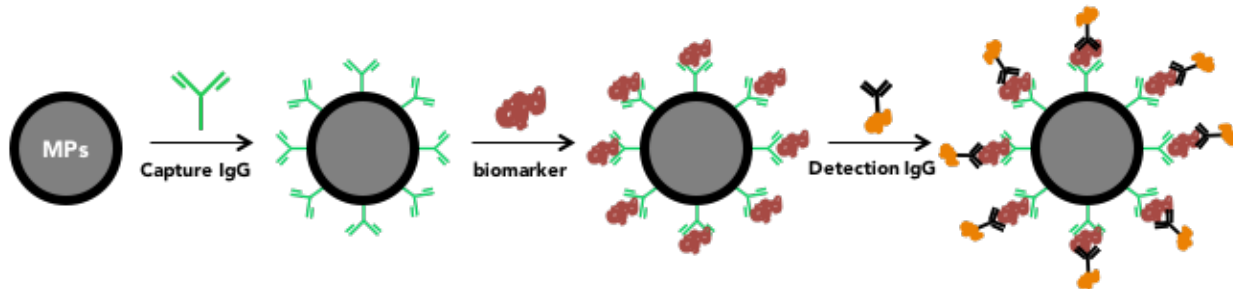


Figure 32. General diagram of an on-bead ELISA format.

around 1cm^2 , but in an on-bead ELISA (OBE), the working surface area can be an order of magnitude greater than using a 96-well plate. Aside from this increase surface area in which to bind analyte, magnetic particles can be manipulated to promote faster analyte-particle interactions. Traditional ELISAs rely on passive diffusion of the analyte to the surface of the well for binding to occur, whereas OBEs can actively mix the capture agent on the surface of the particle with the sample.

This chapter outlines the development of a rapid OBE for the detection of *pf*HRP II from a whole blood sample. As previously discussed, there are a wide range of diagnostic tools available for malaria diagnosis, depending on the level at which the test will be deployed. Many local and/or provincial hospitals are equipped to perform complex diagnostic assays, such as ELISAs and PCR. However, traditional ELISAs can take upwards of 5-6 hours to achieve a result. This in turn slows down the time to result for a patient, who may no longer be at the facility at the end of the assay. In this chapter, two OBE assays for *pf*HRP II are described. The first of which was designed using M(II)NTA particles (where M= Ni or Co). In this design, the assay mimicked the extraction method outlined in Chapter II; however, instead of eluting the protein off the surface of the particle, *pf*HRP II was detected on particle using an anti-*pf*HRP II Ab conjugated with horseradish peroxidase (α -HRP II-HRPx). While initial studies yielded a 500 parasite/ μL limit of detection, problems with blocking the surface of the highly charged

magnetic particles produced significant variability in signal generation and high background noise. To circumvent this challenge, a capture antibody against *pf*HRP-II was conjugated to the surface of a 1 μ m magnetic streptavidin particle, to more closely mimic a traditional ELISA format. Herein, the development and optimization of this assay, to ultimately achieve single parasite/ μ L limits of detection will be discussed in detail.

Materials

Ni(II)NTA Magnetic Agarose Beads (Cat # 36111) were purchased from Qiagen Inc. Co(II)NTA Magnetic His-tag Isolation Dynabeads were purchased from Life Technologies (Cat #10103D). Dynabeads® MyOne™ Streptavidin T1 magnetic particles were purchase from Life Technologies (Cat # 65601). Pooled Human A+ Whole Blood collected in CPD (Cat# HMWBCPD) was purchased from Bioreclamation LLC. Antibodies for the traditional 96-well plate *pf*HRP-II ELISA (Cat # ab9206 and ab30384) were purchased from Abcam Inc. IgG Anti-*pf*HRP-II antibodies for streptavidin particle surface modification as well as the detection antibody for the OBE assay were purchased from Abcam Inc. (Cat # ab9206 and ab30384, respectively). 3,3',5,5'-tetramethylbenzidine (TMB) One solution (Cat # G7431) was purchased from Promega Corporation. Micro Spin Desalting Columns (Cat # 89882) were purchased from Fisher Scientific Inc. EZ-link NHS-PEG₄-Biotin (Cat # 21329) was also purchased from Fisher Scientific Inc. The MagWell 96-well plate magnet was purchased from EdgeBio (Cat # 57624) All other reagents were purchased from Sigma Aldrich Inc. or Fisher Scientific Inc.

Experimental

M(II)NTA On-Bead ELISA General Protocol

All M(II)NTA OBE experiments were performed in plain, polystyrene 96 well plates. Generally, the 10 μ L of the magnetic M(II)NTA particles were added to 100 μ L of sample. After

30 minutes, the plate was placed on the MagWell 96-well plate magnet to pull the beads to the edge of the well. The beads were washed with buffer three times prior to addition of 100 μ L of detection Ab. The MagWell 96-well plate magnet was used in between each solution removal step to ensure minimal loss of beads. After 30 minutes of incubating the *p*fHRP_{II} bound beads with the detection reagent for a given time, the beads were again washed with buffer. Before removing the final wash, all samples were transferred to fresh wells before adding 100 μ L of the detection substrate, TMB. After incubating the beads with TMB for 20 minutes, the plate was again placed on the plate magnet to remove the colorimetric product. This TMB product was placed in a new 96 well plate prior to reading absorbance at 650nm (or 450nm when the reaction is stopped with 2M H₂SO₄). This general protocol was used for optimization of all the assay buffers, reagent concentrations, and other parameters that will be discussed in detail within this chapter.

α -HRP_{II} On-Bead ELISA General Protocol

All α -HRP_{II} OBE experiments were performed in plain, polystyrene 96 well plates. Generally, the 10 μ L of the magnetic α -HRP_{II} particles were added to 100 μ L of sample. α -HRP_{II}-HRP_x was added to the sample with beads as well. After a given incubation time, the plate was placed on the MagWell 96-well plate magnet to pull the beads to the edge of the well. The beads were washed with buffer three times. Before removing the final wash, all samples were transferred to fresh wells before adding 100 μ L of the detection substrate, TMB. After incubating the beads with TMB, the plate was again placed on the plate magnet to remove the colorimetric product. This TMB product was placed in a new 96 well plate prior to reading absorbance at 650nm (or 450nm when the reaction is stopped with 2M H₂SO₄). This general

protocol was used for optimization of all the assay buffers, reagent concentrations, and other parameters that will be discussed in detail within this chapter.

Surface Functionalization of Streptavidin Dynabead Particles with α -HRP II-Ab

Two aliquots (at 15 μ L for each aliquot) of 5.1mg/mL anti-HRP II IgG (abcam Cat#ab9203) were diluted in 300 μ L of 1x PBS. To this 300 μ L solution of antibody, 2.6 μ L of 20mM EZ-link NHS-PEG₄-Biotin (Fisher Scientific Cat#21329) was added and incubated on a rotisserie for 30 minutes. During this biotinylation time, 500 μ L of streptavidin Dynabeads were removed from the stock bottle and washed 2x with 1x PBS using an Eppendorf magnetic rack. The particles were re-suspended in 1x PBS and reserved for later. Additionally, two 0.5 mL 7MWCO desalting columns were prepared to remove excess NHS-PEG₄-Biotin from the Ab. To do so, the storage buffer was removed (1 min, 1500 rcf) and the column was washed with 2x with 300 μ L 1x PBS (1 min, 1500 rcf). 300 μ L of 1x PBS was added to the column after two washes and reserved until the antibody was finished biotinylating. After 30 minutes, the biotinylated antibody solution was desalted using the washed desalting columns by adding 150 μ L to each column and spinning for 2 minutes at 1500 rcf. The two fractions were combined, and 300 μ L of 1x PBS was added to make a total volume of 600 μ L. The buffer was removed from the washed beads. The 600 μ L antibody solution was added to the beads and incubated for 30 minutes on a rotisserie. (Note: 5 μ L of the antibody solution was reserved to compare the concentration of IgG in the supernatant to this original antibody solution after conjugation.) After the 30 minute incubation, the supernatant was removed from the beads. The concentration of IgG remaining was checked using the Take3 plate application on the BioTek SynergyH4 plate reader. (Note: This was compared to the concentration of IgG prior to conjugation to ensure the reaction occurred.) The conjugated beads were washed 2x with 1x

PBS prior to re-suspending in 600 μ L of 1x PBS. 20 μ L of 1 mg/mL D-biotin solution was added and incubated with the beads for 30 minutes to quench the unreacted streptavidin sites on the beads. Finally, the beads were washed 2x with 1x PBS and re-suspended in original volume (500 μ L) of 1x PBS with 0.01% Tween-20.

Spiked Whole Blood Sample Preparation

Human A+ Whole Blood collected in CPD was mixed 1:1 (v:v) with 2X lysis buffer (100mM sodium phosphate, 250mM imidazole, 600mM NaCl, 2% Triton X-100, pH 8.0) and allowed to lyse until the blood became translucent. The lysed blood was filtered through a plastic syringe that was packed with glass wool at the bottom of the syringe. (Note: The size syringe was selected based on the volume of blood needed for each experiment. Blood was lysed freshly for each experiment.) *P. falciparum* culture (at 37,475 parasites/ μ L) was added to appropriate volumes of filtered, lysed blood per experiment.

Results and Discussion

On-Bead ELISA using Ni(II)NTA Magnetic Particles as the Capture Reagent

Since the use of Ni(II)NTA magnetic particles proved to be a very efficient method for capturing *pf*HRP II from a lysed blood sample, incorporating a detection element into this extraction platform was a natural next step. In Chapter III, a cyclometalated iridium probe was synthesized and used to detect *pf*HRP II bound to the Ni(II)NTA agarose particles. Good specificity was obtained when buffer was the sample matrix; however, a more complex matrix, such as plasma, yielded high background noise, as the iridium probe was likely binding to more physiologically abundant histidine containing proteins on the surface of the particles. While additional work is needed for the dual-metal, capture and detection system for *pf*HRP II, a parallel track emerged where the M(II)NTA moiety on the surface of the magnetic particles still

served as the capture agent, but an enzyme conjugated Ab against *pf*HRP_{II} would serve as the detection reagent. The aim of this design was to achieve greater specificity and sensitivity by introducing a detection reagent with higher antigen specificity (Ab > Ni(II)NTA/Ir1 for *pf*HRP_{II}).

A method was first developed using the Ni(II)NTA agarose particles discussed in Chapters II and III. In taking from traditional ELISA protocols, after the capture reagent is immobilized on the assay surface, the rest of the sites must be blocked. Considering the Ni(II)NTA was already on the surface of the particles, the next logical step was to block the

	[HRP_{II} Detection Antibody] µg/mL			
% BSA	0	0.125	0.25	0.5
0.5	0.18	0.404	0.654	1.21
1	0.183	0.334	0.481	
1.5	0.178	0.255	0.409	
3	0.186	0.263	0.356	

Table 2. Checkerboard on-bead ELISA assay to determine effect of BSA and detection antibody concentration on signal at 650nm.

particles, prior to adding the detection Ab. However, this turned out to be not as simple as a 2 hour blocking step. Every attempt at blocking the particles (2 hours to overnight) still led to the same result. A negative sample (0 parasites/µL) and a positive sample (200 parasites/µL) yielded the same colorimetric response after addition of the TMB substrate. The assumption was that the porosity of the agarose coating rendered the particles almost impossible to fully block, which led to non-specific binding of the α-HRP_{II}-HRP_x to the particles. This is also observed on a traditional ELISA as well, if the plates are not fully blocked.

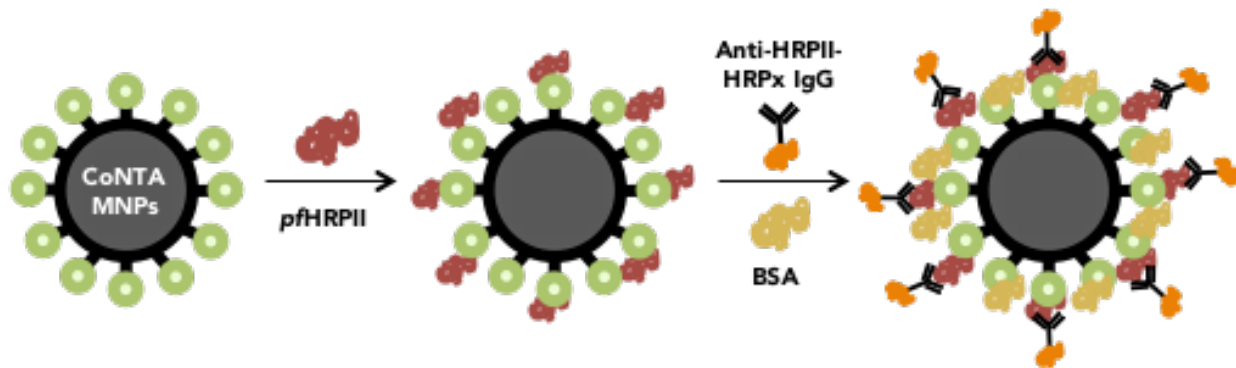


Figure 33. Diagram of Co(II)NTA on-bead ELISA.

Reducing Non-Specific Signal for On-Bead ELISA with Co(II)NTA Magnetic Particles

Instead of continuing to optimize the assay with the Ni(II)NTA agarose particles, focus was shifted to a smaller 1 μm Co(II)NTA magnetic particle (Figure 33). The exact composition of these particles is proprietary, but they are likely comprised of an iron oxide core, a polystyrene coating, and a polyurethane shell. As a first pass, a batch of Co(II)NTA beads were blocked overnight in 5% BSA before testing with a negative and positive sample. The positive sample yielded high signal over background (data not shown), so a checkerboard assay was designed to determine how presence of BSA in the antibody buffer affects non-specific interactions of α -HRP II-HRPx with the particles when *pf*HRP II is not present in the buffer (Table 2). When developing an ELISA method, the amount of BSA in the antibody buffer is tuned to reduce non-specific binding and maximize signal to noise. It was found that 3% BSA served to reduce non-specific background noise across concentrations of α -HRP II-HRPx from 0-0.5 $\mu\text{g}/\text{mL}$. Next, a second checkerboard assay was designed to determine an appropriate concentration of α -HRP II-HRPx over a range of concentrations of *pf*HRP II. Generally, as the concentration of α -HRP II-HRPx increased, the sensitivity of the assay was improved (Table 3). However, the background signal increased as well. It was also noted during these experiments that there was a great deal of variation in batches of blocked Co(II)NTA beads, where the most common issue was such a

high background signal that samples containing *pf*HRP II were indistinguishable from a blank sample. A search of the literature revealed that the particles did not need to be blocked, as long as a high concentration of BSA (3-5%) was in the antibody buffer during the α -HRP II-HRPx incubation step.[86] This would then combine the blocking and Ab incubation steps, where traditionally they are performed sequentially.

	[HRP II] pM				
[α -HRP II-HRPx] μ g/mL	0	1	10	100	1000
0	0.177	0.181	0.181	0.169	0.165
0.125	0.162	0.215	0.243	0.296	0.995
0.25	0.279	0.249	0.288	0.374	1.55
0.5	0.334	0.358	0.346	0.516	2.272

Table 3. On-bead ELISA signal, at 650nm, over a range of HRP II concentrations with increasing detection antibody concentration.

This change in protocol worked to improve batch to batch consistency when the *pf*HRP II was spiked into buffer. Upon switching to lysed whole blood, all the samples, blank and spiked, turned over the substrate, suggesting that non-specific interactions were now a result of increasing the complexity of the initial sample. The 96-well ELISA developed for *pf*HRP II, as outlined in Chapter II, used phosphate buffered saline with Tween-20 (PBST) for all of the assay steps. As such, this was the buffer system used up until this point for OBE development. When searching the literature for approaches to non-specific background reduction, increasing salt in the buffer system seemed to be a common solution. Common recipes for PBST includes 137mM NaCl, 2.7mM KCl, and ~12mM phosphate. Reported literature using magnetic particles in complex matrices suggest using 50mM phosphate and 300mM NaCl to screen the particles from

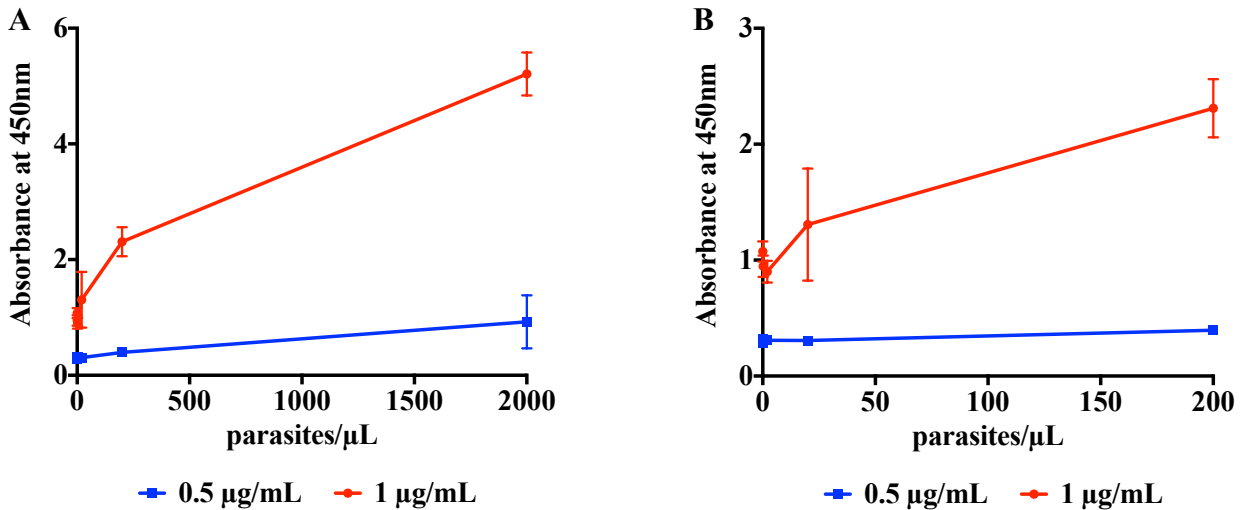


Figure 34. On-bead ELISA response to increasing detection antibody concentrations, where B) focuses on the 0-200 parasites/μL range represented in A).

non-specific protein interactions.[87] Fortunately, this was the buffer composition used for the extraction cassette in Chapter II. In switching from common PBST to this modified phosphate buffer, non-specific interactions were significantly improved and assay to assay variability was greatly reduced (data not shown).

Optimization of the Co(II)NTA On-Bead ELISA

After resolving the non-specific binding issues, it was necessary to optimize the assay for increased sensitivity. A comparison of the improved assay with a sample in buffer versus in lysed whole blood revealed a loss in sensitivity as the sample matrix complexity increased. The first step was to revisit α -HRP_{II}-HRP_x concentration. The plate ELISA protocol for *pf*HRP_{II} outlined in Chapter II used 0.5μg/mL of the detection Ab. Increasing this concentration did indeed increase the signal response at 200 parasites/μL, but an increase in background was also observed. A full OBE over a range of parasite/μL concentrations, using either 0.5μg/mL or 1μg/mL α -HRP_{II}-HRP_x, further demonstrates the effect of adding more detection antibody on

the assay (Figure 34). Again, the sensitivity increased, but the background noise also increased. Linearity of the assay was lost upon increasing the detection antibody concentration, as this concentration of antibody likely promoted signal saturation at higher parasite concentrations. If the concentration of BSA in the detection Ab buffer is increased to 5%, background signal is reduced, but there is a loss in sensitivity (Figure 35). Thus, there seemed to be a trade-off between maximizing overall signal and minimizing background.

After optimizing the detection Ab buffer to contain 5% BSA, the effect of incubation time on signal was explored. The particles incubate with the lysed blood sample for 10 minutes, as decided in Chapter II. The above described experiments then incubated the α -HRP II-HRPx with the *p*/HRP II bound particles for 30 minutes. If this incubation time is reduced to 10 minutes with a α -HRP II-HRPx concentration of 1 μ g/mL, signal loss can be observed at both 200 and 2000 parasites/ μ L (Figure 36). However, if the antibody concentration is increased to 5 μ g/mL with a 10 minute incubation time, signal is recovered. Notably, this increase in antibody does not

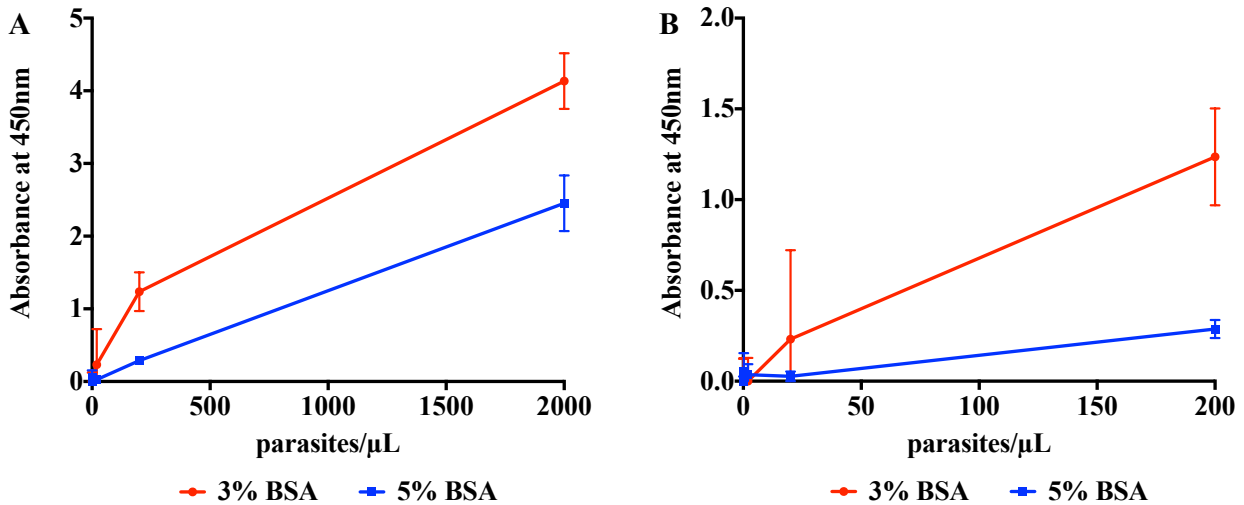


Figure 35. Effect of increasing BSA in blocking buffer on signal response, where B) focuses on the 0-200 parasites/ μ L range represented in A).

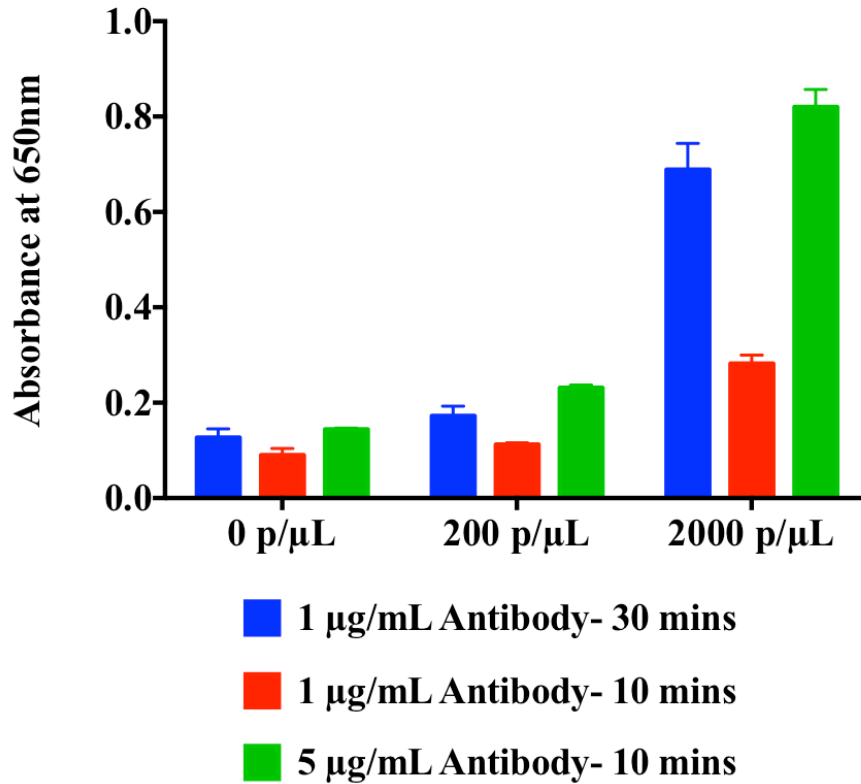


Figure 36. Effect of decreased time and increased detection antibody on on-bead ELISA signal

significantly affect the background noise. With these optimized assay conditions, the limit of detection was calculated as 500 parasites/μL. While these experiments proved the concept that ELISA could be performed on the surface of a magnetic particle, the limit of detection is no better than commercial RDTs. In order to try and improve the limit of detection without increasing assay time or background signal, the OBE platform was reworked in an all-in-one format.

All-in-One On-Bead ELISA with α-HRP II Protein-G Magnetic Particles

As the assay for Co(II)NTA OBE was developed, issues started to arise with the BSA powder used as a blocking agent in the detection Ab buffer. Many commercially available BSA

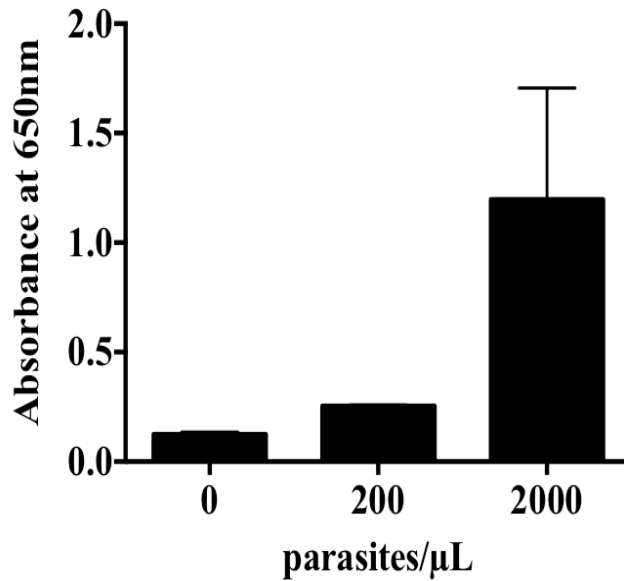


Figure 37. All in one on-bead ELISA proof of concept with Protein-G magnetic particles.

powders have bovine IgG present, which can cross-react with secondary IgG in a given immunoassay.[88] Additionally, the powder can foul over time. When it is used for ELISA, this can result in all of the assay wells turning a “non-specific blue” color because the detection antibody crosslinking with these bovine IgGs. While this could be resolved by simply ordering a fresh lot of BSA or switching to a different blocking agent, this was very concerning considering the assay was being developed for use in developing countries. Reduction of any failure modes in the assay is critical to ensure the test will work every time. Discussions with a collaborator as well as consulting an ELISA kit lead to the development of an all-in-one ELISA. The hypothesis of an all-in-one ELISA is that blood proteins will block the particle surface while allowing specific interactions between the antibody on the particle, the antigen in the blood sample, and the detection antibody to occur. To test this hypothesis, 10 μL of the Co(II)NTA beads were incubated in a lysed blood sample (0, 200, and 2000 parasites/ μL) with 5 $\mu\text{g}/\text{mL}$ of $\alpha\text{-HRP}\text{II-HRPx}$. After a 10 minute incubation in the blood, the beads were washed three times and incubated with TMB for 10 minutes. Unfortunately, no statistical significance between a 0

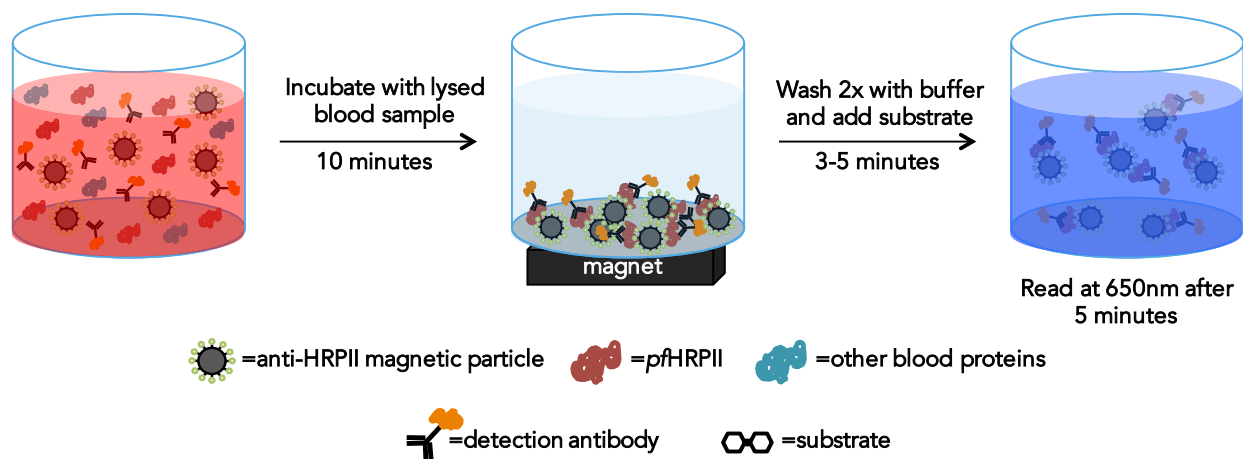


Figure 38. General diagram of the all-in-one on-bead ELISA.

parasite/ μ L sample and a 200 parasite/ μ L sample was observed. While it was promising that adding the Co(II)NTA particles to a lysed blood sample containing *p f*HRP II and α -HRP II-HRPx did not result in non-specific turnover of the substrate, this system was no longer explored. Instead, magnetic particles with antibodies against *p f*HRP II were synthesized. In order to quickly assess whether using an α -HRP II magnetic particle would enhance the sensitivity of the assay, α -HRP II IgG antibodies were immobilized on Protein-G Dynabeads. Protein-G solid phase chemistry is normally used for immunoprecipitation protocols, to isolate IgG from a complex matrix. α -HRP II IgG was incubated with the Protein G beads (according to manufacturer protocols) to create a magnetic capture particle with presumably higher affinity for *p f*HRP II than the M(II)NTA particles (The K_D of α -HRP II-IgG is ~ 1 pM, whereas the K_D for M(II)NTA is low μ M). Using the same all-in-one method described for the Co(II)NTA particles, signal at 200 and 2000 parasites/ μ L was significantly different from 0 parasites/ μ L, and the background noise was lower than seen with any aforementioned protocol (Figure 37). A full titration of *p f*HRP II using this all-in-one method yielded a limit of detection of 40 parasites/ μ L. A general outline of the all-in-one OBE method can be seen in Figure 38.

Optimization of the All-in-One On-Bead ELISA for pfHRP II

While the Protein-G particles worked well to prove the concept of a functional all-in-one ELISA for *pfHRP II* detection, streptavidin Dynabeads were modified with biotinylated α -HRP II IgG to eliminate the possibility of IgG leaching from the surface of the Protein-G particles. The loading capacity of the streptavidin particles was also higher than the Protein-G particles. As seen in Figure 39, the limit of detection was determined to be 0.5 parasites/ μ L using the similar parameters as the Protein-G particles (10 minute incubation in lysed blood, 5 μ g/mL α -HRP II-HRPx, 5 μ L α -HRP II Streptavidin Particles, 10 minute TMB incubation). It was also noted that converting the TMB substrate from blue (650nm) to the yellow product (450nm) afforded greater sensitivity (2.0 parasites/ μ L versus 0.5 parasites/ μ L limit of detection, respectively). However, it was still necessary to understand each variable in the system to ensure OBE method would work at its fullest capacity.

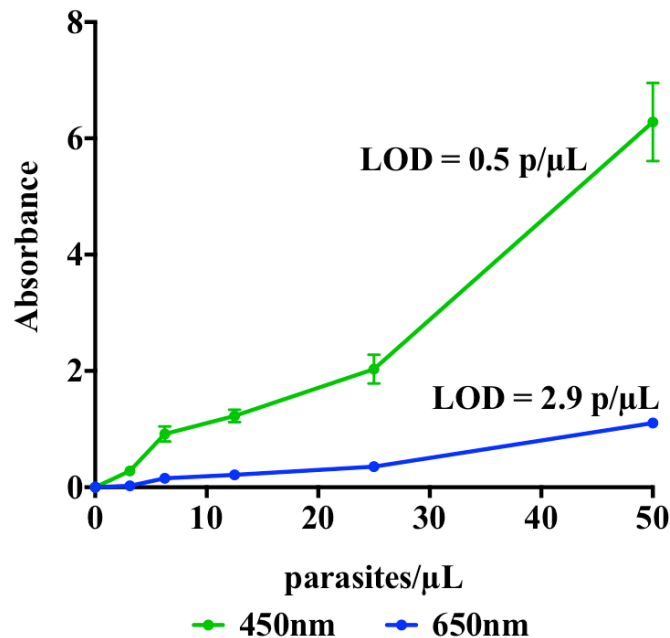


Figure 39. Limit of detection of *pfHRP II* using the proof of concept on-bead ELISA.

First, the effect of incubation time on concentration of *pf*HRP2 remaining in a blood sample was determined. After 1 minute, virtually all of the *pf*HRP2 was removed from the sample (Figure 40- blue line). This is vastly different from the 30 minutes needed to remove most of the protein from the blood sample, using Ni(II)NTA particles (Figure 40- red line). Because such a difference in signal response was seen when the α -HRP2-HRPx was increased from 1 μ g/mL to 5 μ g/mL in the Co(II)NTA system, the effect of concentration of α -HRP2-HRPx on signal was determined. As the concentration of α -HRP2-HRPx is increased, the background signal from a 0 parasite/ μ L sample plateaus at 0.3AU (Figure 41A- blue line). In the presence of 50 parasites/ μ L, maximum signal is achieved at 1 μ g/mL of Ab (Figure 41A- red line). This is likely explained by the Hook-Effect.[89] Up to 1 μ g/mL, interactions between the α -HRP2 IgG

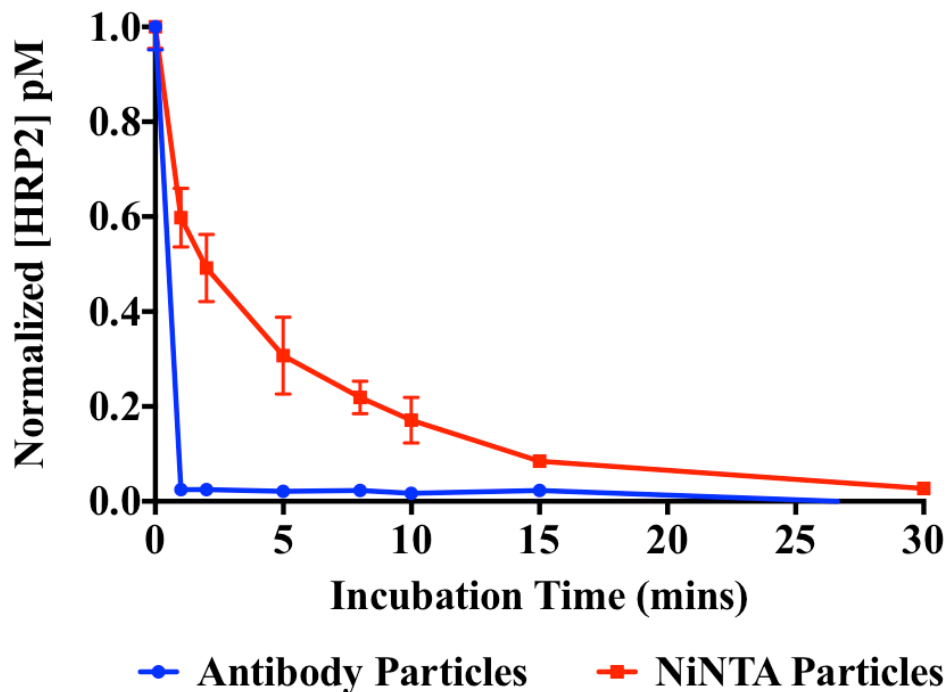


Figure 40. Comparison of *pf*HRP2 depletion, using NiNTA particles or antibody particles, from a blood sample as a function of time.

on the magnetic particle surface, the *pf*HRP_{II} in the lysed blood, and the α -HRP_{II}-HRP_x are favorable. Above 1 $\mu\text{g}/\text{mL}$, there is such a high excess of α -HRP_{II}-HRP_x in solution that the *pf*HRP_{II} molecules are saturated by the detection Ab and unable to bind to the particle surface. This is evidenced by the loss in signal past 1 $\mu\text{g}/\text{mL}$ of antibody. Upon varying the volume of α -HRP_{II} streptavidin particles with 1 $\mu\text{g}/\text{mL}$ of α -HRP_{II}-HRP_x, signal begins to saturate in a 50 parasites/ μL sample at 10 μL of beads (Figure 41B- red line). In a blank lysed blood sample, signal again saturates around 0.3AU (Figure 41B- blue line), which confirms the result from the previously described experiment. Given these results, 1 $\mu\text{g}/\text{mL}$ of α -HRP_{II}-HRP_x and 10 μL of α -HRP_{II} particles were chosen as the optimized reagent concentrations for further assays. Compared to the optimized conditions for the Co(II)NTA OBE, there is less detection antibody but the same volume of beads. This suggests that the greater affinity of the α -HRP_{II} IgG toward *pf*HRP_{II} does indeed promote a more sensitive ELISA.

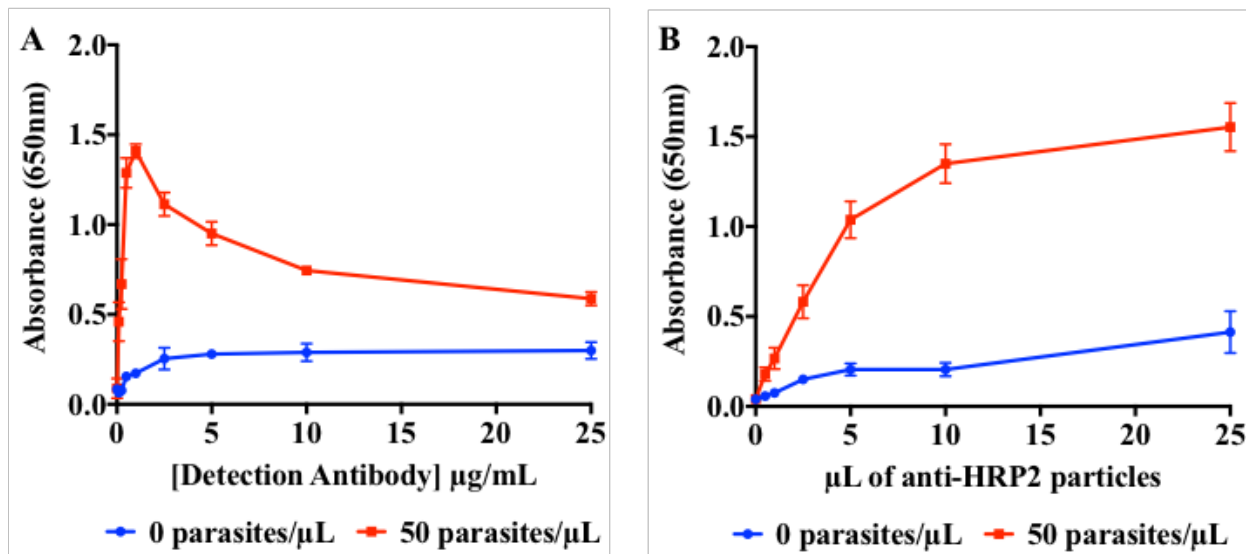


Figure 41. Effect of A) detection antibody concentration and B) particle volume added on on-bead ELISA signal and background noise.

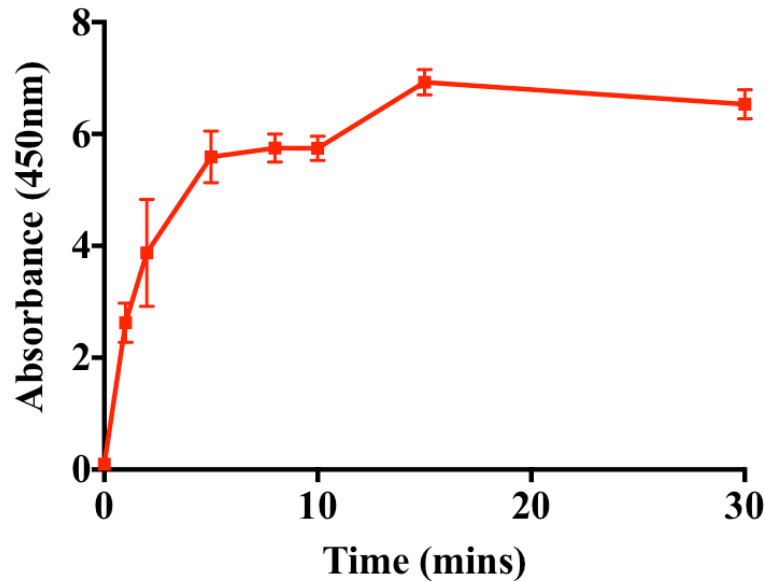


Figure 42. On-bead ELISA signal at various incubation times using optimized reagent concentrations.

After optimizing reagent concentrations for the OBE, the effect of incubation time and signal development time was explored. Based on the incubation study, where all *pf*HRP II was removed from the blood after 1 minute, the effect of incubation time on signal from a 50 parasite/ μ L sample was determined. As seen in Figure 42, signal begins to saturate at 5 minutes, but is fully saturated after 10 minutes. When TMB incubation time is varied at parasite concentrations of 0, 10, and 50 parasites/ μ L, signal starts to saturate at 3 minutes and fully saturates at 10 minutes (Figure 43). The background noise from 0 parasites/ μ L stabilizes around 0.3AU, which again agrees with previous optimization experiments. This confirms that non-specific binding is reduced in this OBE system, and signal generation is solely a result of the presence of *pf*HRP II in the sample. Using these results, titrations were performed over a range of parasite concentrations to fully assess the effect of incubation time on the limit of detection (Figure 44). The limits of detection at 1, 5 and 10 minute sample incubation times were 16

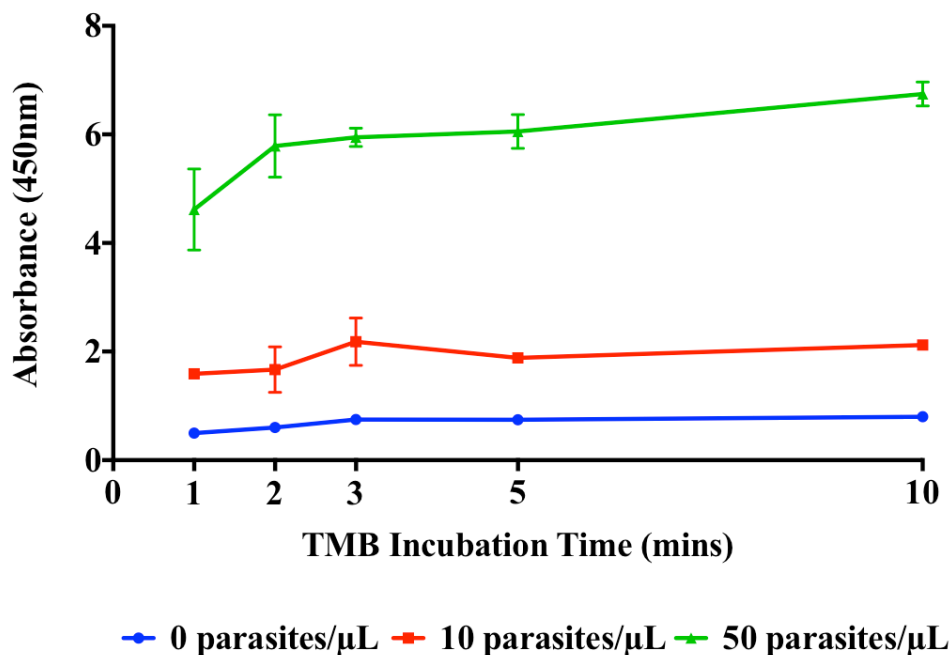


Figure 43. Effect of TMB incubation time on on-bead ELISA signal.

parasites/μL, 6 parasites/μL and 0.1 parasites/μL, respectively. The optimized all-in-one ELISA can achieve sub-parasite/μL limits of detection in under 25 minutes. While there is flexibility to further reduce the time of the assay (ie. ~15 minute assay to detect 10-20 parasites/μL), there will be a trade-off for the limit of detection.

Conclusion

This chapter outlines the development of a series of ELISA protocols that can be performed on the surface of a particle. Initially, the assay was developed on the surface of the Ni(II)NTA particles from Chapter II, but the inability to fully block the particle surface from non-specific binding prevented its use in this format. In switching to less porous Co(II)NTA particles, the assay was optimized to achieve a limit of detection of 500 parasites/μL. Since this form of the assay did not perform any better than RDTs and

was plagued by BSA inconsistencies, efforts were focused on creating an α -HRP_{II}-magnetic particle. Hypothesized to be more selective toward *pf*HRP_{II} and yield a more sensitive assay, development of an all-in-one OBE resulted in a limit of detection of less than 1 parasite/ μ L in under 25 minutes. Considering traditional 96-well format ELISAs take 4-6 hours to achieve the same result, this assay has the potential to bring sensitive, more high-throughput assays to local hospitals in developing nations. With this tool, patients visiting these hospitals will potentially have a faster time to result, with less variation than commercial RDTs. Future directions are aimed at validating the assay against FDA approved ELISA kits for *pf*HRP_{II} diagnosis. Additionally, the all-in-one ELISA will be multiplexed for *Plasmodium* Lactate Dehydrogenase

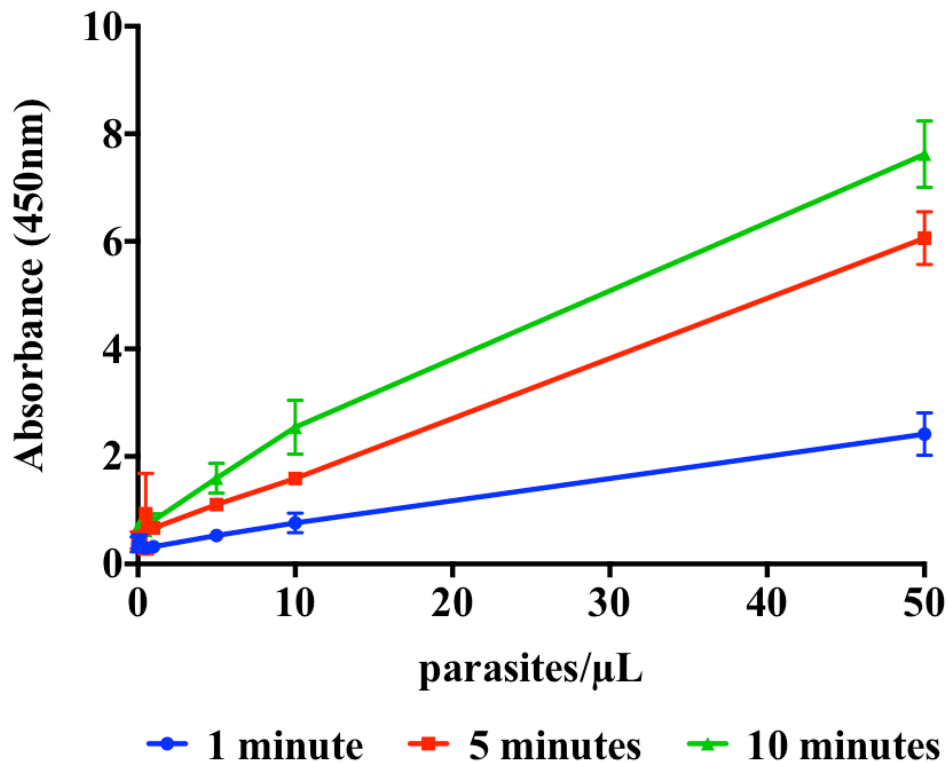


Figure 44. Limit of detection of *pf*HRP_{II}, using optimized on-bead ELISA reagents, at 1, 5 and 10 minute sample incubation times.

detection. *Plasmodium falciparum* is the most prevalent and virulent species of the parasite, but as *P. vivax* infections rise and *pfHRPII* mutations become more abundant, there will be an increased need for rapid and accessible tools for pan-malarial infection. This chapter did not discuss collaborative efforts with the Haselton laboratory in the Biomedical Engineering department to automate the OBE assay, but descriptions of this work can be found in Appendix C.

Acknowledgements

Support for this work was provided by the Bill and Melinda Gates Foundation Grand Challenges in Global Health: Develop Technologies That Allow Assessment of Multiple Conditions and Pathogens at Point-of-Care. K.M.D. was supported by an NSF Graduate Research Fellowship (2012095464).

CHAPTER V

MALARIA RAPID DIAGNOSTIC TESTS: UNCOVERING HOW THEY WORK AND HOW THEY CAN BE IMPROVED

A History of Rapid Diagnostic Tests

The first rapid lateral flow test was developed and marketed by Unipath in 1988 for home pregnancy testing from a urine sample. Where prior “at home” pregnancy tests were sold as mini laboratory kits with a two hour time to result, the purpose of the lateral flow test was to provide quick, home diagnostic testing for an untrained user.[90] Since its development, the lateral flow assay (LFA), also referred to as a rapid diagnostic test (RDT), has inundated the consumer market in the form of a vast selection of at home pregnancy tests. What is not so apparent to the consumer market is how this technology has been extended to rapid detection of a host of infectious and toxic agents, from viruses and bacteria to small molecule toxins and drugs from various sample matrices such as blood, saliva, soil, and food. The first malaria RDT was developed in the early 1990s.[91] To date, there are over 200 brands of malaria RDT available.

Principle of Lateral Flow Assays

The principle behind how lateral flow assays work can be viewed as a combination of chromatography and immunoassays. In thin layer chromatography (TLC), the capillary action of a liquid mobile phase passing along nitrocellulose paper acts to separate molecules based on size (Figure 45). The mobile phase is attracted to the nitrocellulose material via electrostatic interactions. As the buffer molecules migrate down the paper, attractive forces between the molecules themselves serves to wick more liquid material down the paper. If antibodies are immobilized in a region of the nitrocellulose strip, the corresponding antigen in the sample matrix will be immobilized at this region when wicked along the nitrocellulose. All other matrix molecules will continue to flow to the end of the strip. The bound antigen is then visualized upon

the addition of a labeling agent. This labeling agent can be an antibody functionalized particle or dye, but the most common is an antibody conjugated gold nanoparticle (AuNP). In 1992, Tsuda and coworkers demonstrated a novel, rapid dipstick immunoassay for plant viruses from leaf extracts, using antibody functionalized, colored latex particles, that had similar sensitivity to a

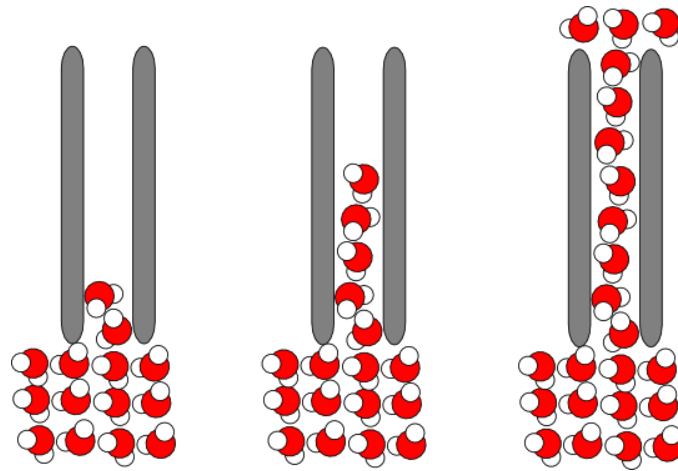


Figure 45. Diagram of capillary action. Image adapted from Physics Stack Exchange.

traditional ELISA for these same viruses.[92] While these rapid immunoassays can be performed like a TLC separation, many lateral flow strips are now manufactured within a plastic cassette.

Components of a Lateral Flow Assay

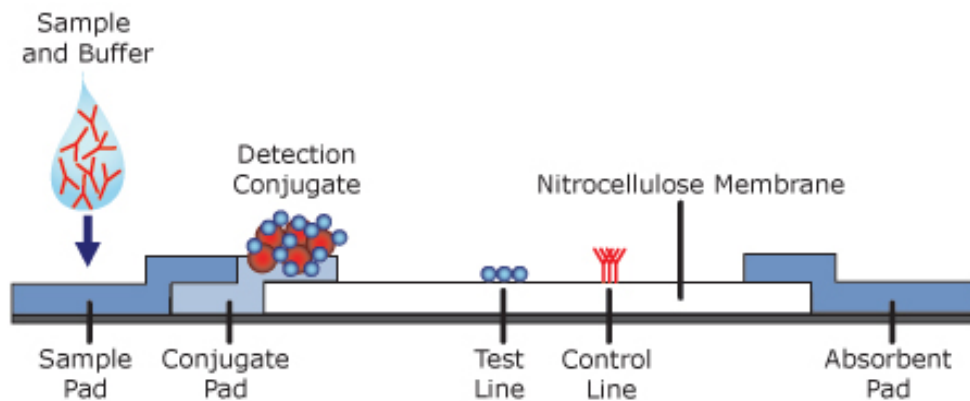


Figure 46. Basic components of a lateral flow immunoassay.[4]

The basic components of a rapid lateral flow strip can be seen in Figure 46.[4] The components of the lateral flow strip and their function are easily explained from point of adding

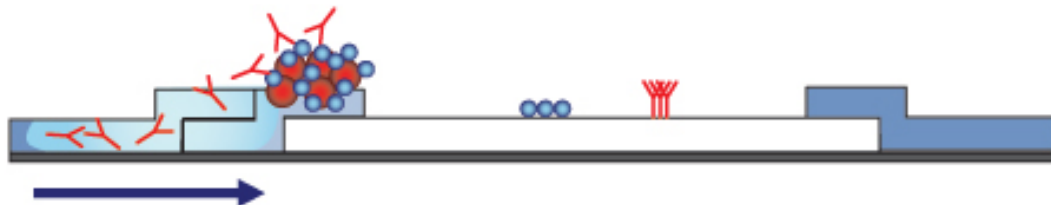


Figure 47. Interaction of sample with AuNPs on lateral flow conjugate pad.[5]

a sample to the test. As the lateral flow strip itself is very small (usually 600mm long x 5mm wide), a small volume of sample is applied to the sample pad. For a blood sample, this is usually around 5 μ L. The sample pad is composed of cellulose or glass fiber and acts to prepare the sample for the assay and reduce sample to sample variability. Addition of buffer reagents, surfactants, salts, and blocking proteins to the sample pad help normalize any variation in sample pH, ionic strength, or nonspecific protein interactions while preparing the sample for flow down the strip. The conjugate pad is arguably the most important part of the assay strip, as it houses the visualization reagent for the assay. 40nm AuNPs are functionalized with antibodies against the antigen of interest before deposition on the conjugate pad. Available as glass fiber or other woven material (e.g. polyester), the conjugate pad is also pre-treated with buffering reagents to facilitate specific interactions of the analyte with the conjugate and reduce non-specific binding. As the sample is released from the sample pad and comes in contact with the conjugate, antibody-antigen interactions immediately occur (Figure 47).[5] Considering these AuNPs must flow down the strip as the test runs, it is important to assess the release characteristics of the pad materials.

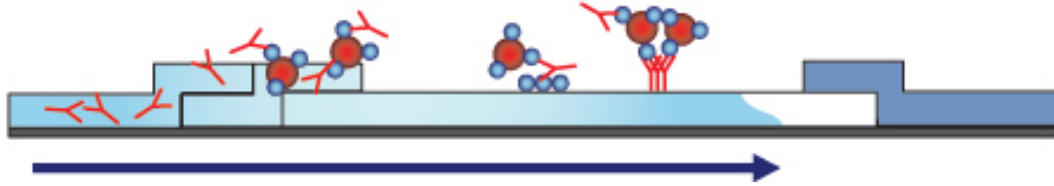


Figure 49. Wicking of antigen bound AuNPs down the nitrocellulose strip. [5]

As aforementioned, nitrocellulose has long been used for chromatographic separations. In the lateral flow format, the nitrocellulose provides both a platform for the immunoassay to be performed on as well as an inherent sample purification method, as unbound biological materials are wicked along the strip via capillary action. Antibodies are immobilized in stripes to form a test line and a control line. The porosity of the nitrocellulose will govern the speed at which the sample and AuNP conjugate is wicked down the strip. This pore size must be optimized for the assay as the speed at which the conjugate flows down the pad can lead to low sensitivity or high background. Much like the sample and conjugate pads, the nitrocellulose membrane is also pretreated with blocking buffer to reduce non-specific interactions along the assay strip. If antigen is present, the AuNP conjugate will be sandwiched at the test line, as the immobilized antibody is specific for the antigen. Excess unbound AuNP conjugate will flow past this line to the control line, where immobilized antibody against AuNP conjugate will capture the excess particles (Figure 49).[5] This control line serves to tell the user the test is working, and thus should always be visualized, regardless of whether the result is negative or positive. The

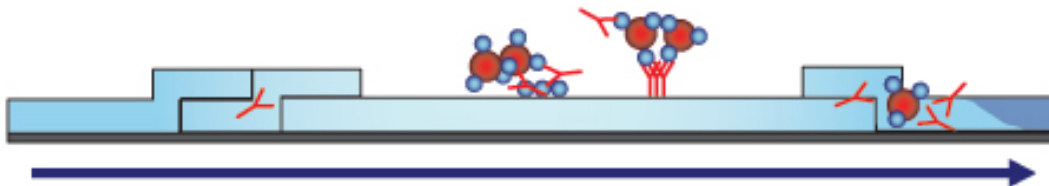


Figure 48. Trapping of excess reagents by the wicking pad. [5]

wicking pad at the end of the lateral flow strip acts to promote capillary flow of the sample and buffer down the membrane as the assay runs (Figure 48).[5] This pad is typically a cellulosic material able to hold 100-200 μ L of fluid. Most lateral flow strips are manufactured to process 100 μ L of total liquid volume (sample and running buffer combined). A plastic adhesive backing card serves as the structural platform for the paper components of the lateral flow assay and ensures that all the assay components stay in contact. This is vital to assay performance, as all of the pads and membranes must remain in contact with one another post-manufacturing and during the test itself.

Rapid Diagnostic Tests for Malaria

Figure 50 demonstrates a generalized lateral flow assay for *P.falciparum* malaria

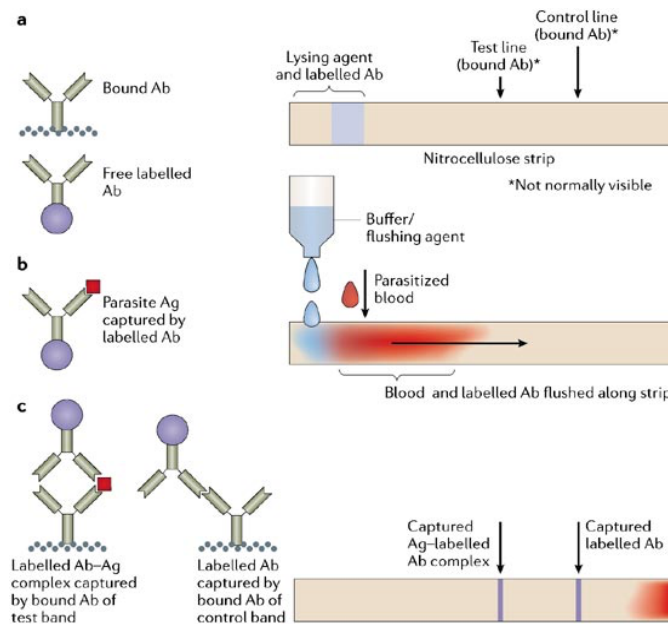


Figure 50. Generalized diagram of a *Plasmodium* RDT.[1]

detection. Several companies in the US and around the world manufacture malaria rapid diagnostic tests. Since 2006, the World Health Organization has qualified RDT performance

with clinical samples at 200 parasites/ μL and 2000 parasites/ μL for *P. falciparum* and *P. vivax*. The WHO has released an annual report of these results since 2009 detailing the performance characteristics (sensitivity, specificity, heat stability, other performance anomalies) of each brand tested, in order to inform clinical acquisition. As can be seen by the description of the lateral flow assay components, there is a great deal of complexity in manufacturing what will ultimately become a simple, easy to use RDT. These manufacturing companies are well equipped to

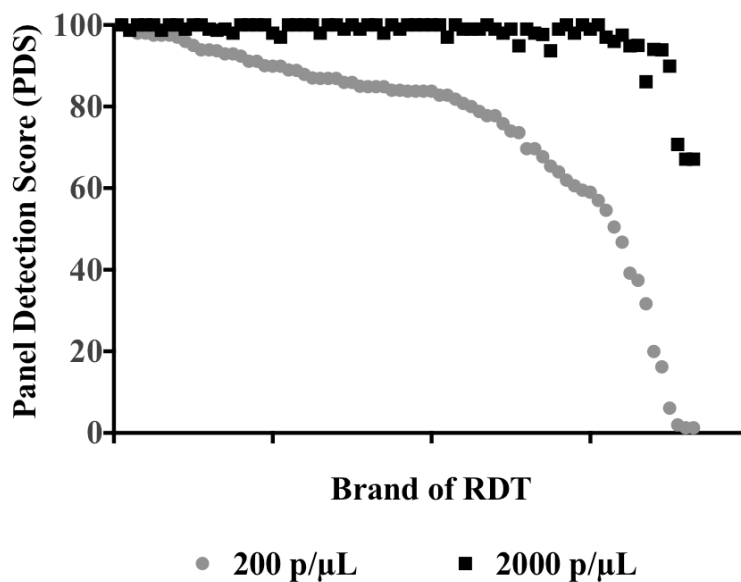


Figure 51. Panel detection scores of malaria RDT brands tested by the WHO.

produce large volumes of product, but quality control and assurance of the diagnostic assay has proven to be a concern. Lack of antibodies on the test and control lines and no conjugate sprayed on the conjugate pad are just two of the many issues observed in manufactured RDTs. Figure 51 shows a plot of the panel detection score (PDS) of all the brands tested at 200 and 2000 parasites/ μL . This score is determined as *the percentage of malaria samples in the panel that give a positive result in two RDTs per lot at the lower parasite density or by a single RDT per lot at the higher parasite density.*[1] An example of this calculation is shown in Figure 52.

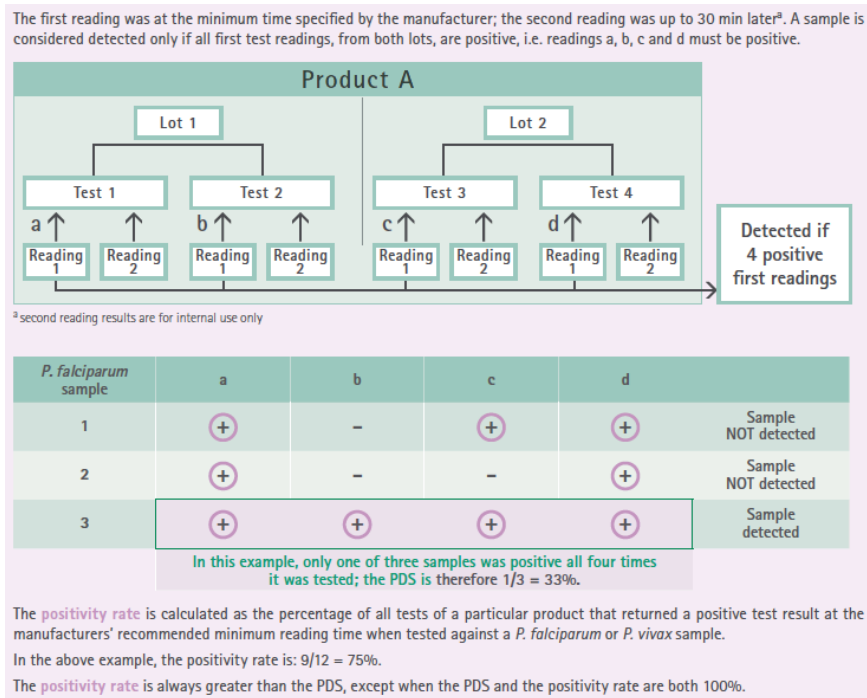


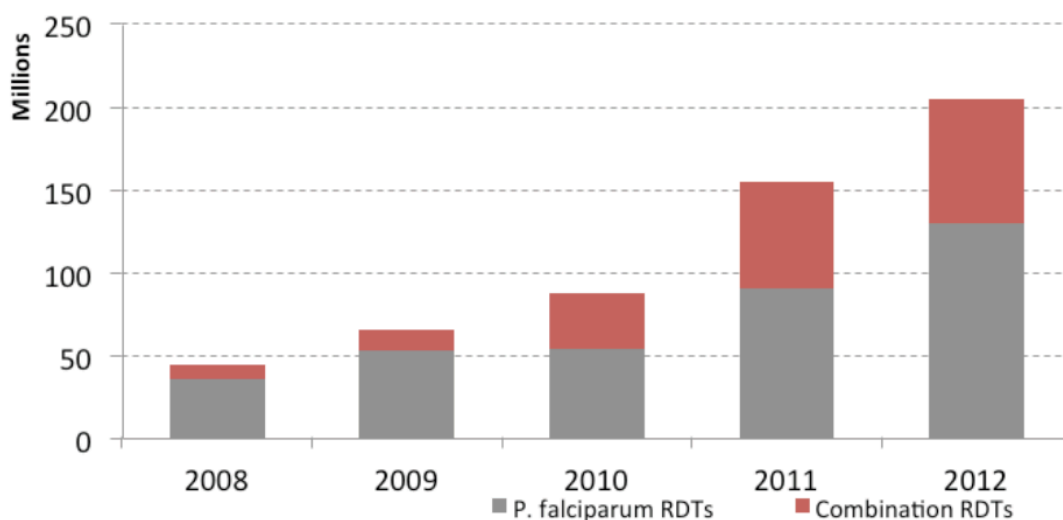
Figure 52. Example of panel detection score calculation. [1]

While PDS is different from clinical sensitivity, it predicts performance in the field at low parasite densities from the combination of positivity rate and inter-lot consistency. 78.6% and 42.4% of the products tested had a PDS score $\geq 75\%$ for *P. falciparum* and *P. vivax*, respectively. All products tested were seen to have issues with sample clearance. 62% of the tests demonstrated cases of samples completely failing to migrate. Given these tests guide patient diagnosis and treatment, it is imperative to ensure quality products are being delivered to these areas, regardless of brand or manufacturer. Hence, the WHO has outlined selection criteria for clinical RDT procurement as:

- a) PDS against *Pf* and *Pv* samples should be at least 75% at 200 parasites/ μ L.
- b) False positive rate should be less than 10%.
- c) Invalid rate should be less than 5%.

These iterative rounds of testing and reports and establishment of selection criteria have helped inform clinical procurement of validated RDTs.

Malaria RDT Landscape



Source: 2012 World malaria report. Geneva: WHO; 2012 (based on responses from manufacturers participating in the WHO Malaria Product Testing Programme for Malaria RDTs; 31 suppliers in 2008–2010, 24 suppliers in 2011–2012).

Figure 53. Number of malaria RDTs (*Pf* and Combo tests) purchased between 2008-2012.[7]

Malaria RDT demand has grown significantly in recent years. 45 million tests were sold in 2008, and this number rose to 205 million in 2012 (Figure 53).[7] The estimated need for malaria RDTs, in Africa alone, is 1.6 billion between the years of 2013-2016, but the funded demand only supports 400 million tests. This is reflected in the statistic that only 62% of suspected African malaria cases in 2013 received a diagnostic test. Of the \$5.1 billion dollars projected to achieve global malaria control and elimination, only \$2.7 billion was available, domestically and internationally, in 2013. The average price of a *Pf* test and a *Pf*/Pan test were \$0.32 and \$0.38, respectively. The market has consolidated around three major manufacturers: Access Bio (US/South Korea), Standard Diagnostics (South Korea) and Premier Medical

Corporation (India). Additionally, half of the countries have shifted from procurement of *Pf* only tests to *Pf/Pan* tests. As the market landscape for RDT use shifts, manufacturers must adapt their standards and product lines to ensure proper coverage. However, as the price of RDTs approaches the cost of production, there is little incentive for quality improvement and innovation. Two areas of innovation most needed for elimination campaigns are increased sensitivity for asymptomatic infection and better pan-malarial diagnostic tests.

While academic, non-profit and government organizations cannot force the private sector to adapt manufacturing practices, a willingness to work with these companies and show initiative toward innovation can push toward global malarial elimination. This chapter outlines an approach toward enhancement of commercially manufactured malaria rapid diagnostic tests, as preliminarily shown in Chapter II. **Chapter VI** demonstrates the utilization of the extraction device from Chapter II for the enhancement of six malaria RDT brands. A semi-quantitative approach was taken to calculate this enhancement factor via image processing. Parasite densities indicative of asymptomatic infection were detectable on commercial RDTs with the addition of a sample preparation. In efforts to further streamline the enhancement process, **Chapter VII** outlines a proof-of-concept method for one-step sample concentration for RDT enhancement. Instead of fully purifying *pfHRP*II from a blood sample using the extraction cassette, *pfHRP*II bound to Ni(II)NTA particles were deposited directly on the sample pad of an RDT. Modification of the manufactured running buffer with imidazole allowed for *pfHRP*II release directly on the RDT strip. The design and preliminary testing of a device, deemed the RDT garage, for more user-enabled processing is also discussed in this chapter. Lastly, a discussion on future directions of this research and perspectives on the malaria RDT landscape, as a result of this work, is provided.

CHAPTER VI

SIMPLE SAMPLE PROCESSING ENHANCES MALARIA RAPID DIAGNOSTIC TEST PERFORMANCE

Introduction

The advent of point of care (POC) diagnostic tools has been a major part in providing access to affordable healthcare in nations affected by the ongoing spread of infectious diseases.[25] Molecular based diagnostic methods such as enzyme immunoassays (ELISA) and quantitative polymerase chain reaction (qPCR) are powerful tools for the detection of protein and nucleic acid biomarkers of infectious diseases, but reagent instability and cost of these assays in addition to time and expertise needed to perform the test limits their use in underdeveloped areas.[93] Light microscopy is currently the gold standard for blood-borne disease detection, but intermittent access to functional microscopes and trained microscopists prevents its widespread use. Lateral flow immunochromatographic rapid diagnostic tests (RDTs), which operate much like a commercial pregnancy test, were developed to circumvent these challenges and bring affordable disease diagnosis to low-resource areas.[91; 94] Several advantages of RDTs include low-cost, rapid time to result, and ease of use and interpretability.[21] Additionally, these tests have been widely used in public health programs to aid with patient management, disease surveillance and treatment campaigns.[95] In 2006, over 16 million RDTs were delivered to underdeveloped nations for the detection of malaria alone.[94]

Despite the many advantages of RDTs, the changing climate of infectious disease education, prevention, and treatment has highlighted the need for improved tests. The World Health Organization (WHO) periodically reviews all malaria RDTs manufactured

for diagnostic use, and qualifies the limit of detection for these tests at 200 parasites/ μ L.[96] While this limit of detection is sufficient for the diagnosis of symptomatic malaria infection, many asymptomatic (or submicroscopic) patients are missed by these tests due to their limitations in this range of parasitemia. Additionally, poor manufacturing standards and storage conditions render many brands of malaria RDTs inoperable and unreliable.[97] There are an estimated 60 brands and 200 types of tests manufactured for the detection of malaria, and according to the WHO, less than 10% of those tests are effective at detecting 200 parasites/ μ L parasite densities.[96] Unfortunately, tests are often acquired based on government sanctions, history of use, and cost instead of acquisition based on reliability of the brand.[98] This variability in test performance, sensitivity and reliability undermines the progress made in malaria disease prevention.[23]

Effecting a change in low-resource diagnostics and global healthcare may not necessarily require a complete reworking of the system, but simply using innovation to

	Brand	WHO PDS	Catalog #	Lot #	Date of Manufacture	Expiration Date	Manufacturer
1	Paracheck Pf	96.0	30301025	311310	02/12	01/14	Orchid Biomedical Systems
2	One Step Pf	67.7	522352	201209025	N/A	09/14	Blue Cross Biomedical
3	ParaHit Pf	80.8	551C101-50	4000006366	3/24/11	3/24/13	Span Diagnostics
4	ParaHit Total	35.4	551C204-50	4000007699	11/24/11	1/24/13	Span Diagnostics
				4000010071	12/31/12	12/31/14	Span Diagnostics
5	ICT Dual	78.8	ML03	50130	09/12	09/14	ICT Diagnostics
6	ICT Pf	86.9	ML01	10006	05/12	05/14	ICT Diagnostics
				50131	05/12	05/14	ICT Diagnostics

Table 4. Malaria RDT specifications for RDT enhancement.

make the existing constructs work better. This was observed in Chapter II, as a simple sample preparation step served to improve the limit of detection of one brand of RDT 8 fold. Since these tests operate by sandwiching the biomarker of interest between a strip of nitrocellulose paper and a gold nanoparticle on a test region of the RDT, any technology that can deliver a higher concentration of biomarker to the test line should improve the test. Likewise, any test should be able to be improved, regardless of manufacturer or WHO detection score. In order to choose the RDT brands to be evaluated in this study, the WHO report on the performance of all manufactured malaria RDTs was consulted. Given this report, a range of RDT brands (low, medium and high performing) were selected (Table 4). Because of the nature of extraction device, the hypothesis was that RDTs could be improved, regardless of WHO PDS, by application of a small volume of concentrated, purified *pfHRP2*. This chapter outlines the utility of the extraction cassette developed in Chapter II for improvement of six malaria RDTs below the WHO limit of detection of 200 parasites/ μL . Additionally, this chapter outlines development of a method to quantify the level of enhancement by converting the visual signal on the RDT to a quantifiable peak area. In doing so, enhancement factors and limits of detection can be calculated for the analyzed RDTs.

Materials

Both pooled and individual donor human whole blood in citrate phosphate dextrose (Cat # HMWBCPD) were purchased from Bioreclamation LLC. For the enhancement study pooled blood was used. For the individual donor effect study, individual donor blood was used as shown in Table 5. This study was blinded, as we did not know the identity of the donors. *Plasmodium falciparum* D6 strain was cultured in

Donor	Lot #	Gender	Age	Race
1	BRH701920	Male	46	Black
2	BRH701915	Male	29	Black
3	BRH701919	Male	41	Black
4	BRH701918	Male	66	Hispanic
5	BRH701916	Male	50	Black

Table 5. Specifications of individual blood donor samples.

the laboratory. Tygon tubing was purchased from McMaster Carr (Cat # ACF00002). Ni-NTA Magnetic Agarose Beads (Cat # 36113) were purchased from Qiagen Inc. Donut magnet used in this study was purchased from Emovendo LCC. Paracheck (Pck), ParaHit Dipstick (PDip), ParaHit Total (PTot), ICT Pf (IPf), ICT Dual (IDual) and Blue Cross One Step Pf (OsPf) rapid diagnostic tests were acquired from their respective manufacturers. Hewlett Packard Color LaserJet CM3530fs MFP scanner was used to image the RDTs. Image J software was downloaded from the National Institute of Health website (<http://rsbweb.nih.gov/ij/>). OriginPro 9.0 Software was employed for RDT analysis. The remaining products were purchased from either Fisher Scientific or Sigma Aldrich.

Experimental

Blood Sample Preparation

Human whole blood samples were combined in 1:1 (v:v) ratio with 2X lysis buffer (100 mM potassium phosphate pH = 8.0, 600 mM NaCl, 250 mM imidazole, 2% Triton X-100). Subsequently, the blood sample was filtered through glass wool that was placed in the bottom of a plastic syringe. Following filtration, a 200 parasite/ μ L stock blood sample was made by adding a specific amount of D6 *P. falciparum* culture (at ~52000

parasites/ μL) to the lysed and filtered sample. The remaining parasitemias were achieved by serial dilution of the 200 parasites/ μL stock. For the mimic patient study, this process was modified slightly in that the specific amount *P. falciparum* culture required for the desired parasitemia was spiked into the sample before filtration. Thus, the samples were prepared individually without dilution.

Extraction and Analysis with RDTs

Extraction devices were constructed and prepared blood samples were purified and concentrated as described previously.[77] Briefly, a 9-inch piece of Tygon tubing was injected with three 100 μL wash chambers (50 mM PB, pH 8.0, 300 mM NaCl, 125 mM imidazole, and 0.05% Tween-20) each separated by a 0.25 μL mineral oil valve. An elution chamber consisting of 10 μL of elution buffer (50 mM potassium phosphate (PB), pH 8.0, 300 mM NaCl, 500 mM imidazole, 0.05% Tween-20) was injected at the end of the tube. One end of the Tygon tube was blocked with a capillary tube and a PCR tube was placed on the other end as the sample chamber. 200 μL of the blood sample were placed into this chamber with 10 μL of Ni-NTA magnetic agarose beads. After incubation in the chamber, the beads were pulled through the wash chambers into the elution chamber with a magnet. After incubating in the elution chamber the beads were pulled back into the adjacent oil valve. The elution chamber was then cut off with a razor and the contents were spotted onto an RDT. In the enhancement study, this process was done, in triplicate, on six types of RDTs, at six parasitemias (0, 12.5, 25, 50, 100 and 200 parasites/ μL). For the individual donor effect study, the process was done in triplicate for three parasitemias (0, 10 and 100 parasites/ μL) with each donor sample, on three RDT brands, PTot, IPf and Pck, of low to high performance, respectively, based on the WHO

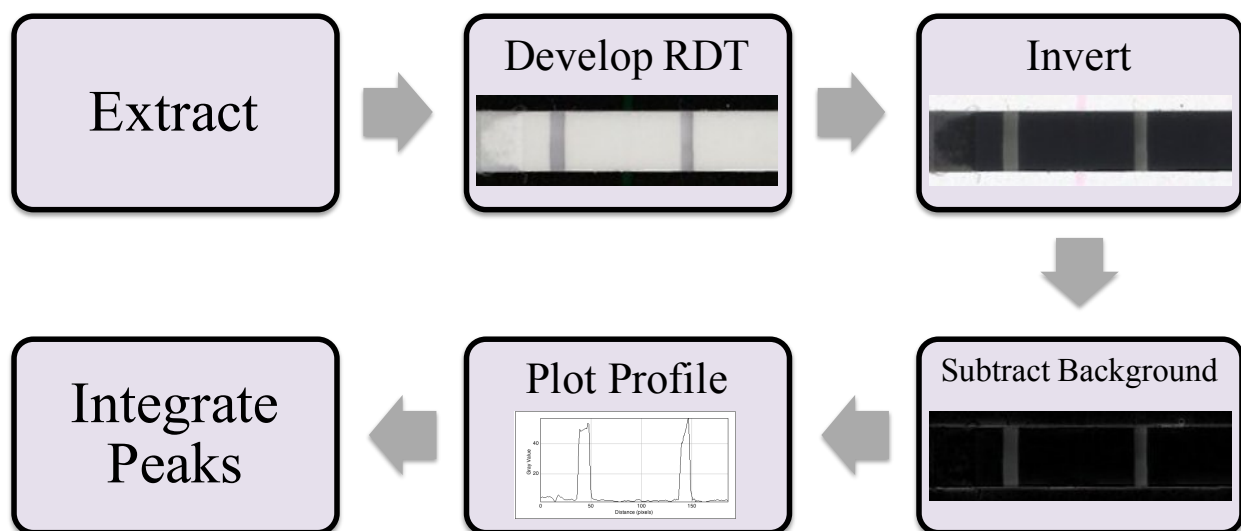


Figure 54. Workflow for RDT processing.

report. For both studies, standard analysis of the blood samples that were not extracted consisted of spotting 5 μL of parasite spiked blood sample directly onto the RDT and processing according to manufacturer's specifications. These unextracted samples served as reference standards.

Image Analysis

The process used for analysis of the RDTs is outlined in Figure 54. To begin the image analysis portion of this workflow, the immunochromatographic test strip, housed within the plastic cassette of the RDT, was removed. The absorption pad at the end of the strip was detached to aid in the drying of the strip. The strips were dried overnight prior to imaging with a Hewlett Packard Color LaserJet CM3530fs MFP scanner. This drying step did not affect peak signal over time (data not shown). Specific settings were used (darkness = 8, background = 1, sharpness = 4) and the highest image quality was selected. The image was then manipulated in

Image J. First, the image was inverted. This is a processing step commonly performed in RDT reader algorithms to present the data in an intuitive manner.[99] Secondly, the background was subtracted (rolling ball radius = 15 pixels, smoothing disabled). Once this was accomplished, a plot profile containing the test and control line was generated. This profile was imported into Origin® software, where the peak in the plot profile associated with the test line was integrated using the Peak Analysis tool. When using this tool, the automatic background line was used. A test was considered positive if the height of the test line peak on the plot profile was at least 3% of the control peak. Peak width was determined manually by the user, and the result of the integration was generated by the software. This result was used to quantitate the intensity of the test line in the form of an integrated area.

Results and Discussion

Enhancement in RDT Performance

The advent and implementation of rapid diagnostic tests have made an invaluable impact on the diagnosis and treatment of infectious diseases in third world countries. The efficacy of these tests at high parasitemias was demonstrated in this study, as all RDT brands analyzed were found to produce detectable signal given unextracted samples at a parasite density of 2000 parasites/ μL . But as discussions about eradication strategies begin in earnest, the challenge becomes how to effectively identify the untreated asymptomatic patient reservoir. Management of submicroscopic malarial infections has become a challenge in the field, as current rapid diagnostics are unable to detect these patients.[100] The effect of sample preprocessing on RDT performance can be seen in

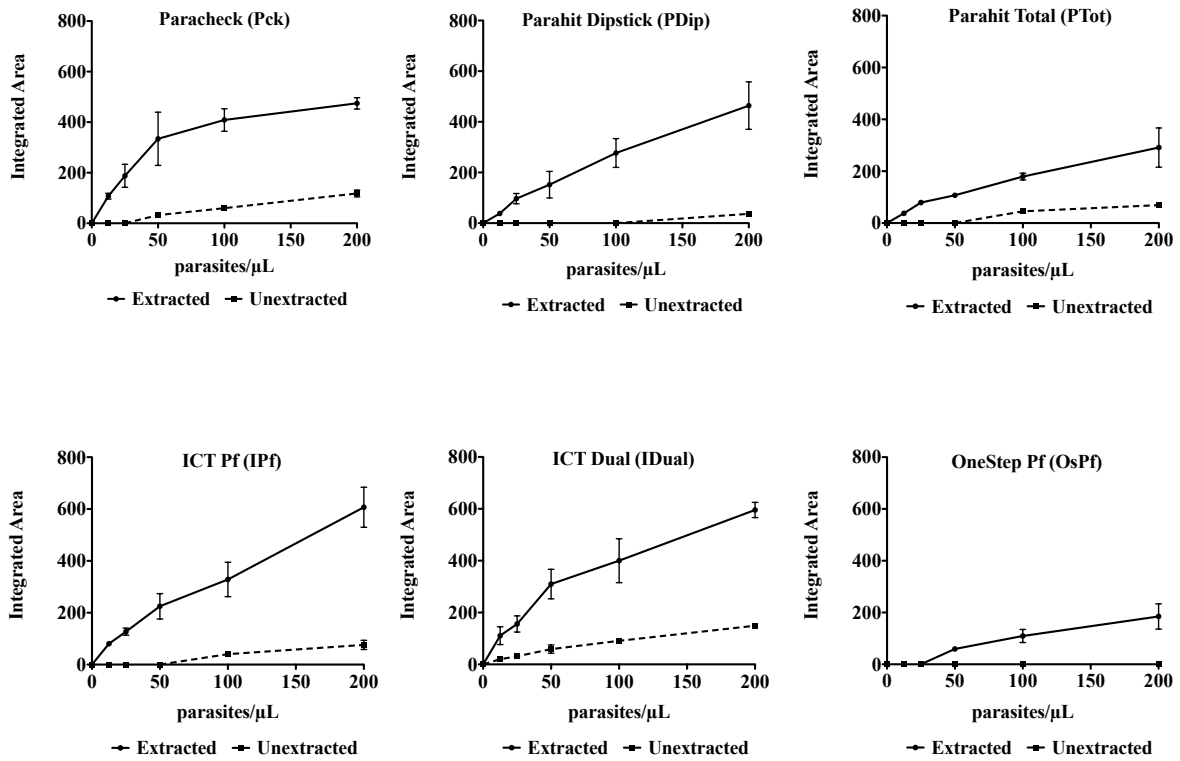


Figure 55. RDT enhancement curves before and after sample processing.

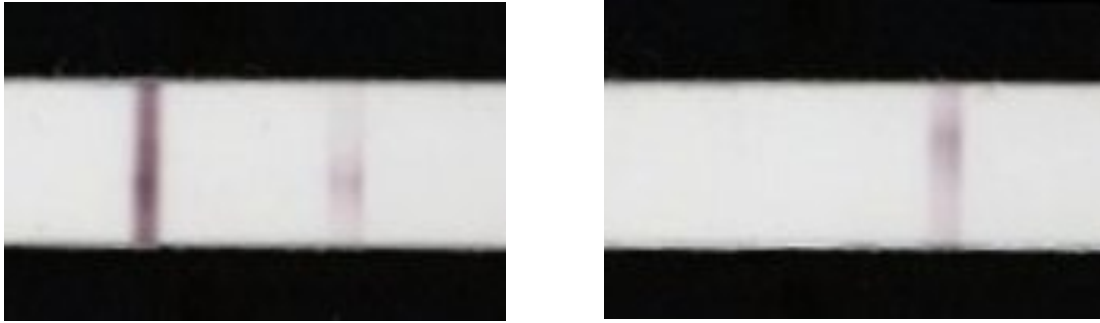


Figure 56. Example of a missing control line (right image). Both RDTs were from the same manufacturer.

Figure 55. This analysis showed five of the six RDT brands tested were able to detect 200 parasites/ μL from an unextracted sample. Four brands detected 100 parasites/ μL , as compared to only two at 50 parasites/ μL . Only IDual detected unextracted samples at 25 and 12.5 parasites/ μL . After extraction, all brands were improved to detect parasite concentrations of 12.5 parasites/ μL and higher, with the exception of OsPf. However, the control line was missing on random tests from one lot (Lot #10006) of IPf RDTs (Figure 56). Upon switching to a new lot, this issue was resolved.

To quantitate performance, the lateral flow strips within each cassette for all brands were scanned and the corresponding plot profiles analyzed using peak integration software. Analysis methods of this type are common in recently developed RDT readers.[99] The degree of enhancement in RDT signal that occurs with extraction of the sample (enhancement factor) was calculated for 200 parasites/ μL by the following relationship:

$$\textit{Enhancement Factor} = \textit{Integrated Area}_{\textit{Extracted}} / \textit{Integrated Area}_{\textit{Unextracted}}$$

This enhancement factor ranged from 4 to 13 among the five brands that produced a detectable signal at 200 parasites/ μL unextracted. For OsPf, the enhancement was

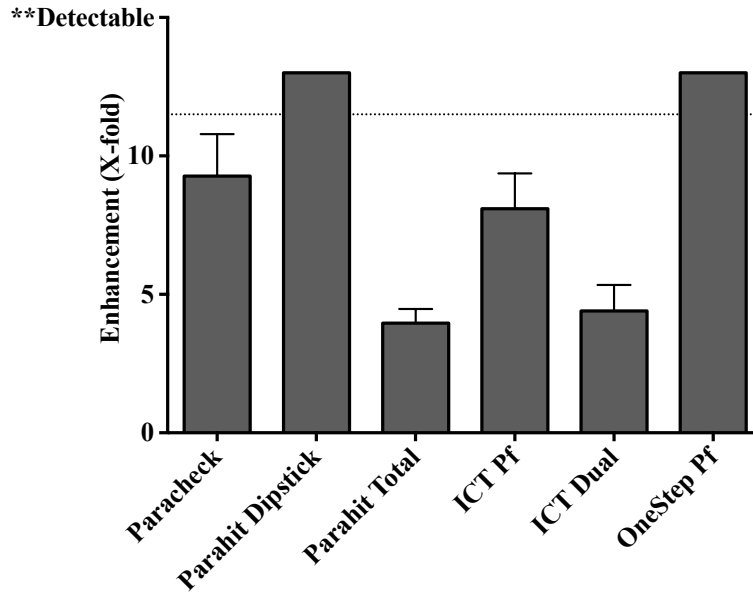


Figure 58. Calculated enhancement factors at 200 parasites/ μ L.

practically infinite, as the unextracted sample was not detected at 200 parasites/ μ L (Figure 58). Analysis of RDT signal as a function of parasitemia from 12.5 to 200 parasites/ μ L generally pointed to an enhancement in test performance after sample processing as compared to an unextracted sample. Improvement in test performance was benchmarked on changes in the signal intensity of the *pf*HRP_{II} test line. Despite the observed enhancement, visual and pixel analysis of the tested brands revealed several brand-to-brand discrepancies. The most noted was in the case of OsPf, where smearing of the sample and RDT components on the test strip increased the background, preventing



Figure 57. Faulty sample clearance across the nitrocellulose strip of the RDT.

detection of low parasitemias in this brand (Figure 57). This failure of the test strip to clear the sample and reagents prevented proper development of the test line and peak identification. Other brand-to-brand differences were observed by comparing the shape of the titration curves. Pck reached saturation in signal intensity after 100 parasites/ μ L, whereas PTot and IPf remained linear through 200 parasites/ μ L, where our analysis stopped (Figure 59). These differing trends suggest a greater concentration of active antibody on the test line of IPf and PTot RDTs, thus providing a wider linear range for calculations made through our algorithm.

Limit of Detection of Enhanced RDT Signal

Given the nature of the algorithm used to detect the peaks on the scanned RDT image, the smallest detectable signal was found as a percentage of the control peak

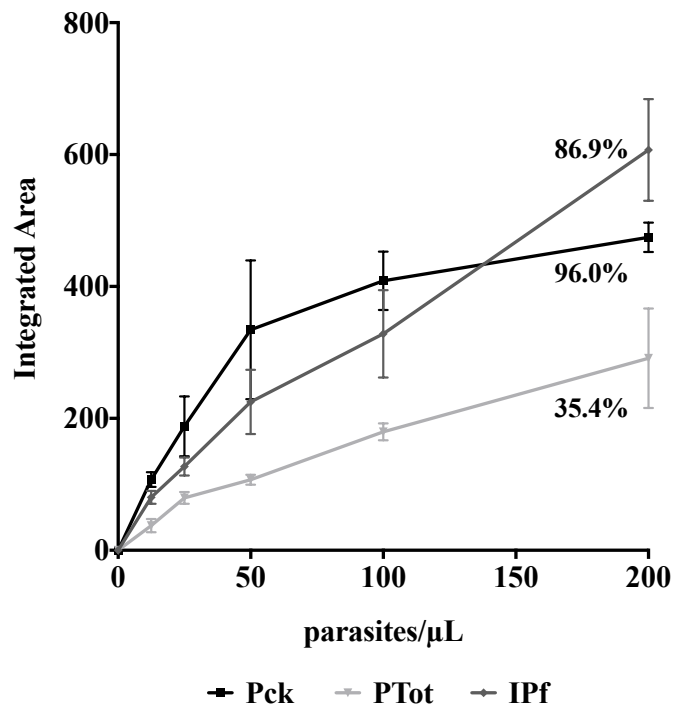


Figure 59. Comparison of enhancement curves of three different RDTs.

(threshold height). For each brand tested, the integrated area for all of the control lines analyzed were averaged and converted to the 3% threshold height maximum. This threshold height was visible to the naked eye. Given this threshold height, the LOD was found for extracted and unextracted samples of each brand. Both Pck and IDual had LODs of 3 parasites/ μ L after extraction (Table 1). According to the WHO, the limit of

	Unextracted	Extracted
Paracheck (Pck)	21.7 \pm 7.4	3 \pm 0.2
Parahit Dipstick (PDip)	143.7 \pm 39.5	10.7 \pm 0.9
Parahit Total (PTot)	70.2 \pm 12.4	17.3 \pm 1.5
ICT Pf (IPf)	51.1 \pm 7.9	5.6 \pm 0.8
ICT Dual (IDual)	15 \pm 1	2.9 \pm 0.2
One Step Pf (OsPf)	ND	32.6 \pm 4.5

Table 6. Calculated limit of detection (in parasites/ μ L) for all brands tested.

detection for malaria RDTs is required to be at least 200 parasites/ μ L.[96] Given an unextracted sample, five out of six of these brands were found to have limits of detection ranging from 15-150 parasites/ μ L. OsPf did not detect any unextracted samples within the LOD recommended by the WHO. When samples were extracted, the limits of detection were found to be between 3-33 parasites/ μ L (Table 6). Of the six brands tested, five were enhanced to detect below the set detection limit of 20 parasites/ μ L, which is representative of asymptomatic and submicroscopic levels of malaria infection. IDual was the only brand tested that was able to detect at this level before extraction. To our

knowledge, no previously developed method for RDT analysis has allowed for the detection of such low parasitemias.

It is also intriguing to observe how sample preprocessing affects the deviation of replicate measurements. There was quite a bit of variation from test to test when 5 μ L of the unextracted sample was applied to the test. However, upon extraction, not only was the limit of detection improved, the variation among replicate tests was reduced. As a best case, the standard deviation of processed samples on PDip tests was reduced by two orders of magnitude. This result speaks not only to the enhancement potential upon preprocessing, but also to the effect of cleaning up the sample prior to RDT development. Application of a purer, more concentrated sample to the RDT likely reduces the variability from test to test.

Effect of Individual Donor Samples on RDT Performance

To focus the study on the correlation between donor source and WHO panel detection score (PDS) and the RDT signal intensity, three RDT brands of low, medium and high performance were selected. The performance of each RDT brand is based on the WHO PDS which is established by the RDT brand's inter-test and inter-lot consistency.[96] The three brands were selected by their WHO PDS and Pck fell in the high (>90%), IPf in the medium (50-90%) and PTot in the low (10-40%) range. These three brands were tested with unextracted and extracted samples at 0, 10 and 100 parasites/ μ L to demonstrate their utility at low parasitemias. As can be observed in Figure 60, the extracted donor samples at 100 parasites/ μ L had average signal intensities that were statistically different among brands and trended with their respective PDS. The highest signal intensities for the extracted samples were observed for Pck, which had a

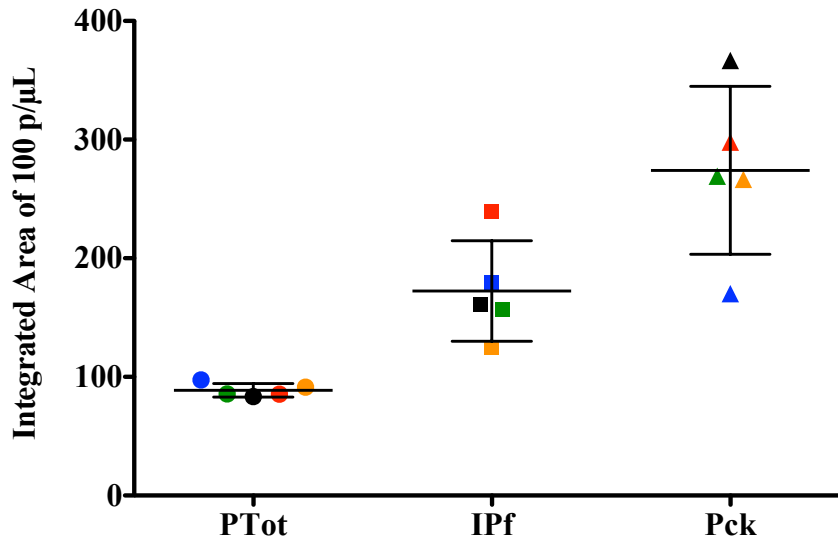


Figure 60. Effect of donor sample on RDT signal. Donor 1 (red), Donor 2 (green), Donor 3 (yellow), Donor 4 (black), Donor 5 (blue).

PDS of 96.0%. Signal intensity decreased for IPf followed by PTot, whose detection scores were 86.9% and 35.4%, respectively.

In Figure 61 it can be seen that when unextracted donor samples were spiked to contain 100 parasites/ μ L, only Paracheck and ICT Pf yielded a signal. Two false negatives were seen for ICT Pf at this parasitemia. No brand tested was able to detect 10 parasites/ μ L in any of the donor samples. Additionally, Parahit Total afforded no signal at any parasitemia before extraction. Upon extraction, Paracheck and ICT Pf yielded signal at 10 and 100 parasites/ μ L, while Parahit Total only recognized 100 parasites/ μ L. Only one false negative was observed for ICT Pf at 10 parasites/ μ L extracted. A 4 to 5-fold difference in signal intensity between the 10 and 100 parasites/ μ L extracted samples for Pck and IPf was observed. Generally, all samples of the same parasitemia, analyzed by the same RDT brand, experienced similar enhancements, which seems to point to no

individual donor sample effect on the signal. Thus, any variations in signal intensity of a given RDT observed for samples with the same preparation and parasitemia were attributed to manufacturing and brand differences.

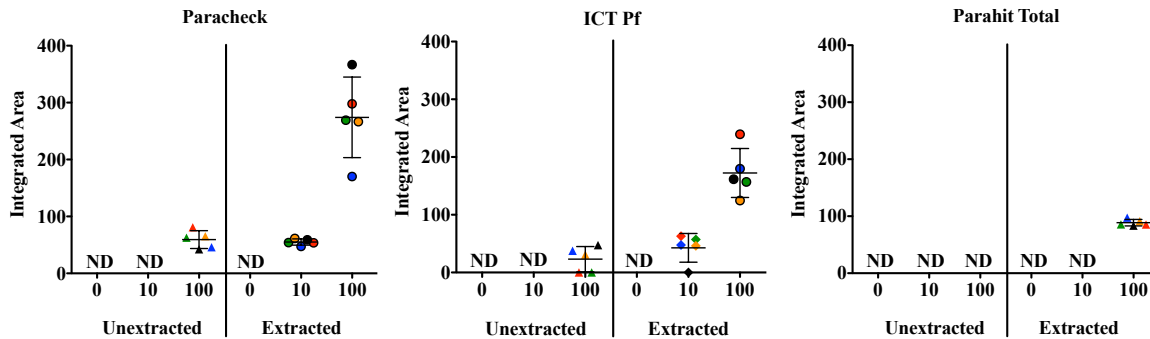


Figure 61. Plots of the average peak areas from the RDT test lines for each mimic donor sample, extracted and unextracted, at all parasitemias. Donor 1 (red), Donor 2 (green), Donor 3 (yellow), Donor 4 (black), Donor 5 (blue).

The data collected from this portion of the study was also used to observe trends in RDT performance. An increase in integrated peak area from PDip to IPf to Pck was found to correspond to an increase in signal intensity between these brands. This increase in signal followed the trend in the increasing PDS reported by the WHO for these RDT brands. Although the signals of low and medium performing tests were not enhanced to that of high performing test, enhancement in overall performance was observed across the range of the panel detection scores. Analysis of these three RDT brands also showed that sample extraction reduced the incidence of false negative test results. For example, in the case of IPf, at 100 parasites/μL, only 3/5 of the unextracted donor samples were detected but upon extraction 5/5 of the donor samples produced detectable signal. The inclusion of

the extraction step makes seemingly bad RDTs work better, by increasing signal and thus reducing false negatives and could be invaluable to malaria management programs to enhance the performance of brands available for use.

Conclusion

This chapter describes a method for improving existing rapid diagnostic tests for the detection of malaria by adding a simple sample preparation step prior to performing the test. Regardless of the panel detection scores assigned to the selected brands by the World Health Organization, five of six brands were improved upon sample preprocessing and detected parasitemia within asymptomatic levels of infection--a regime of diagnosis that RDTs have traditionally been unable to detect. Both the visual signal and limit of detection gained a 4-fold and in some cases 100-fold enhancement. Limits of detection, after extraction, were estimated to be as low as 3 parasites/ μ L for two brands. Several labs are currently developing cell phone RDT readers, which use an algorithm similar to that was described in this chapter to convert the visual test signal to a quantitative one.[99; 101; 102] Additionally, many companies are manufacturing standalone RDT readers that can be synced up to cloud-based databases. This combination of removing test interpretation bias from the human eye with diagnostic result logging has the potential to greatly impact patient case management. By combining the basic extraction technology outlined in Chapter II with these developing resources, there is potential to provide more sensitive diagnostic tools to community health workers at the point-of-care, as the push for malaria elimination grows.

Acknowledgements

“K.M. Davis, L.E. Gibson, F.R. Haselton, and D.W. Wright, Simple sample processing enhances malaria rapid diagnostic test performance. *Analyst* 139 (2014) 3026-3031. Reproduced by permission of The Royal Society of Chemistry.”

Partial support for this work was provided by the Bill and Melinda Gates Foundation Grand Challenges in Global Health: Develop Technologies that Allow Assessment of Multiple Conditions and Pathogens at Point-of-Care. Additional support was provided through the Vanderbilt-Zambia Network for Innovations in Global Health Technologies (NIH D43 TW009348). Support for KMD was provided by an NSF Graduate Research Fellowship (GRFP2012095464). We thank M.F. Richards for critical comments concerning this manuscript. We thank Dr. Phil Thuma and Dr. Sungano Mharakurwa for their support in this work.

CHAPTER VII

FUTURE DIRECTIONS: TOWARD DEVELOPMENT OF A NEW RAPID DIAGNOSTIC PLATFORM FOR MALARIA DETECTION

Introduction

Throughout this dissertation, there have been discussions about the current state of the malaria epidemic, what populations need to be targeted for diagnosis, current strategies for point-of-care diagnosis, as well as potential alternative assays for sensitive detection of malaria. If one were to visit a local health outpost, one would observe that the lateral flow diagnostic tests discussed in Chapter V are the most widely used diagnostic tests, not only for malaria but for other infectious diseases. When considering a level 0, in the village, diagnostic scenario, this is not a coincidence. The characteristic ease of use, rapid time to result, and low cost of these tests promote their widespread use at the point of care (POC). There is an estimated need for 1.4 billion malaria tests in Africa alone, between the years of 2013-2016.[7] While current innovations toward new point of care diagnostic tools show promise, is a complete reworking of the system the best pathway for timely malaria elimination?

In December 2011, the Bill and Melinda Gates Foundation announced over \$31 million dollars in grants to fund new, innovative ideas for POC diagnostics in developing nations.[103] As a part of the Point of Care Diagnostics (POC Dx) Initiative, these grants were aimed at “developing new technologies and identifying implementation issues to address the key barriers for clinical diagnostics in the developing world.” Several academic and government labs and industrial teams were funded, in this first phase, to address what were deemed the key components of a POC diagnostic: sample collection, sample preparation, sample detection, and diagnostic implementation. The Wright and Haselton labs were funded under this initiative for

sample preparation, which lead to the development of the extraction cassette outlined in Chapter II and other publications. The goal of the first phase was to identify and select key players from each diagnostic component class to move on to a Phase 2 funding period. This phase would involve integration and further development of the design, validation of the assays, and potential partnership with industrial manufacturers. The Wright and Haselton labs were again selected for funding, but for a “phase 1.5” part of the program. As opposed to integrating components from the first phase, the foundation selected four of the 23 teams to instead design their own diagnostic “box,” in this 1.5 phase, to meet a certain target product profile for ELISA, nucleic acid testing (NAT), clinical chemistry and cell counting, in which part of the efforts toward automated ELISA tests for *pf*HRP II are outlined in Appendix C. This type of innovative research and development is absolutely necessary as the push for new tools to meet emerging challenges in infectious disease research grows. However, when considering the case of malaria as a part of the Accelerate to Zero campaign, the timescale to reach malaria elimination by 2025 does not seem to support a reworking of the current system.[104]

In order to find and treat all cases of malaria before the threat of drug resistance, sensitive diagnostic tools for asymptomatic patients must be rolled out as soon as possible. Chapter II outlined the development of an extraction cassette for rapid purification and concentration of *pf*HRP II from a blood sample. Preliminary data suggested that application of the concentrated product to commercially available malaria RDTs served to improve the sensitivity of these tests 8-fold. Upon further investigation, as outlined in Chapter VI, this extraction method improved a six different brands of malaria RDTs of varying performance levels (according to the WHO RDT report). It was found that the limits of detection were reduced by an order of magnitude, and there was significant improvement in variability between replicate tests. Despite these results,

the extraction cassette, in its present form, was likely too complicated for a level 0 community health worker to operate, as an off-line sample preparation step before RDT development. In order to maintain this level of RDT enhancement but improve the user experience, the extraction protocol was streamlined to only require one off-line extraction step while maintaining the same level of performance as seen with the entire extraction cassette. This chapter outlines the pathway to this discovery, validation of the enhancement against results from Chapter VI, design of the RDT garage for ease of use, as well as future directions toward implementation in the field.

Materials

Ni(II)NTA magnetic agarose particles (Cat # 36111) were purchased from Qiagen Inc. Co(II)NTA magnetic particles (Cat # Cat #10103D) were purchased from Life Technologies. Pooled human whole blood collected in CPD (Cat# HMWBPCPD) was purchased from Bioreclamation LLC. Paracheck Pf RDTs (Cat# 30301025) were acquired from Orchid Biomedical Systems. 500 μ L flat cap PCR tubes (Cat# AB-0350) were purchased from Fisher Scientific. The RDT garage was printed on a ProJet HD 3000 plus 3D printer. All other materials were purchase from Fisher Scientific.

Methods

Proof of Concept RDT Enhancement via Elution Off-Beads

An extraction cassette was prepared as outlined in Chapter II; however the elution chamber was not included in the cassette. Two tubes were prepared with oil as the final valve after the third wash chamber. Two additional tubes were prepared with air as the final valve. A lysed blood sample at 0 and 200 parasites/ μ L was processed, as previously outlined, through both tubes. After processing, the tube was cut between the packet of beads and the Meltemp

capillary. Using a magnet, the beads were slid out of the tube and deposited directly onto the sample pad of a Paracheck RDT. Paracheck running buffer, spiked to contain 500mM imidazole, was placed on the buffer port, and the RDT was allowed to develop for 30 minutes. After developing, the lateral flow strips were taken out of the cassette, scanned, and processed as described in Chapter VI.

Proof of Concept RDT Enhancement via Elution Off-Beads without Purification

A 200 μ L PCR tube with the bottom end cut off was inserted into a 1” length of Tygon R-3603 tubing. The rounded end of a Meltemp glass capillary was inserted into the opposite end of the Tygon tubing. This Tygon tubing was filled with mineral oil, up to the cut end of the PCR tube, using a 1mL syringe fitted with a 27 ½ gauge needle. 200 μ L of lysed and filtered whole blood, spiked to contain 200 parasites/ μ L, was added to the PCR tube with 10 μ L of Ni(II)NTA magnetic beads. Three tubes were made at this concentration. The tubes were placed on a rotisserie for 10 minutes. After 10 minutes, a magnet was used to pull the beads out of the blood and into the oil in the Tygon tubing. The tubing was cut between the packet of beads and the Meltemp capillary tubing. Using the magnet, the beads were slid out of the oil and deposited directly onto the sample pad of a Paracheck RDT. Paracheck running buffer, spiked to contain 500mM imidazole, was placed on the buffer port, and the RDT was allowed to develop for 30 minutes. After developing, the lateral flow strips were taken out of the cassette, scanned, and processed as described in Chapter VI.

RDT Enhancement using the RDT Garage

After designing a prototype “hands-free” device for RDT enhancement, a workflow was established for magnetic bead deposition on the RDT strip. The first prototype can be seen in Figure 62 as a frame of reference. Briefly, a 100 μ L lysed blood sample was incubated with



Figure 62. Prototype RDT garage.

20 μ L of Ni(II)NTA magnetic beads for 10 minutes on a benchtop vortexer. During mixing, the RDT was removed from the packaging and inserted into the garage with the buffer port going in first. After mixing, the sample with the beads was transferred to the bottom of a 500 μ L PCR tube, whose bottom was cut off using a razor blade, using a plastic transfer pipette. This was done by holding the cut PCR tube with the closed cap side down and inserting the sample from the top of the cut side with the transfer pipette. The cut PCR tube was inverted right side up and placed in the sample port of the RDT garage (Note: Surface tension within the PCR tube with the cap closed keeps the fluid inside. It is important to keep the cap closed during this process, otherwise the sample flows out of the tube.) The tube was allowed to rest within the garage for 30 seconds to collect the magnetic beads at the bottom of the tube, via the presence of the magnet. After 30 seconds, the top of the PCR tube was gently depressed to blot the beads on to the sample pad. (Note: Some blood will also transfer.) The RDT was removed from the garage prior to adding 4 drops of imidazole modified running buffer. (Note: To modify any RDT

brand's running buffer, the buffer is spiked to contain 500mM imidazole). The RDT was allowed to develop for 30 minutes prior to removing from cassette for image processing.

Haiti Field Trial Workflow

A weeklong field trial using the RDT garage was conducted alongside St. Matthew's Catholic Church's annual medical mission in January 2014 in Gobert, Haiti. If a patient at the clinic was suspected to have malaria, they were sent to the malaria testing station and diagnosed using a Paracheck RDT. The patient's finger (or heel if the patient was an infant or toddler) was cleaned with an alcohol swab prior to pricking their finger. Using the blood collection wand in the RDT packet, 5 μ l of the patient's blood was run on the RDT, per manufacturer's instructions. After 20 minutes, the patient was informed of the result. Using a glass capillary tube, regulated to hold 200 μ L of blood, 50-100 μ L of the patient's blood was then collected for enhancement data. (Note: The results of the enhancement was not shared with the patient, as the enhancement method being tested is not CLIA, Clinical Laboratory Improvement Amendments, waived.) 100 μ L of lysis buffer was pipetted into the top end of the glass capillary to flush and simultaneously lyse the blood sample into a 500 μ L PCR tube. To this lysed sample, 20 μ L of Ni(II)NTA agarose magnetic beads were added and vortexed using a modified, battery powered personal massager. Dr. Nick Adams of the Haselton laboratory was the originator of this idea. Holes were drilled into the cup of the massager to act as tube holders. Upon turning on the massager, with the tubes in place, the motor motion acted to vortex the samples. The workflow proceeded as previously mentioned in the preceding RDT garage method. The lateral flow strips for the enhanced and unenhanced tests were labeled and saved. Additionally, blood spots were obtained for each patient for later analysis by ELISA or PCR.

Results and Discussion

On-RDT Elution of pfHRP II for RDT Signal Generation

In Chapter II and Chapter VI, enhancement of commercially available RDTs was demonstrated upon extraction and concentration of *pfHRP II* from a 100 μ L whole blood sample into a 10 μ L purified solution. If the protein could be eluted off the particles, directly on the RDT sample pad surface, this could serve to reduce processing steps toward RDT enhancement. To prove this concept, the *pfHRP II* bound Ni(II)NTA beads were processed through the extraction cassette. However, instead of eluting the bound protein, the beads were deposited directly onto the RDT sample pad using a magnet. A strong signal was observed on the test line, from a 200 parasites/ μ L sample (365.2 integrated area vs. 474.6 when eluted in solution prior to placement on the RDT), when the running buffer was spiked to contain 500mM imidazole (Figure 63). When compared to an unextracted sample, a 3-fold enhancement was observed. This is slightly less than what was reported in Chapter VI (4-fold enhancement using an eluted sample from the extraction cassette). When the beads are blotted on the sample pad of the RDT, they are often in

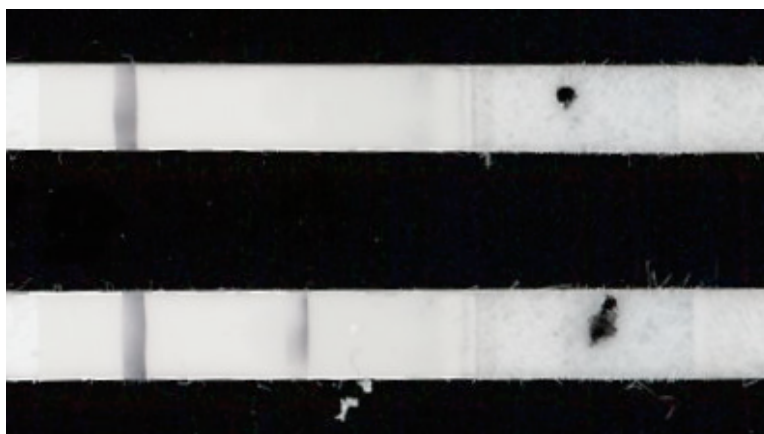


Figure 63. On-RDT enhancement from a negative (0 parasites/ μ L) and positive (200 parasites/ μ L) lysed blood sample.

a tight packet, instead of uniformly dispersed across the pad. This phenomenon likely contributes to the decrease in observed enhancement, because imidazole is unable to penetrate the center of the packet to fully elute the bound protein. Regardless, as a proof of concept, it was demonstrated that the protein could be eluted off the beads directly on the RDT without prior elution.

RDT Enhancement without Purification Steps

Lateral flow strips have inherent purification qualities, as the flow of proteins is guided down the nitrocellulose strip by wicking action. When a 5 μ L blood sample is applied to the



Figure 64. Proof of concept RDT enhancement without sample purification.

RDT, the hemoglobin and other cellular debris is cleared by the strip to yield a test and control line with little background (given proper manufacturing of the strips). High purity of extracted *p*fHRP II was necessary for molecular based detection methods; however, it seemed that RDT enhancement was governed mainly from applying a more concentrated sample to the pad in an equivalent volume normally used on the tests. To test this hypothesis, the beads needed to be deposited on the strip without any wash steps. It was previously determined that the carryover volume of 10 μ L of Ni(II)NTA beads from an aqueous solution was around 1 μ L. If 20 μ L of *p*fHRP II bound beads were deposited on the RDT, theoretically only 2-3 μ L of liquid would accompany that bead packet. After incubation with a 200 parasites/ μ L lysed blood sample, the

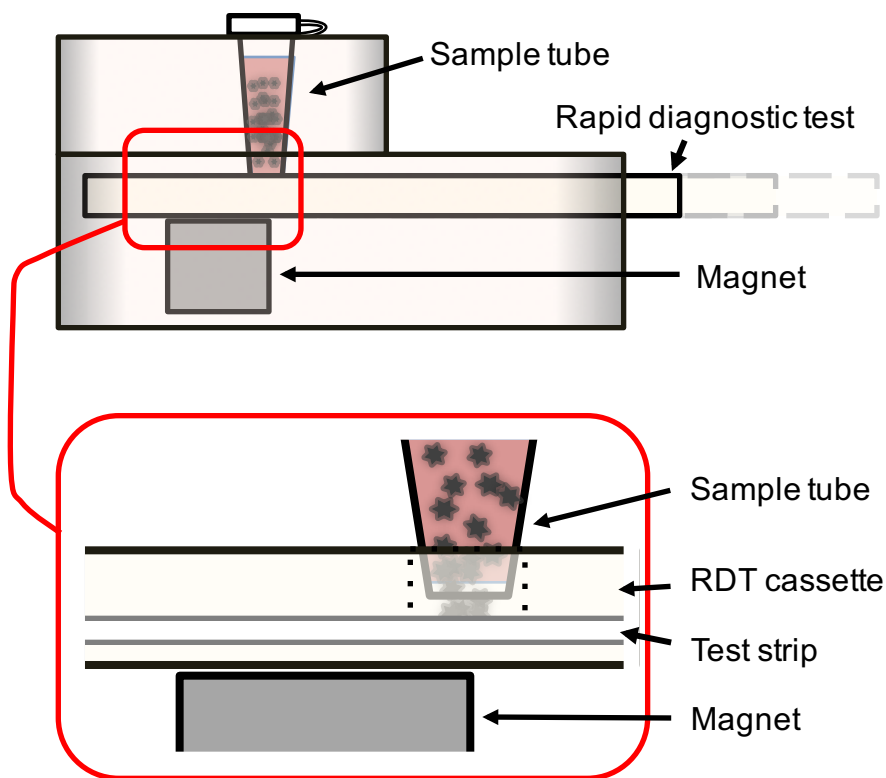


Figure 65. General schematic of the RDT garage. Image graciously provided by Dr. Nick Adams.

beads were transferred through an oil valve and deposited on the RDT strip. Flowing imidazole modified running buffer over the bead packet yielded an integrated peak area (test line) of 412.8, which agreed very well with the peak area determined in Chapter VI (474.6) (Figure 64). This result confirmed that the observed enhancement was driven predominantly by concentration of *p*fHRPII as opposed to both concentration and purification using the full extraction cassette.

Design and Evaluation of a User-Enabled Device for RDT Enhancement

Given the proof of concept that RDTs could be enhanced by delivering *p*fHRPII bound magnetic particles directly to the RDT pad, a prototype device was designed to better aid an endpoint user in the enhancement workflow. When considering the workflow, the major components of a device needs to include: a) sample tube, b) magnet, and c) plastic housing to

orient the RDT and sample tube. After sketching out a design, our collaborators in the Haselton laboratory 3D printed a device we deemed the RDT Garage. As can be seen in Figure 65, the RDT Garage was designed seamlessly integrate with current RDT cassette designs. There is a port in the 3D printed housing for the sample and the buffer, as well as a viewing window for the test result. Underneath the RDT is a fixed 0.75” magnet. This magnet serves to collect the beads, after incubation, for deposition on the test.



Figure 66. Comparison of Paracheck RDT unenhanced (top) and enhanced using the RDT garage (bottom) at 200 parasites/ μ L.

To test the design, 500 μ L thin walled PCR tubes were cut at the bottom to leave a hole approximately 1mm in diameter. This would allow the biomarker bound magnetic beads to be deposited on the sample pad of the RDT. A filtered, lysed blood sample at 200 parasites/ μ L was incubated with the Ni(II)NTA magnetic particles in an uncut PCR tube. After incubation, the blood and beads were transferred from this tube to the cut PCR tube and inserted into the garage. Upon blotting the particles on the pad and eluting the protein with modified running buffer,

enhancement over an unextracted sample was observed (Figure 66). The integrated area of the enhanced RDT was similar to that observed from a fully eluted sample from Chapter VI.

Previous data had shown that the 50 μ m agarose beads were unable to pass through an aqueous/air interface, due to their high porosity and density. While the blotting method was proven to work well for RDT enhancement, a small volume (5-10 μ L) of lysed blood is transferred to the sample pad upon blotting. This was observed to be regulated by the size of the hole at the bottom of the sample tube and the length of time the tube was depressed on the pad to blot the beads. RDTs are manufactured to handle 100 μ L of total liquid volume. Therefore, if too much blood is transferred during the blotting process, all of the sample was unable to clear. Even though this scenario was rare in the laboratory setting, the failure mode must be taken into account when considering a community healthcare worker in a developing nation. If the magnetic particles can “jump” to the sample pad upon entering the RDT garage, this could potentially reduce user error. The 1 μ m Co(II)NTA particles were validated to be able to traverse an aqueous/air interface, and thus were tested in this design. However, it was noted that ability to traverse from the lysed blood sample to the sample pad, without blotting, was unreliable. If a meniscus formed at the base of the sample tube, the particles formed more of a ring structure around the opening and were unable to “jump” onto the sample pad. In instances where the particles were able to form a dense packet at the base of the sample tube, they were able to pass through the interface. It was also noted that these particles, when deposited on the sample pad, flowed down the lateral flow strip when the RDT was removed from the garage. Despite producing an enhanced signal at the test line, this flow obscured the signal on the test line and increased the background (Figure 67). If the test is allowed to fully develop within the garage,

the particles are held on the conjugate pad, due to the presence of the magnet. While this is a potential solution to the issue, it will slow down the throughput in the field.

In each chapter discussing sample preparation and detection using magnetic particles, the blood sample was lysed and filtered through glass wool to avoid agglomeration of the particles by the cellular debris. Regardless of the particle size or composition, this agglomeration of the particles was observed. For a level 0/level 1 diagnostic setting, the fewer patient sample processing steps the better. For normal RDT use, the patient sample is placed directly on the sample pad for diagnosis. In order to assess whether the sample needs to be filtered, lysed blood

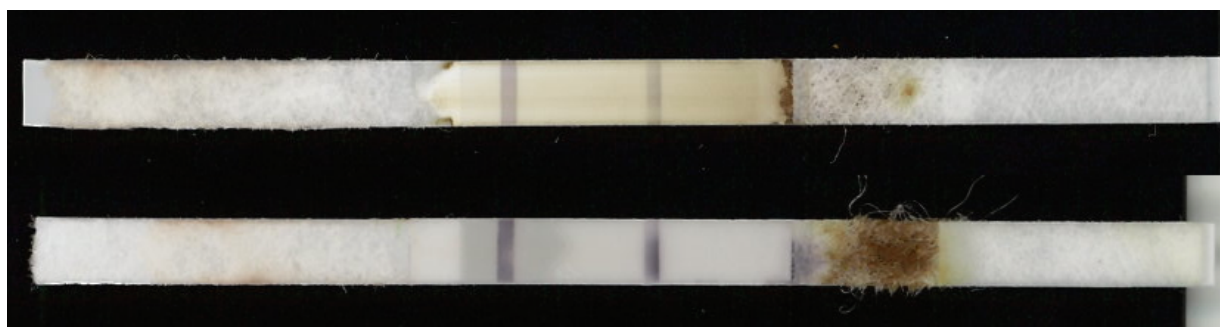


Figure 67. Flow of Co(II)NTA Dynabeads across the nitrocellulose (top strip). In the presence of a magnetic field this flow is prevented (bottom strip).

at 200 parasites/ μ L was processed using the RDT garage without filtering. Three mixing methods were used: vortexer, rotisserie (which was used for Chapter II studies), and shaking by hand. While shaking by hand depends on the user, it was included in this conceptual study as a 100% electricity free mode for mixing. It can be seen in Figure 68 that vortexing and shaking by hand yielded strong bands on the RDT (integrated area similar to lysed and filtered samples). Samples processed on the rotisserie did not perform as well, due to the gentle mixing of this method. A visual inspection of the beads after mixing showed no particle agglomeration

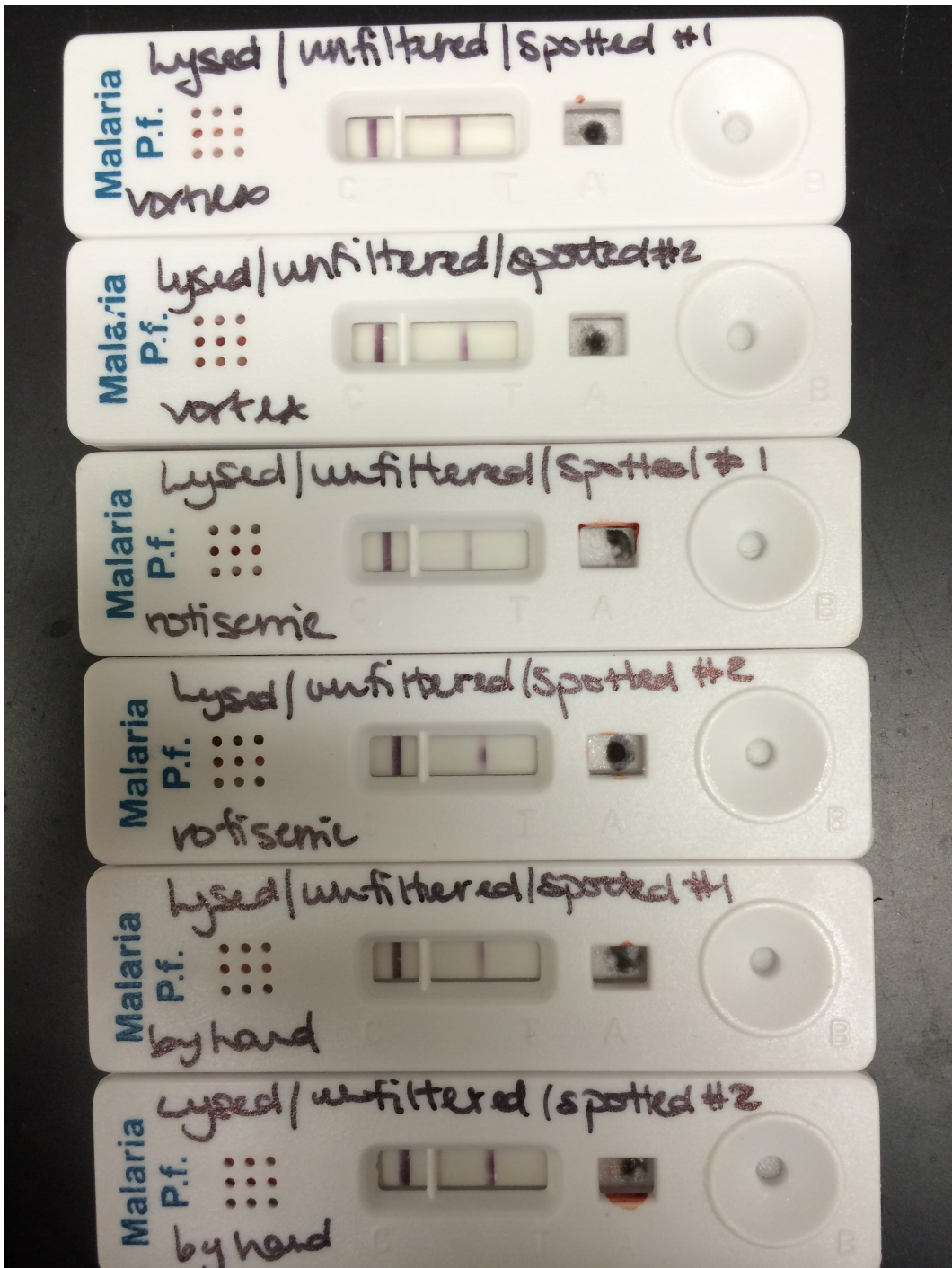


Figure 68. Effect of mixing mode on enhanced RDT signal.

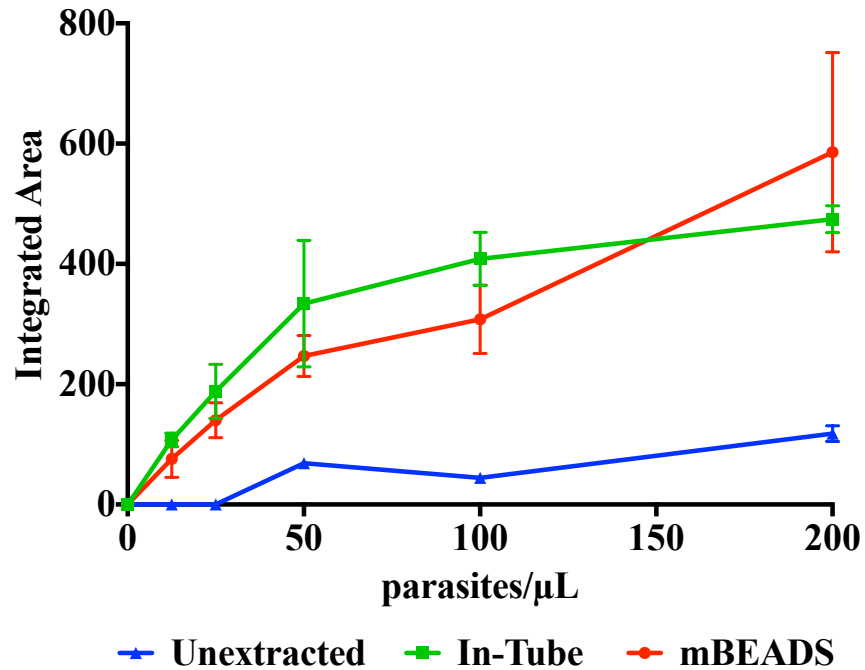


Figure 69. Comparison of Chapter VI and Chapter VII enhancement methods.

from the vortexer and mixing by hand, but the particles were gelled by the cellular debris using the rotisserie. These preliminary results were promising in helping design the field trial, to be discussed later.

Enhancement with the RDT Garage

Due to the unreliability of the 1μm Co(II)NTA particles, a full enhancement curve was generated by blotting the 50μm Ni(II)NTA agarose particles on the sample pad, within the RDT garage (Figure 69). Comparing the signal enhancement using the garage versus the previously discussed method in Chapter VI revealed significant overlap between the two methods (Figure 69- green curve vs. red curve). This is promising, in that eluting the protein from the surface of the particles directly on the RDT works as well as depositing a purified protein concentrate. Additionally, comparable enhancement was achieved by a simple 10 minute processing step as compared to the 30 minute extraction set. A 30 minute sample preparation time is ideal for well-

equipped laboratory settings, especially considering most sample preparation techniques can take several hours. However, RDTs only take 20 minutes to run. Essentially doubling the time to test is not beneficial for level 0 healthcare, despite increasing the sensitivity of these tests. Streamlining the enhancement process could potentially have great implications on the use of these rapid malaria diagnostics at the point of care.

Prototype Field Trial in Gobert, Haiti

After designing the prototype device and validating RDT enhancement over a wide range of parasitemias, we had the opportunity to test the device at the point of care. Small field trials are important when designing field deployable devices, as bottlenecks in the workflow can be identified. Using discarded blood samples from a week-long medical mission with St. Matthew Catholic Church of Franklin, TN, we tested our RDT enhancement workflow on upwards of 200



Figure 70. Processing candidate patient samples for the RDT garage field trial in Gobert, Haiti.

patients (Figure 70). Out of all the patients tested, no one was diagnosed with *P. falciparum* infection from an enhanced or an unenhanced tests. While this was a good result for the patients, it was a seemingly poor result for our field trial. Gobert is located in the mountains of central



Figure 71. Lysed candidate patient blood samples processed using the handheld mixer designed by Dr. Nick Adams.

Haiti. Additionally, January is the dry season in Haiti. The climate and geographical location of Gobert during this time of the year lead us to believe that malaria transmission was low. Despite these results, the field trial did provide some valuable insight into the workflow and how it could be improved. We expected to be able to get 100 μ L of blood from a fingerprick, but this was

proven difficult, as the blood viscosity of many patients was very high. This could be due to malnutrition and poor hydration. Some of the men had such thick calluses on their fingers, from a life of manual labor, that getting any blood from a finger prick proved challenging. In some instances, even attempting to obtain blood from the side of the finger proved difficult.

After collecting the blood from the fingerprick in the capillary tube, lysis buffer was used to flush the blood into a 500 μL PCR tube. In the time allotted to prepare for the trip, this was the best collection method we could design, but there were some flaws. There were four transfer steps between the fingerprick and sample incubation: 1) blood collection by glass capillary, 2) acquisition of 100 μL of lysis buffer via pipette, 3) flushing of the blood through the capillary with lysis buffer, and 4) addition of 20 μL of Ni(II)NTA particles. For a trained laboratory technician, use of a calibrated pipette and glass capillary tube is routine. For a community health worker, these steps are outside of the normal training received for performing RDTs. Additionally, some of the blood samples began to coagulate, even after lysis. Normal blood collection tubes have some form of anticoagulant in them (e.g. Lithium heparin, EDTA, sodium citrate). We know that citrate based anticoagulants work well for Ni(II)NTA chelation, as was demonstrated by the work in Chapter II. The glass capillary tubes employed in this trial did not have an anticoagulant coating, as it was assumed lysis was sufficient to prevent coagulation.

These observations alluded to the fact that the sample collection tube is arguably the key component in this point of care RDT enhancement device. An ideal tube would need to be designed to a) collect the patient sample, b) lyse the sample after collection via liquid or lyophilized lysis reagents and magnetic particles, c) withstand incubation for 10 minutes via vortexing, and d) have a removable bottom to allow for bead deposition on the sample pad. With such a design, RDT enhancement using magnetic beads as a sample concentrator becomes four

steps. First, the sample is collected and lysed in the sample tube. Then, the sample is mixed for 10 minutes with the handheld vortexer (Figure 71). After mixing, the bottom of the tube is snapped off and placed in the garage before the magnetic beads are transferred to the sample pad. Finally, the RDT is developed by adding modified sample buffer to the test. While further design and field testing of this device is needed, these initial results are promising for utilizing, but enhancing currently accepted diagnostic tools.

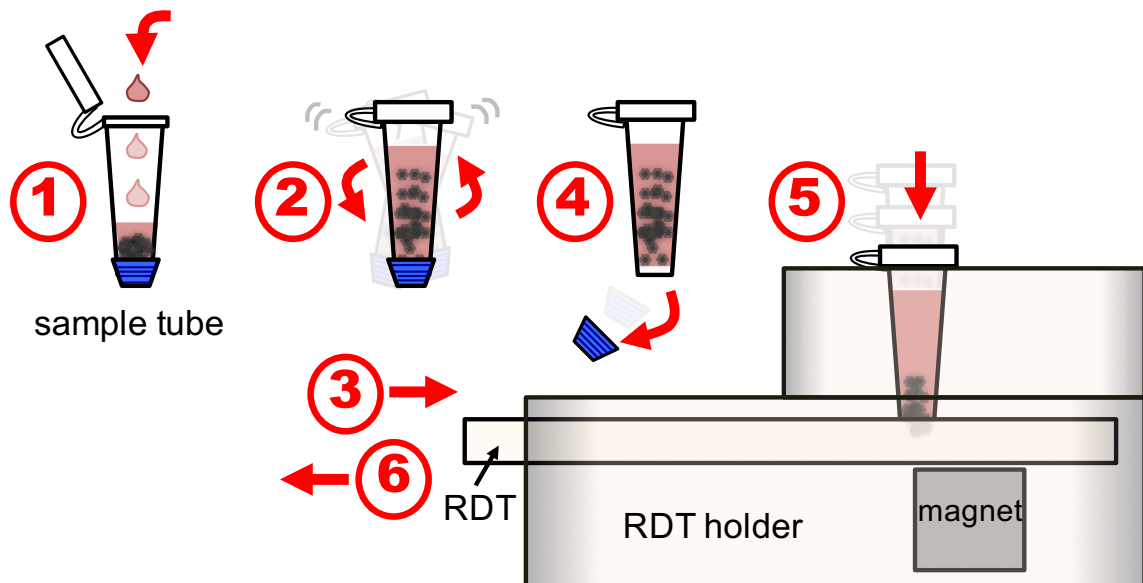
Conclusions

This chapter detailed the design of a user-enabled device for enhancing malaria rapid diagnostic tests. Taking inspiration from Chapter II and Chapter VI, the enhancement process was condensed to a single 10 minute incubation and transfer step. By modifying the manufacturer supplied running buffer to contain a high concentration of imidazole, *p*fHRPII was eluted from the surface of the particles after deposition on the sample pad. It was demonstrated that similar enhancement can be generated on the RDT with and without sample purification. The design of a 3D printed device, deemed the RDT garage, provided an easier means toward sample preparation and RDT enhancement of blood samples within the asymptomatic range of infection. Further development of this concept would allow for detection of malaria transmission reservoirs without disrupting the currently accepted diagnostic tool used at the point of care in developing nations.

Future Directions and Perspectives

The field trial in Haiti revealed many areas where the RDT garage can be improved for a second attempt at deployment. An ideal workflow using the RDT garage prototype, as is, is outlined in Figure 72. The Wright laboratory, in collaboration with the Haselton laboratory, is currently working on a second generation of this device, deemed mBEADS, where mBEADS

stands for a *magnetically-enabled biomarker enhancement and delivery system*. With funding from the Gates Foundation, PATH and Intellectual Ventures, we are beginning to explore how best to design the device to facilitate the highest signal enhancement as well as promote user experience at the point of care. While this chapter outlined the proof of concept work toward the idea that biomarker bound magnetic particles can be deposited on an RDT and signal can be enhanced after release of the biomarker, there is considerable future work that can be done to make the assay work better for *pfHRP2* and for other biomarkers of infectious disease. For the *pfHRP2* model, fully understanding the interactions at the front end of the workflow (i.e. the



- | | |
|--------------------------------------|--|
| ① Add sample to tube | ④ Break away tube cap |
| ② Mix sample with magnetic particles | ⑤ Insert tube to transfer particles to RDT |
| ③ Insert RDT into holder | ⑥ Remove test and add running buffer |

Figure 72. Ideal workflow using the RDT garage.

incubation step) will inform the signal enhancement. Theoretically, there should be a 20x enhancement in signal (100 μ L of *p*/HRP_{II} concentrated to 5 μ L particle volume). We observed anywhere between 4-13x enhancement in Chapter VI, depending on the RDT brand. In order to get as close to the theoretical maximum, we must fully optimize the buffer conditions (What concentration of blocking imidazole is necessary?), mixing strategy (Is vortexing the best method?), incubation time (Do we need more or less than 10 minutes?), sample handling (How many particles are lost during transfer steps?), and elution on the sample pad (Is all of the protein fully eluted from the particles prior to interacting with the gold conjugate?). With funding from Gates/PATH and Intellectual Ventures to explore these variables, we hope to get as close to the 20x enhancement as possible.

This system is unique for using Ni(II)NTA particles as a capture reagent, as *p*/HRP_{II} has a high affinity for M²⁺ chemistry. Additionally, imidazole facilitates rapid release of the protein without significantly affecting downstream protein interactions. Direct extension of this platform to other biomarkers of infectious disease is not as straightforward, if classical antibody/antigen pairs are used. Harsh conditions (high salt, heat, low pH) are needed to “elute” an antigen from the surface of an antibody functionalized particle; however these conditions are hard to incorporate into current RDTs without destroying the functionality of the RDT itself. To take advantage of the rapid release kinetics and compatibility of imidazole with the RDT, we are designing hexaHis-tagged antibodies for a “catch-and-release” approach toward generalizing the RDT enhancement platform. By attaching a hexa-His tag to an antibody, the Ni(II)NTA particles can be made to capture any biomarker of interest. After binding of the antigen to the antibody, the entire antigen/antibody complex is released by imidazole modified running buffer

to be captured at the test line. This could potentially allow for enhancement of a wider range of RDTs for infectious disease.

Despite these enhancement capabilities, we are ultimately limited by current RDT manufacturing practices. In the laboratory, teasing out and reducing the variability in our enhancement method can be easily done. Yet, lot to lot variability of a manufactured test cannot be controlled. The reality is there is no incentive for these manufacturers to put more resources into research and development of these tests because it is not profitable for them. As an academic laboratory, we are beginning to see ways in which these tests can be improved without completely altering the basic core of the RDT itself. A team of Wright and Haselton laboratory members took a training course at Diagnostics Consulting Network (DCN) in Carlsbad, Ca to learn the concepts of RDT design as well as make our own lateral flow test. We are taking what we learned there in addition to observations from years of RDT enhancement data to think about how we would redesign the RDT. While we are currently using the *p/HRPII* RDT as a model, we aim to extend our findings to other RDT formats for infectious disease biomarkers.

I have immense hope in the ability of our team here at Vanderbilt to make a mark in point of care diagnostics for developing nations. I firmly believe our perspective toward research and development is driven by design for what the end user needs. Visiting these countries and fully understanding their day to day life and how diagnostics fits into their standard of care is absolutely necessary for effecting a change in diagnosis of infectious disease. Many non-profit organizations are invaluable in providing funds for this research, but truly striving toward an infectious disease elimination campaign will take more than meetings and thinktanks to envision a next generation “bells and whistles” device. A prime example of this is the tribulations Cepheid has had with cost and failure of their GeneXpert instrument for tuberculosis diagnosis.[105]

There is power in simplicity, and this is evidenced by the great success of the RDT. This is why we are orienting our research to improve these devices without completely altering the understood workflow, because this technology is what community health workers know and understand. This is not to say next generation diagnostic devices cannot be utilized at the point of care, but the design should be informed by the end user, affordable, and robust. To do so, there must be crosstalk between R&D, funding agencies, and the governments in which these tools will be deployed. Additionally, there must be a push toward more policy and education at the point of care so the healthcare workers and patients fully understand the diseases we are trying to diagnose and treat as well as how our new developments will lead to a healthier future for them and generations to come. As a member of a global community, it is important to realize that all lives have value. Truly working together to ensure these lives maintain their value is how we will achieve a healthier world.

Acknowledgements

Partial support for this work was provided by the Bill and Melinda Gates Foundation Grand Challenges in Global Health: Develop Technologies that Allow Assessment of Multiple Conditions and Pathogens at Point-of-Care. Additional support was provided through the Vanderbilt-Zambia Network for Innovations in Global Health Technologies (NIH D43 TW009348). Support for KMD was provided by an NSF Graduate Research Fellowship (GRFP2012095464). We thank St. Matthew's Catholic Church Medical Mission of Franklin, TN, Our Lady of Miracles of Gobert, Haiti, and the people of Gobert for support and cooperation during the field trial.

REFERENCES

- [1] World Malaria Report 2014, World Health Organization, 2014.
- [2] Malaria Parasites, Centers for Disease Control, 2012.
- [3] Microscopic Tests, Malaria Site, 2015.
- [4] Lateral Flow Test Components, PATH, 2015.
- [5] Lateral flow tests: How they work, PATH, 2015.
- [6] G. Walther, Enabling POC Diagnostics through Standard Setting, Bill and Melinda Gates Foundation, 2012.
- [7] Malaria Diagnostics Technology and Market Landscape, UNITAID, 2014.
- [8] M. Doucleff, Dr. Seuss on Malaria: 'This is Ann... She Drinks Blood.', National Public Radio, 2012.
- [9] L.J. Panton, P. McPhie, W. Lee Maloy, T.E. Wellems, D.W. Taylor, and R.J. Howard, Purification and partial characterization of an unusual protein of Plasmodium falciparum: histidine-rich protein II. *Molecular and Biochemical Parasitology* 35 (1989) 149-160.
- [10] The History of Malaria, An Ancient Disease, Centers for Disease Control, 2012.
- [11] Lifecycle of Malaria, National Institutes of Health, 2012.
- [12] C. JM, and H. SL, *Medical Microbiology*, University of Texas Medical Branch at Galveston, Galveston, TX, 1996.
- [13] T. Bousema, L. Okell, I. Felger, and C. Drakeley, Asymptomatic malaria infections: detectability, transmissibility and public health relevance. *Nat Rev Micro* 12 (2014) 833-840.
- [14] D. Laishram, P. Sutton, N. Nanda, V. Sharma, R. Sobti, J. Carlton, and H. Joshi, The complexities of malaria disease manifestations with a focus on asymptomatic malaria. *Malaria Journal* 11 (2012) 29.

- [15] C. Ohrt, Purnomo, M.A. Sutamihardja, D. Tang, and K.C. Kain, Impact of Microscopy Error on Estimates of Protective Efficacy in Malaria-Prevention Trials. *Journal of Infectious Diseases* 186 (2002) 540-546.
- [16] D.W. Taylor, M. Parra, G.B. Chapman, M.E. Stearns, J. Rener, M. Aikawa, S. Uni, S.B. Aley, L.J. Panton, and R.J. Howard, Localization of *Plasmodium falciparum* histidine-rich protein 1 in the erythrocyte skeleton under knobs. *Molecular and Biochemical Parasitology* 25 (1987) 165-174.
- [17] E. Rock, K. Marsh, A. Saul, T. Wellems, D. Taylor, W. Maloy, and R. Howard, Comparative analysis of the *Plasmodium falciparum* histidine-rich proteins HRP-I, HRP-II, and HRP-III in malaria parasites of diverse origin. *Parasitology* 95 (1987) 209-227.
- [18] P. Verma, S. Biswas, T. Mohan, S. Ali, and D.N. Rao, Detection of histidine rich protein & lactate dehydrogenase of *Plasmodium falciparum* in malaria patients by sandwich ELISA using in-house reagents. *The Indian Journal of Medical Research* 138 (2013) 977-987.
- [19] I.M. Bashir, N. Otsyula, G. Awinda, M. Spring, P. Schneider, and J.N. Waitumbi, Comparison of PfHRP-2/pLDH ELISA, qPCR and Microscopy for the Detection of *Plasmodium* Events and Prediction of Sick Visits during a Malaria Vaccine Study. *PLoS ONE* 8 (2013) e56828.
- [20] C. Murray, and J. Bennett, Rapid Diagnosis of Malaria. *Interdiscip Perspect Infect Dis* 2009 (2009) 415953.
- [21] D. Bell, and R.W. Peeling, Evaluation of rapid diagnostic tests: malaria. *Nature Reviews Microbiology* 4 (2006) S34.
- [22] Mapping the landscape of diagnostics for sexually transmitted infections., 2002.
- [23] V. Gubala, L.F. Harris, A.J. Ricco, M.X. Tan, and D.E. Williams, Point of Care Diagnostics: Status and Future. *Analytical Chemistry* 84 (2011) 487-515.
- [24] V. Linder, S.K. Sia, and G.M. Whitesides, Reagent-Loaded Cartridges for Valveless and Automated Fluid Delivery in Microfluidic Devices. *Analytical Chemistry* 77 (2004) 64-71.
- [25] P. Yager, G.J. Domingo, and J. Gerdes, Point-of-Care Diagnostics for Global Health. *Annual Review of Biomedical Engineering* 10 (2008) 107-144.

- [26] R.S. Gaster, D.A. Hall, and S.X. Wang, nanoLAB: An ultraportable, handheld diagnostic laboratory for global health. *Lab on a Chip* 11 (2011) 950-956.
- [27] P. Yager, T. Edwards, E. Fu, K. Helton, K. Nelson, M.R. Tam, and B.H. Weigl, Microfluidic diagnostic technologies for global public health. *Nature* 442 (2006) 412+.
- [28] H. Parsa, C.D. Chin, P. Mongkolwisetwara, B.W. Lee, J.J. Wang, and S.K. Sia, Effect of volume- and time-based constraints on capture of analytes in microfluidic heterogeneous immunoassays. *Lab on a Chip* 8 (2008) 2062-2070.
- [29] D.J. Beebe, G.A. Mensing, and G.M. Walker, Physics and applications of microfluidics in biology. *Annual Review of Biomedical Engineering* 4 (2002) 261-286.
- [30] C. Lui, N. Cady, and C. Batt, Nucleic Acid-based Detection of Bacterial Pathogens Using Integrated Microfluidic Platform Systems. *Sensors* 9 (2009) 3713-3744.
- [31] K.M. Schilling, A.L. Lepore, J.A. Kurian, and A.W. Martinez, Fully Enclosed Microfluidic Paper-Based Analytical Devices. *Analytical Chemistry* 84 (2012) 1579-1585.
- [32] A.W. Martinez, S.T. Phillips, and G.M. Whitesides, Three-dimensional microfluidic devices fabricated in layered paper and tape. *Proceedings of the National Academy of Sciences* 105 (2008) 19606-19611.
- [33] K. Sur, S.M. McFall, E.T. Yeh, S.R. Jangam, M.A. Hayden, S.D. Stroupe, and D.M. Kelso, Immiscible Phase Nucleic Acid Purification Eliminates PCR Inhibitors with a Single Pass of Paramagnetic Particles through a Hydrophobic Liquid. *The Journal of Molecular Diagnostics* 12 (2010) 620-628.
- [34] S.M. Berry, E.T. Alarid, and D.J. Beebe, One-step purification of nucleic acid for gene expression analysis via Immiscible Filtration Assisted by Surface Tension (IFAST). *Lab on a Chip* 11 (2011) 1747-1753.
- [35] S. Mitsuhiro Shikida and Kentaro Takayanagi and Hiroyuki Honda and Hiroshi Ito and Kazuo, Development of an enzymatic reaction device using magnetic bead-cluster handling. *Journal of Micromechanics and Microengineering* 16 (2006) 1875.
- [36] D. Chen, M. Mauk, X. Qiu, C. Liu, J. Kim, S. Ramprasad, S. Ongagna, W. Abrams, D. Malamud, P. Corstjens, and H. Bau, An integrated, self-contained microfluidic cassette for

isolation, amplification, and detection of nucleic acids. *Biomedical Microdevices* 12 (2010) 705-719.

[37] K. D.M., S. K., and P. Z., *Barriers for Facilitating Biological Reactions*, Northwestern University, US, 2009.

[38] S. Berry, L. Strotman, J. Kueck, E. Alarid, and D. Beebe, Purification of cell subpopulations via immiscible filtration assisted by surface tension (IFAST). *Biomedical Microdevices* 13 (2011) 1033-1042.

[39] G.P. Stone, R. Mernaugh, and F.R. Haselton, Virus detection using filament-coupled antibodies. *Biotechnology and Bioengineering* 91 (2005) 699-706.

[40] H. Bordelon, N.M. Adams, A.S. Klemm, P.K. Russ, J.V. Williams, H.K. Talbot, D.W. Wright, and F.R. Haselton, Development of a Low-Resource RNA Extraction Cassette Based on Surface Tension Valves. *ACS Applied Materials & Interfaces* 3 (2011) 2161-2168.

[41] N.M. Adams, A.E. Creecy, C.E. Majors, B.A. Wariso, P.A. Short, D.W. Wright, and F.R. Haselton, Design criteria for developing low-resource magnetic bead assays using surface tension valves. *Biomicrofluidics* 7 (2013) 014104.

[42] P. Ghimire, J.C. Samantaray, B.R. Mirdha, A.K. Patra, and A.K. Panda, Purification and partial characterization of PfHRP-II protein of *Plasmodium falciparum*. *Southeast Asian Journal of Tropical Medicine and Public Health* 34 (2003) 739-743.

[43] J.D. Swartz, C.P. Gulka, F.R. Haselton, and D.W. Wright, Development of a Histidine-Targeted Spectrophotometric Sensor Using Ni(II)NTA Functionalized Au and Ag Nanoparticles. *Langmuir* 27 (2011) 15330-15339.

[44] D.C. Harris, *Quantitative Chemical Analysis*, W.H. Freeman and Company, 2007.

[45] A.L. Jones, M.D. Hulett, and C.R. Parish, Histidine-rich glycoprotein: A novel adaptor protein in plasma that modulates the immune, vascular and coagulation systems. *Immunol Cell Biol* 83 (2005) 106-118.

[46] W.T. Morgan, The histidine-rich glycoprotein of serum has a domain rich in histidine, proline, and glycine that binds heme and metals. *Biochemistry* 24 (1985) 1496-1501.

- [47] I.K.H. Poon, K.K. Patel, D.S. Davis, C.R. Parish, and M.D. Hulett, Histidine-rich glycoprotein: the Swiss Army knife of mammalian plasma. *Blood* 117 (2011) 2093-2101.
- [48] R.L. Lundblad, Considerations for the Use of Blood Plasma and Serum for Proteomic Analysis. *The Internet Journal of Genomics and Proteomics* 1 (2005).
- [49] A.L. Golden, C.F. Battrell, S. Pennell, A.S. Hoffman, J. J. Lai, and P.S. Stayton, Simple Fluidic System for Purifying and Concentrating Diagnostic Biomarkers Using Stimuli-Responsive Antibody Conjugates and Membranes. *Bioconjugate Chemistry* 21 (2010) 1820-1826.
- [50] M. de Souza Castilho, T. Laube, H. Yamanaka, S. Alegret, and M.I. Pividori, Magneto Immunoassays for Plasmodium falciparum Histidine-Rich Protein 2 Related to Malaria based on Magnetic Nanoparticles. *Analytical Chemistry* 83 (2011) 5570-5577.
- [51] P. Lodemann, G. Schorer, and B. Frey, Wrong molar hemoglobin reference values-a longstanding error that should be corrected. *Annals of Hematology* 89 (2010) 209.
- [52] A. Kuzmenko, S. Tankov, B.P. English, I. Tarassov, T. Tenson, P. Kamenski, J. Elf, and V. Hauryliuk, Single molecule tracking fluorescence microscopy in mitochondria reveals highly dynamic but confined movement of Tom40. *Sci. Rep.* 1 (2011).
- [53] A. Sassolas, B.D. Leca-Bouvier, and L.J. Blum, DNA Biosensors and Microarrays. *Chemical Reviews* 108 (2007) 109-139.
- [54] A. Miyawaki, A. Sawano, and T. Kogure, Review: Lighting up cells: labelling proteins with fluorophores. *Nature Cell Biology* 5 (2003) S1-S7.
- [55] M. Liu, C. Jia, Y. Huang, X. Lou, S. Yao, Q. Jin, J. Zhao, and J. Xiang, Highly sensitive protein detection using enzyme-labeled gold nanoparticle probes. *Analyst* 135 (2010) 327-331.
- [56] X. Michalet, F.F. Pinaud, L.A. Bentolila, J.M. Tsay, S. Doose, J.J. Li, G. Sundaresan, A.M. Wu, S.S. Gambhir, and S. Weiss, Quantum Dots for Live Cells, in Vivo Imaging, and Diagnostics. *Science* 307 (2005) 538-544.
- [57] A. Thibon, and V. Pierre, Principles of responsive lanthanide-based luminescent probes for cellular imaging. *Analytical and Bioanalytical Chemistry* 394 (2009) 107-120.

[58] T. Steinkamp, and U. Karst, Detection strategies for bioassays based on luminescent lanthanide complexes and signal amplification. *Analytical and Bioanalytical Chemistry* 380 (2004) 24-30.

[59] E. Holder, B.M.W. Langeveld, and U.S. Schubert, New Trends in the Use of Transition Metal–Ligand Complexes for Applications in Electroluminescent Devices. *Advanced Materials* 17 (2005) 1109-1121.

[60] P.S. Wagenknecht, and P.C. Ford, Metal centered ligand field excited states: Their roles in the design and performance of transition metal based photochemical molecular devices. *Coordination Chemistry Reviews* 255 (2011) 591-616.

[61] S. Lamansky, P. Djurovich, D. Murphy, F. Abdel-Razzaq, H.-E. Lee, C. Adachi, P.E. Burrows, S.R. Forrest, and M.E. Thompson, Highly Phosphorescent Bis-Cyclometalated Iridium Complexes: Synthesis, Photophysical Characterization, and Use in Organic Light Emitting Diodes. *Journal of the American Chemical Society* 123 (2001) 4304-4312.

[62] M.-L. Ho, Y.-A. Chen, T.-C. Chen, P.-J. Chang, Y.-P. Yu, K.-Y. Cheng, C.-H. Shih, G.-H. Lee, and H.-S. Sheu, Synthesis, structure and oxygen-sensing properties of Iridium(III)-containing coordination polymers with different cations. *Dalton Transactions* 41 (2012) 2592-2600.

[63] N.D. McDaniel, F.J. Coughlin, L.L. Tinker, and S. Bernhard, Cyclometalated Iridium(III) Aquo Complexes: Efficient and Tunable Catalysts for the Homogeneous Oxidation of Water. *Journal of the American Chemical Society* 130 (2007) 210-217.

[64] D.-L. Ma, W.-L. Wong, W.-H. Chung, F.-Y. Chan, P.-K. So, T.-S. Lai, Z.-Y. Zhou, Y.-C. Leung, and K.-Y. Wong, A Highly Selective Luminescent Switch-On Probe for Histidine/Histidine-Rich Proteins and Its Application in Protein Staining. *Angewandte Chemie International Edition* 47 (2008) 3735-3739.

[65] Y. You, and W. Nam, Photofunctional triplet excited states of cyclometalated Ir(III) complexes: beyond electroluminescence. *Chemical Society Reviews* (2012).

[66] Q. Zhao, M. Yu, L. Shi, S. Liu, C. Li, M. Shi, Z. Zhou, C. Huang, and F. Li, Cationic Iridium(III) Complexes with Tunable Emission Color as Phosphorescent Dyes for Live Cell Imaging. *Organometallics* 29 (2010) 1085-1091.

- [67] C. Li, M. Yu, Y. Sun, Y. Wu, C. Huang, and F. Li, A Nonemissive Iridium(III) Complex That Specifically Lights-Up the Nuclei of Living Cells. *Journal of the American Chemical Society* 133 (2011) 11231-11239.
- [68] G. Park, and J. Seo, New Heteroleptic Tris-Cyclometalated Iridium(III) Complexes Containing Difluorophenylpyridine and Phenylpyridine. *Journal of the Korean Physical Society* 50 (2007) 1729-1734.
- [69] E.L. Schneider, and M.A. Marletta, Heme Binding to the Histidine-Rich Protein II from *Plasmodium falciparum*†. *Biochemistry* 44 (2004) 979-986.
- [70] J. Ziegler, R.T. Chang, and D.W. Wright, Multiple-Antigenic Peptides of Histidine-Rich Protein II of *Plasmodium falciparum*: Dendrimeric Biomineralization Templates. *Journal of the American Chemical Society* 121 (1999) 2395-2400.
- [71] B. Schmid, F.O. Garces, and R.J. Watts, Synthesis and characterizations of cyclometalated iridium(III) solvento complexes. *Inorganic Chemistry* 33 (1994) 9-14.
- [72] J. Xu, C. Yang, B. Tong, Y. Zhang, L. Liang, and M. Lu, The Effects of Different Solvents and Excitation Wavelength on the Photophysical Properties of Two Novel Ir(III) Complexes Based on Phenylcinnoline Ligand. *Journal of Fluorescence* (2013) 1-11.
- [73] B. Verity, and S.W. Bigger, The dependence of quinine fluorescence quenching on ionic strength. *International Journal of Chemical Kinetics* 28 (1996) 919-923.
- [74] P. Atkins, and J. De Paula, *Physical Chemistry*, Oxford University Press, 2006.
- [75] S. Haneder, *Correlation Between Electronic Structure and Light Emission Properties in Phosphorescent Emitters*, Physics, Ludwig-Maximilian-Universitat Munchen, Munich, 2009.
- [76] D.A. Giljohann, and C.A. Mirkin, Drivers of biodiagnostic development. *Nature* 462 (2009) 461-464.
- [77] K.M. Davis, J.D. Swartz, F.R. Haselton, and D.W. Wright, Low-Resource Method for Extracting the Malarial Biomarker Histidine-Rich Protein II To Enhance Diagnostic Test Performance. *Analytical Chemistry* 84 (2012) 6136-6142.

[78] R.M. Lequin, Enzyme Immunoassay (EIA)/Enzyme-Linked Immunosorbent Assay (ELISA). *Clinical Chemistry* 51 (2005) 2415-2418.

[79] Overview of ELISA, Life Technologies, 2015.

[80] S. Zhang, A. Garcia-D'Angeli, J.P. Brennan, and Q. Huo, Predicting detection limits of enzyme-linked immunosorbent assay (ELISA) and bioanalytical techniques in general. *Analyst* 139 (2014) 439-445.

[81] M. Robers, F.F. Van der Hulst, M.A.J.G. Fischer, W. Roos, C.E. Salud, H.-G. Eisenwiener, and J.F.C. Glatz, Development of a Rapid Microparticle-enhanced Turbidimetric Immunoassay for Plasma Fatty Acid-binding Protein, an Early Marker of Acute Myocardial Infarction. *Clinical Chemistry* 44 (1998) 1564-1567.

[82] D.A.A. Vignali, Multiplexed particle-based flow cytometric assays. *Journal of Immunological Methods* 243 (2000) 243-255.

[83] F. Liu, Y. Li, X.-L. Su, M. Slavik, Y. Ying, and J. Wang, QCM immunosensor with nanoparticle amplification for detection of *Escherichia coli* O157:H7. *Sensing and Instrumentation for Food Quality and Safety* 1 (2007) 161-168.

[84] H.-T. Kuo, J.Z. Yeh, P.-H. Wu, C.-M. Jiang, and M.-C. Wu, Application of immunomagnetic particles to enzyme-linked immunosorbent assay (ELISA) for improvement of detection sensitivity of HCG. *Journal of Immunoassay and Immunochemistry* 33 (2012) 377-387.

[85] F.M. Rubio, J.A. Itak, A.M. Scutellaro, M.Y. Selisker, and D.P. Herzog, Performance characteristics of a novel magnetic - particlebased enzyme - linked immunosorbent assay for the quantitative analysis of atrazine and related triazines in water samples. *Food and Agricultural Immunology* 3 (1991) 113-125.

[86] R. De Palma, G. Reekmans, W. Laureyn, G. Borghs, and G. Maes, The Optimization of Magnetosandwich Assays for the Sensitive and Specific Detection of Proteins in Serum. *Analytical Chemistry* 79 (2007) 7540-7548.

[87] Ni-NTA Magnetic Agarose Beads Handbook, 2001.

[88] I. Buchwalow, V. Samoilova, W. Boecker, and M. Tiemann, Non-specific binding of antibodies in immunohistochemistry: fallacies and facts. *Scientific Reports* 1 (2011) 28.

- [89] J. Tate, and G. Ward, Interferences in Immunoassay. *The Clinical Biochemist Reviews* 25 (2004) 105-120.
- [90] R. Davies, *Handbook of Biosensors and Biochips*, John Wiley and Sons, 2007.
- [91] C.K. Murray, R.A. Gasser, A.J. Magill, and R.S. Miller, Update on Rapid Diagnostic Testing for Malaria. *Clinical Microbiology Reviews* 21 (2008) 97-110.
- [92] S. Tsuda, M. Kameya-Iwaki, K. Hanada, Y. Kouda, M. Hikata, and K. Tomaru, A novel detection and identification technique for plant viruses: Rapid immunofilter paper assay (RIPA). *Plant Disease* 76 (1992) 466-469.
- [93] N. Tangpukdee, C. Duangdee, P. Wilairatana, and S. Krudsood, Malaria Diagnosis: A Brief Review. *Korean J Parasitol* 47 (2009) 93-102.
- [94] C.K. Murray, and J.W. Bennett, Rapid Diagnosis of Malaria. *Interdisciplinary Perspectives on Infectious Diseases* 2009 (2009).
- [95] D. Bell, and M. Perkins, Malaria Diagnostics: Lighting the Path. in: H.M. Staines, and S. Krishna, (Eds.), *Treatment and Prevention of Malaria*, Springer Basel, 2012, pp. 293-307.
- [96] Malaria Rapid Diagnostic Test Performance: Results of WHO product testing of malaria RDTs- Round 3, World Health Organization, 2011.
- [97] C. Wongsrichanalai, M.J. Barcus, S. Muth, A. Sutamihardja, and W.H. Wernsdorfer, A Review of Malaria Diagnostic Tools: Microscopy and Rapid Diagnostic Test (RDT). *The American Journal of Tropical Medicine and Hygiene* 77 (2007) 119-127.
- [98] D. Bell, C. Wongsrichanalai, and J.W. Barnwell, Ensuring quality and access for malaria diagnosis: how can it be achieved? *Nat Rev Micro* 4 (2006) 682-695.
- [99] O. Mudanyali, S. Dimitrov, U. Sikora, S. Padmanabhan, I. Navruz, and A. Ozcan, Integrated rapid-diagnostic-test reader platform on a cellphone. *Lab on a Chip* 12 (2012) 2678-2686.
- [100] L.C. Okell, T. Bousema, J.T. Griffin, A.L. Ouedraogo, A.C. Ghani, and C.J. Drakeley, Factors determining the occurrence of submicroscopic malaria infections and their relevance for control. *Nat Commun* 3 (2012) 1237.

[101] S. Shekalaghe, M. Cancino, C. Mavere, O. Juma, A. Mohammed, S. Abdulla, and S. Ferro, Clinical performance of an automated reader in interpreting malaria rapid diagnostic tests in Tanzania. *Malaria Journal* 12 (2013) 141.

[102] S. Feng, R. Caire, B. Cortazar, M. Turan, A. Wong, and A. Ozcan, Immunochromatographic Diagnostic Test Analysis Using Google Glass. *ACS Nano* 8 (2014) 3069-3079.

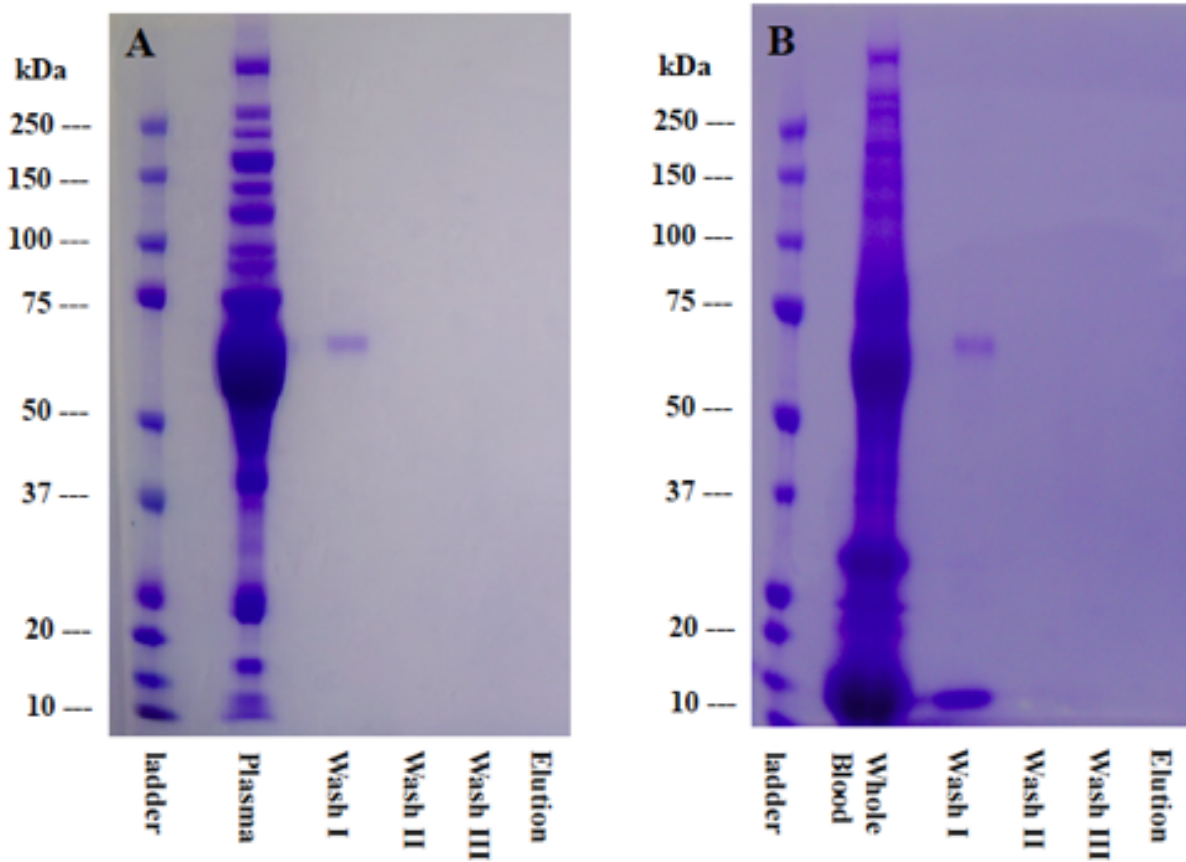
[103] Foundation and Grand Challenges Canada Announce over \$31 Million for Point-of-Care Diagnostics | Bill & Melinda Gates Foundation, Bill and Melinda Gates Foundation, 2011.

[104] A. Ghani, *Malaria 2025: Accelerate to Eliminate*, World Health Organization, 2014.

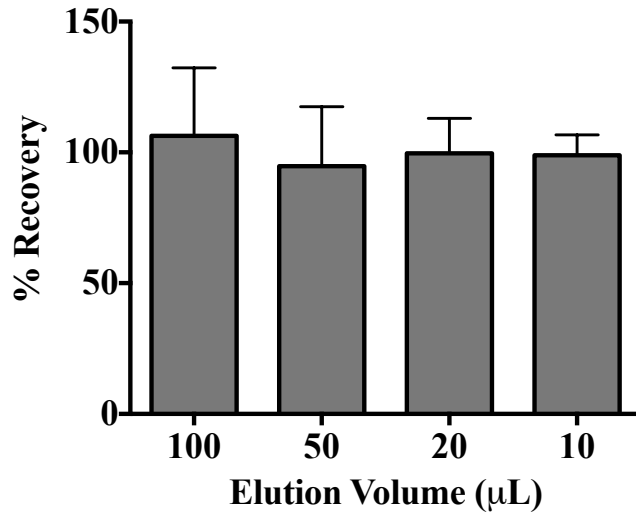
[105] OPEN LETTER Re: Cartridge prices, extended warranties and business in Russia and the People's Republic of China, Global Tuberculosis Community Advisory Board Treatment Action Group, 2014.

APPENDIX A

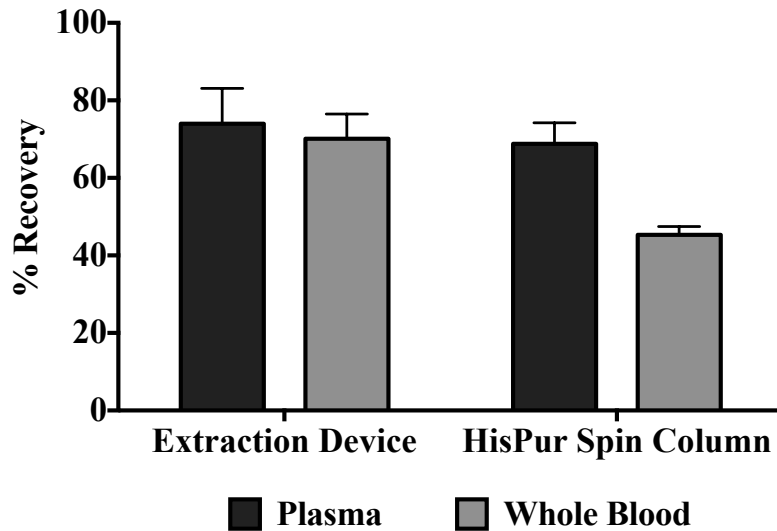
SUPPORTING INFORMATION: CHAPTER II



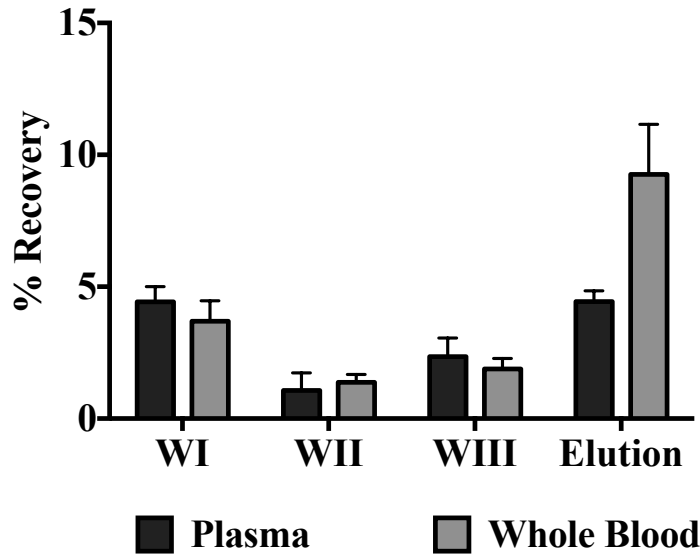
Supporting Information Figure II.1. SDS-PAGE gel of all chambers from 200 parasites/ μ L extractions out of (A) plasma and (B) whole blood, both with 125mM imidazole. Bands were stained with Coomassie Blue. The band at 67kDa in the Wash I lanes corresponds to the presence of HSA. For the whole blood gel, the band at 14kDa in the Wash I lane corresponds to the monomer of hemoglobin. The presence of HSA and hemoglobin was only observed in the first wash chamber, and thus demonstrates the efficacy of the wash chambers in limiting carryover contamination.



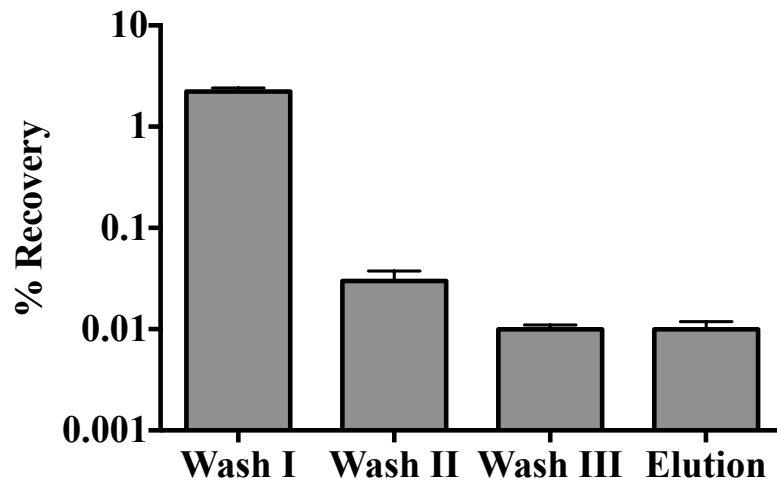
Supporting Information Figure II.2. Recovery of *pfHRPII* as a function of elution chamber volume.



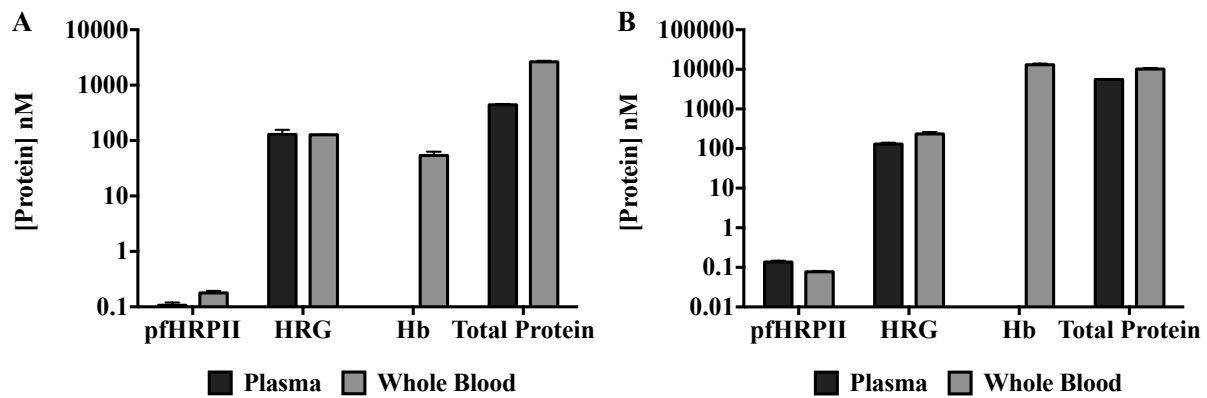
Supporting Information Figure II.3. Recovery of *pfHRPII* from a 200 parasites/µL spiked plasma and blood sample using the extraction cassette versus the commercial spin column.




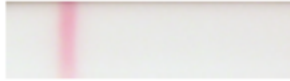









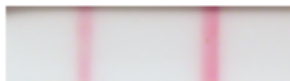
Supporting Information Figure II.4. Recovery of histidine rich glycoprotein (HRG) across the processing chambers of the extraction cassette. All chambers were normalized to the concentration of HRG in the blood sample.



Supporting Information Figure II.5. Recovery of hemoglobin (Hb) across the processing chambers of the extraction cassette. All chambers were normalized to the concentration of Hb in the blood sample.



Supporting Information Figure II.6. Comparison of final concentration of non-specific protein interferents and pfHRP II from plasma (black bars) and whole blood (gray bars) using A) the extraction device and B) HisPur Ni(II)NTA spin column.

Parasites/ μ L	Surrogate Patient Sample	Elution from Blood
0		
12.5		
25		
50		
100		
200		

Supporting Information Figure II.7. Comparison of the limits of detection of manufactured RDTs at parasitemias below the WHO limit of detection. Mimic patient samples were compared to the elution chamber extracted from spiked whole blood samples at 125mM imidazole. In the pictures, the the leftmost line is the control line and the rightmost line is the *pfHRP2* line. The visual limit of detection (with confidence) is 12.5 parasites/ μ L.

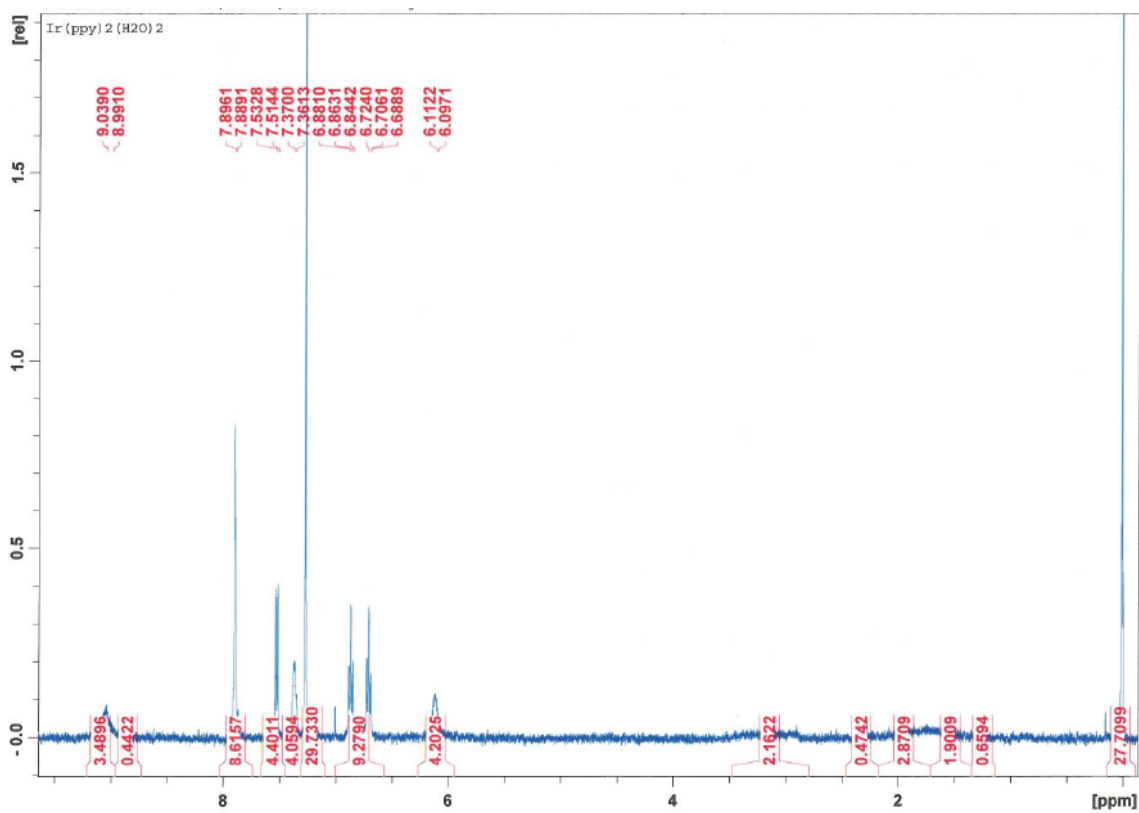
Acknowledgements

“Reprinted with permission from K.M. Davis, J.D. Swartz, F.R. Haselton, and D.W. Wright, Low-Resource Method for Extracting the Malarial Biomarker Histidine-Rich Protein II To Enhance Diagnostic Test Performance. *Analytical Chemistry* 84 (2012) 6136-6142. Copyright 2012 American Chemical Society.”

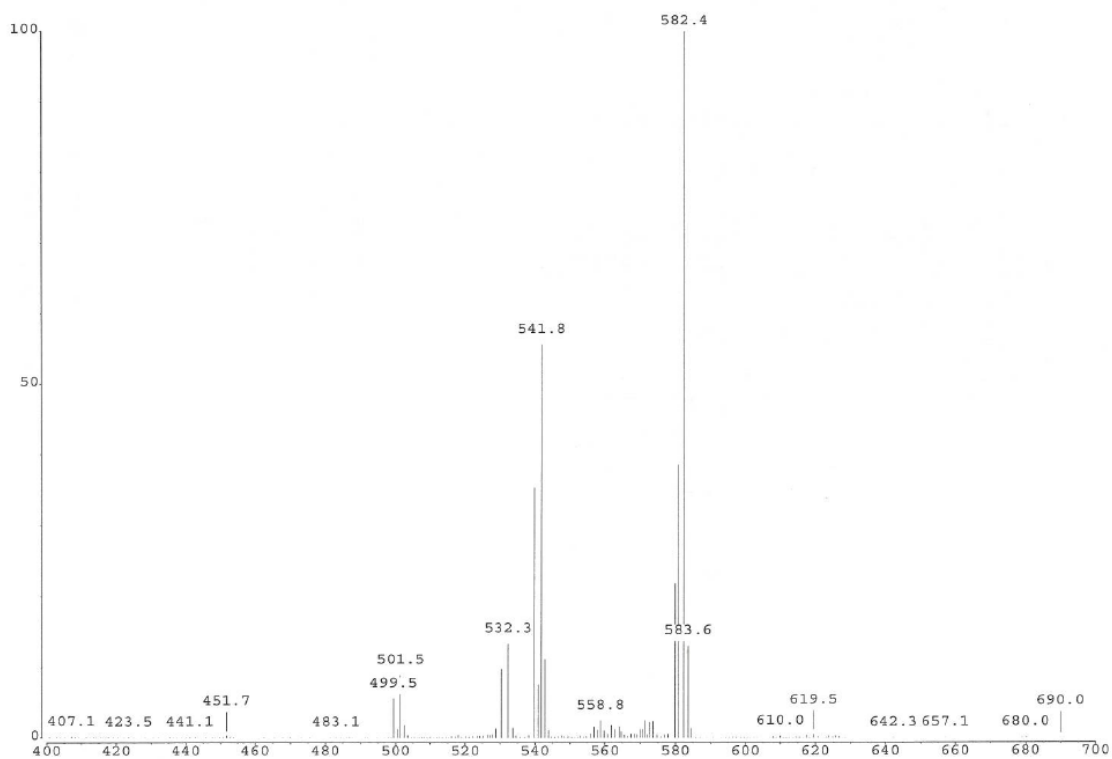
Support for this work was provided by the Bill and Melinda Gates Foundation Grand Challenges in Global Health: Develop Technologies that Allow Assessment of Multiple Conditions and Pathogens at Point-of-Care. We thank Nick Adams and Catherine Majors for experimental design suggestions. We thank M.F. Richards for critical comments concerning this manuscript.

APPENDIX B

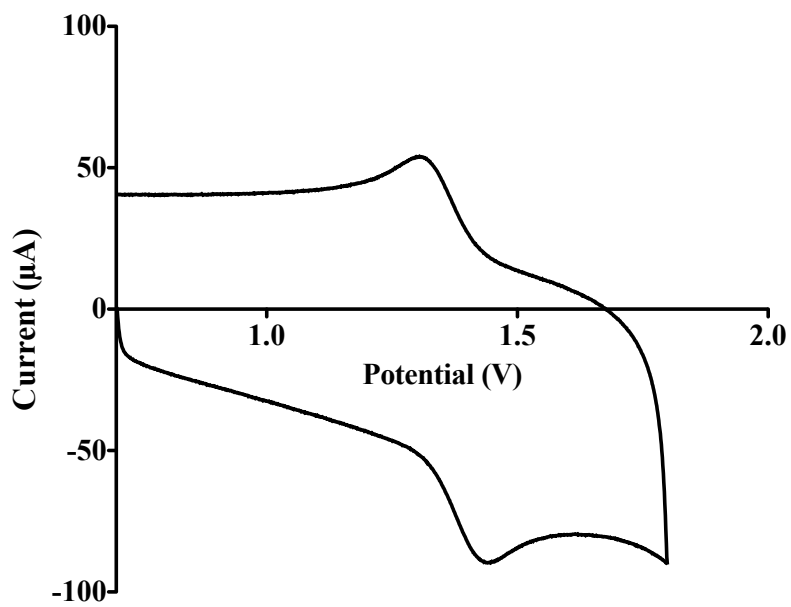
SUPPORTING INFORMATION: CHAPTER III



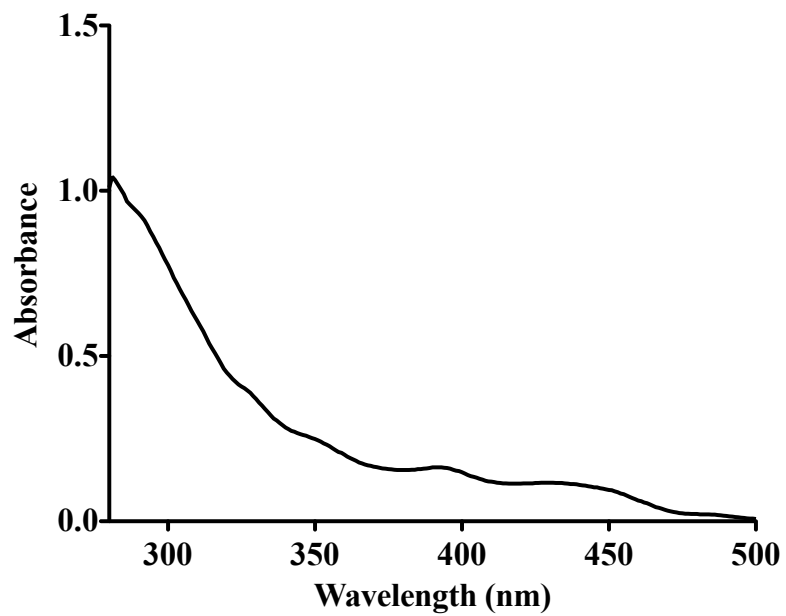
Supporting Information Figure III. 1. ^1H NMR of Ir1.



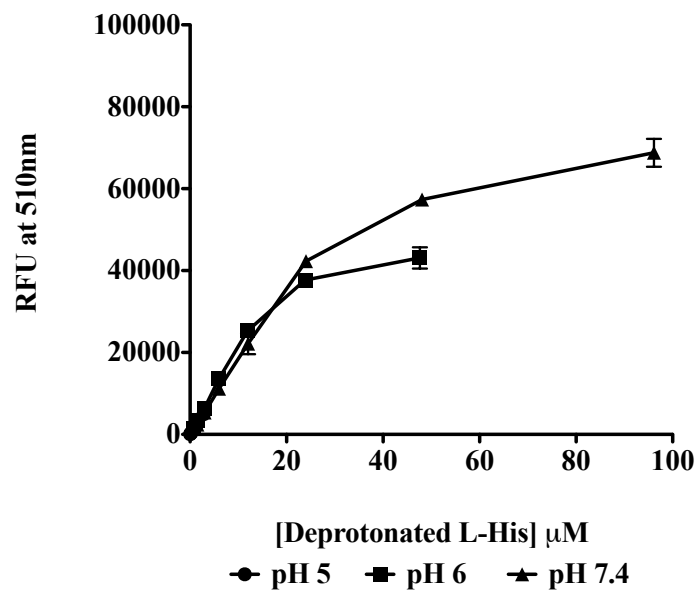
Supporting Information Figure III. 2. ESI of Ir1.



Supporting Information Figure III. 3. CV of Ir1 in MeOH.



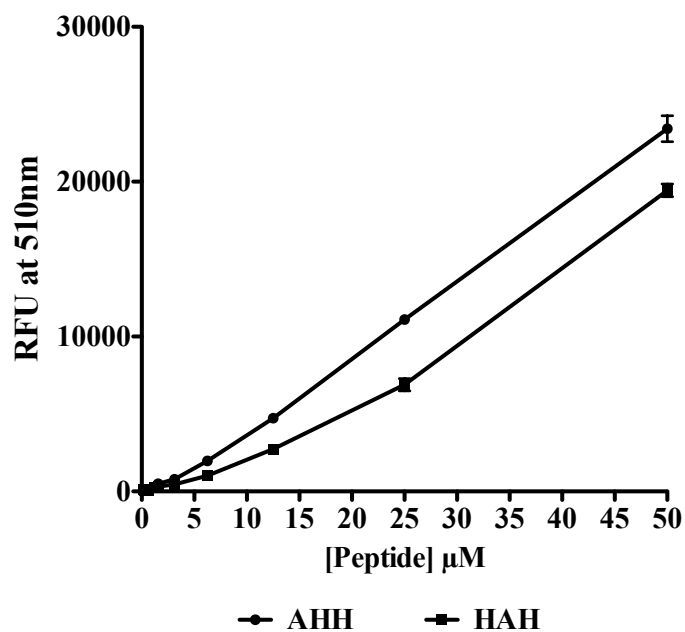
Supporting Information Figure III. 4. Absorbance of 100µM Ir1 in MeOH.



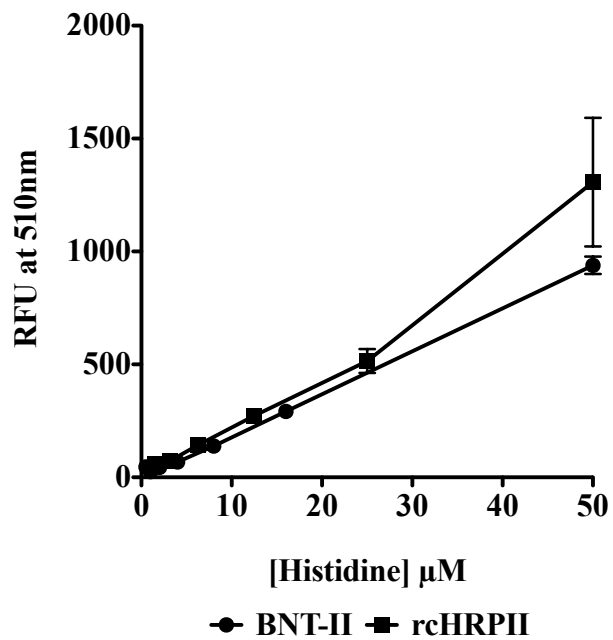
Supporting Information Figure III. 6. Signal intensity of L-His with 50μM Ir1 as a function of concentration of deprotonated histidine at each pH

Sample	Quantum Yield
Ir1	<0.1%
Ir1/L-His	7.0%
Ir1/BNT-II	8.3%

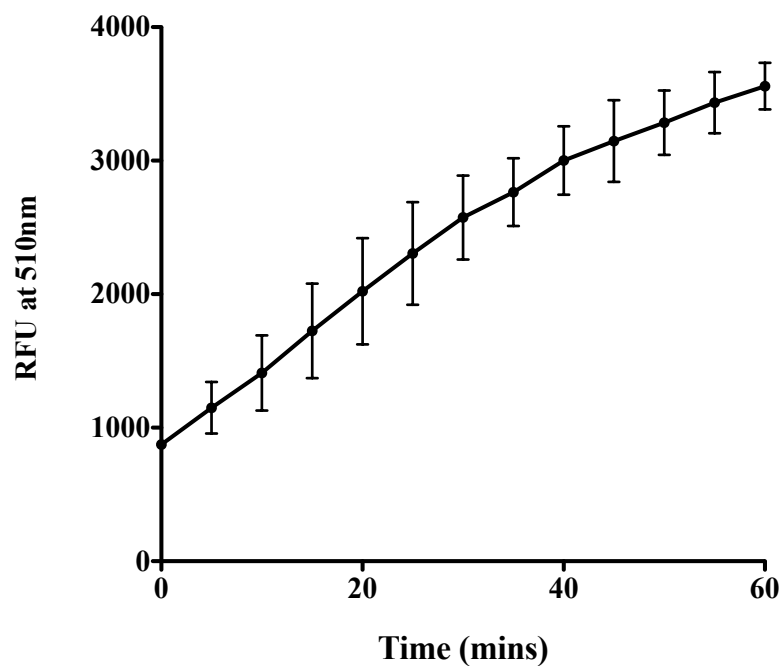
Supporting Information Figure III. 5. Quantum yield of 50μM Ir1 with 400μM L-Histidine and 100μM BNT-II in HBS. Quinine Sulfate was used as the reference compound ($\phi=0.546$ in 0.5M H₂SO₄; $\lambda_{ex}=366\text{nm}$).



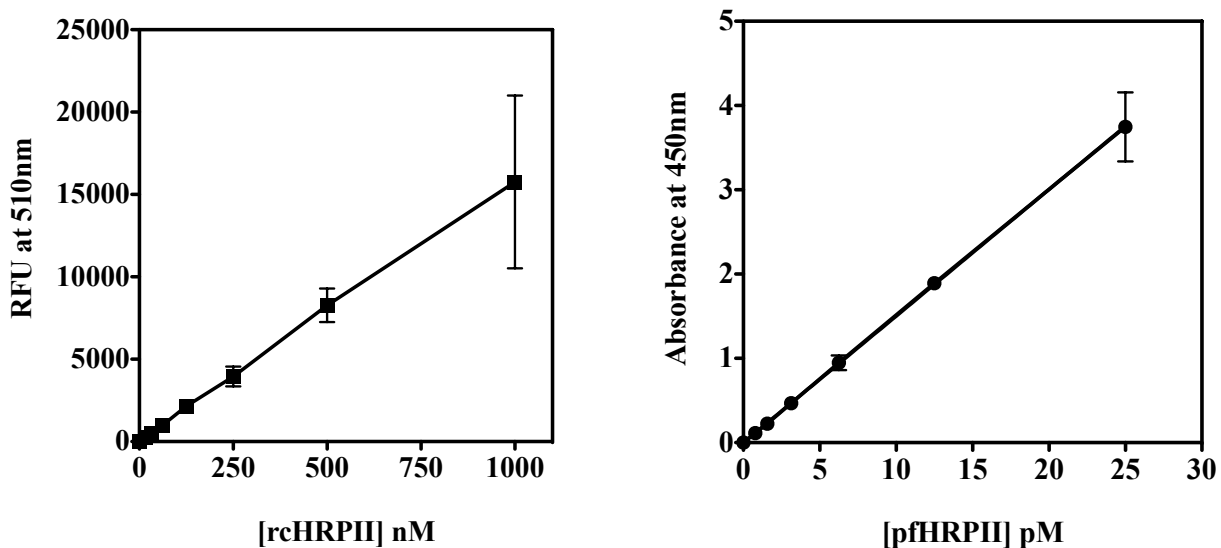
Supporting Information Figure III. 7. Signal intensity of tripeptides AHH and HAH with $50\mu\text{M}$ Ir1 in HBS. Tripeptides were allowed to incubate with Ir1 for 10 minutes before measuring signal at 510nm (365ex). $\text{Slope}_{\text{AHH}}=456\pm 9$. $\text{Slope}_{\text{HAH}}=356\pm 19$. While the two curves are statistically different, this data shows that Ir1 can bind both adjacent and split histidines within the AHHAHHAAD motif of *pf*HRP11.



Supporting Information Figure III. 8. Correlation between relative fluorescence signal intensity and concentration of total histidine in BNT-II and rcHRPII with 50 μM Ir1 in HBS.



Supporting Information Figure III. 9. Signal generated from 50µM Ir1 coordinating to 100nM rCHRPII bound to the surface of 50µm Ni(II)NTA agarose particles over 60 minutes.



Supporting Information Figure III. 10. Side by side comparison of the linear range of our on-bead Ir1 assay (left graph) and a traditional ELISA (right graph) for the detection of pfHRP II. The slope of the line for the on-bead assay and ELISA are 15.93 ± 0.13 and 0.1502 ± 0.0003 , respectively.

Potential Strategies for Creating and Ir-Based Molecular Recognition Element (MRE)

Of the data shown in Chapter III, using Ir1 as an alternative reagent for protein detection is promising, as the signal is robust and long-lived. However, non-specific binding of the probe to other histidine containing proteins (HRG, HSA) poses a problem for its use as a specific pfHRP II probe, as these proteins are in much higher abundance than pfHRP II, even after purification (See Supporting Information Figure II.5). Additionally, the probe is unique for histidine, and thus cannot be used as a general-use reagent for protein detection/staining. To circumvent these challenges, it was thought that BNT-II, preloaded with Ir1, could be covalently coupled to an aptamer or antibody against a specific target. In this design, specific recognition of the protein is governed by

the chosen aptamer/antibody. The iridium bound BNT-II, covalently linked to the aptamer/antibody, then yields the signal response. In this way, the iridium probe is no longer used as a “switch-on” probe, but as a labelling reagent. Since the iridium would constantly be in the “on” state, as it is bound to the BNT-II peptide region of the MRE, excess reagent must be washed away before detection. This makes the use of magnetic particles attractive, as washing and immobilization steps are easily performed.

Francisco Guevara, an REU student in the summer of 2013, began preliminary work on coupling a histidine rich peptide, (AHHAHHAAD)₂, to an aptamer against *p*LDH (aptamer was provided from AMBiotech). He first synthesized and purified the peptide, in high yields, using both manual and automatic synthesis methods. After characterizing the peptide by MALDI, he attached sulfo-SMCC to the N-terminus of the peptide. This succinimide functionalized peptide was purified and characterized by MALDI to confirm the coupling reaction. Lastly, the disulphide bond of the provided aptamer was deprotected using DTT, before coupling with the SMCC-functionalized aptamer. Excess unreacted peptide was removed using a size exclusion spin column. Reaction of Ir1 with this purified solution yielded a signal response at 510nm, indicating some of the peptide coupled to the aptamer. In order to separate any unreacted aptamer from the total MRE complex (aptamer+peptide), Ni(II)NTA magnetic particles were used to bind the histidine rich peptide in the MRE complex. Upon elution of the particles with 500mM imidazole, no aptamer was found in the eluate. MALDI was attempted on the MRE product, but no fragmentation was observed. Thus, the hypothesis was that the 22kDa aptamer was likely assuming some folding structure around the peptide—which would make it unable to bind Ni(II)NTA surfaces or fragment on MALDI. Further

characterization and purification is needed to pursue this aptamer/peptide MRE as a potential reagent for protein detection.

A second approach was taken to create a MRE by covalently coupling an amine terminated BNT-II peptide to an α -HRP II IgG (from Abcam; ab9203). The acetylated BNT-II peptide was synthesized by hand on Fmoc 4-branch MAPS resin. Synthesis was confirmed by MALDI. Prior to conjugation to the IgG, the peptide was pre-loaded with Ir1 by incubating 2mg of the peptide with an excess of Ir1. Any unbound Ir1 was removed by passing the peptide through a desalting column. After lyophilisation, the product was placed under broadband UV light to determine whether the loading was successful (Figure III.11).



Supporting Information Figure III. 11. Luminescent signal from Ir1 bound to BNT-II, after lyophilization

After successful synthesis and loading of the BNT-II peptide, it was conjugated to the aforementioned IgG via EDC/sulfo-NHS coupling. This coupling method crosslinks amines to sulfhydryl groups. This method was chosen as conjugation to sulfhydryl groups on the IgG is less likely to reduce IgG avidity in the Fab region. After conjugation, the solution was passed through a 30kDa spin filter to remove any unbound Ir1/BNTII peptide. Visual inspection, by broadband UV light, of the concentrated solution remaining in the filter revealed bright blue-green luminescence—indicating the peptide did indeed bind to the antibody. Future directions on this method are aimed at purifying any unreacted IgG away from the complete MRE. Since the histidines on the BNT-II are bound by Ir1, Ni(II)NTA chromatography likely cannot be used. If the Ir1 probe does not bind the IgG, the MRE could be “loaded” with the probe after synthesis and purification. This would then allow for the use of Ni(II)NTA to purify the complete MRE. After purification and characterization of the MRE, it must be tested against *pf*HRPII to determine its sensitivity and specificity. If enhanced sensitivity is needed, electrochemiluminescence (ECL) can be explored as a potential technique, as the Ir1 probe is redox active. Details of the aptamer and antibody approach toward a MRE can be found in Francisco’s laboratory notebook (labelled FG REU 2013) and my 4th notebook (NB4 pgs 104-108, 113-114, and 128-129).

Acknowledgements

“Reprinted with permission from K.M. Davis, A.L.Bitting, and D.W. Wright, On-particle detection of Plasmodium falciparum histidine rich-protein II by a “switch-on” iridium (III) probe. Analytical Biochemistry 445(7) (2014). Copyright 2014 Elsevier.”

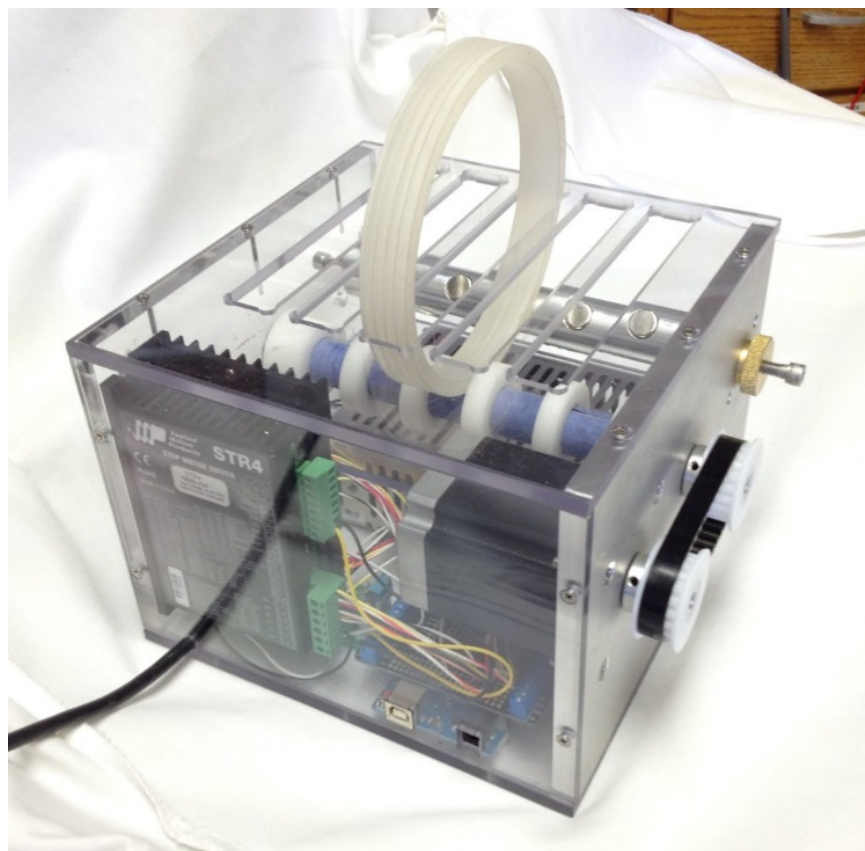
Support for this work was provided by the Bill and Melinda Gates Foundation Grand

Challenges in Global Health: Develop Technologies That Allow Assessment of Multiple Conditions and Pathogens at Point-of-Care. K.M.D. was supported by an NSF Graduate Research Fellowship (2012095464). We would like to thank E. Gizzie for assistance with the CV measurement of **Ir1**, A. Balinski for ESI, and M.F. Richards for critical comments in the preparation of the manuscript.

APPENDIX C

AUTOMATED EXTRACTION OF *PFHRPII* FROM BIOLOGICAL SAMPLES

In collaboration with the Haselton laboratory in the Biomedical Engineering Department at Vanderbilt University, we have designed an automated extraction device to process biomarker bound beads through the extraction cassette outlined in Chapter II. All studies detailed in Chapter II and Chapter IV were performed manually. However, part of the Gates Phase 1 POC Initiative grant milestones were to create an automated device to



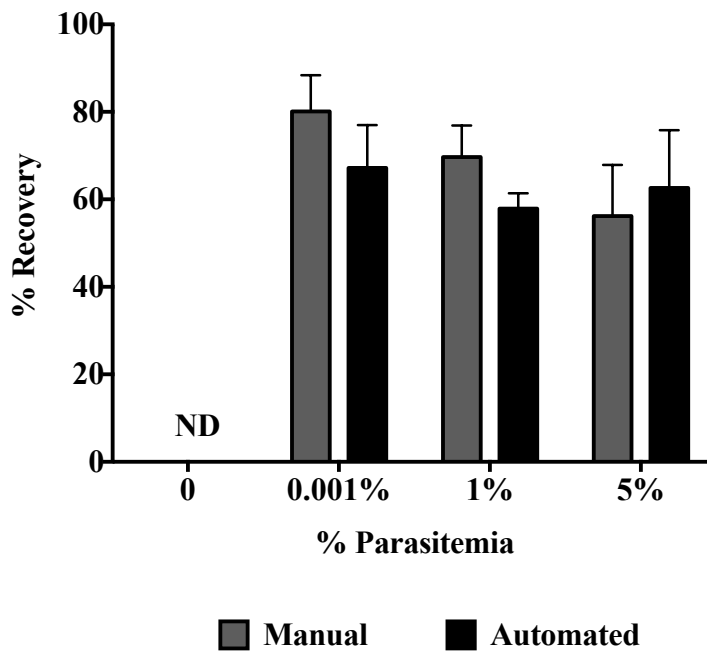
Supporting Information Figure IV. 1. Hotdog roller (HDR) automated extraction device.

perform the sample preparation. The first iteration was deemed the “hot dog roller,” and the name informs the extraction motion (Figure IV.1). The extraction tubing was fitted around a plastic disk with channels carved into them. This disk served as the support for

the assay tubing during the extraction process. The disk was placed on the HDR to perform the extraction. The HDR was programmed to move the biomarker bound magnetic particles down the assay tube to purify the biomarker away from the sample, but the program was designed to be agnostic to the assay type. The assay tubing was laid out similarly to that detailed in Chapter II.. The Ni(II)NTA beads were allowed to mix with a lysed blood sample for 10 minutes. After this period, particles were manually moved into the following oil chamber prior to loading on the plastic disk. The HDR program moved the beads through each chamber. The elution chamber was modified to contain 2M imidazole (versus 500mM from Chapter II) as the beads were not able to spend 10 minutes in this chamber. This ensured the *pfHRP*II would elute from the beads in the time allotted by the HDR program. ELISA was used to determine the percent recovery of *pfHRP*II from both a manual and automated extraction of malaria samples provided to us by PATH. The details of these samples and the extraction data are outlined below (Figure IV.2). Recovery using the manual and automated extraction methods agreed nicely (Figure IV.3). The automated HDR extraction device proved successful at extracting and

Pathogen	Analyte	Matrix	Biomarker Detected	Sample Concentration			
				Negative	Low	Medium	High
Malaria	Parasites	Blood	Protein	0	0.001%	1%	>5%
Panel Results (% Recovery) →				0%	80 ± 8%	70 ± 7%	56 ± 12%
Panel Results (RDT) →				-	-	+	+

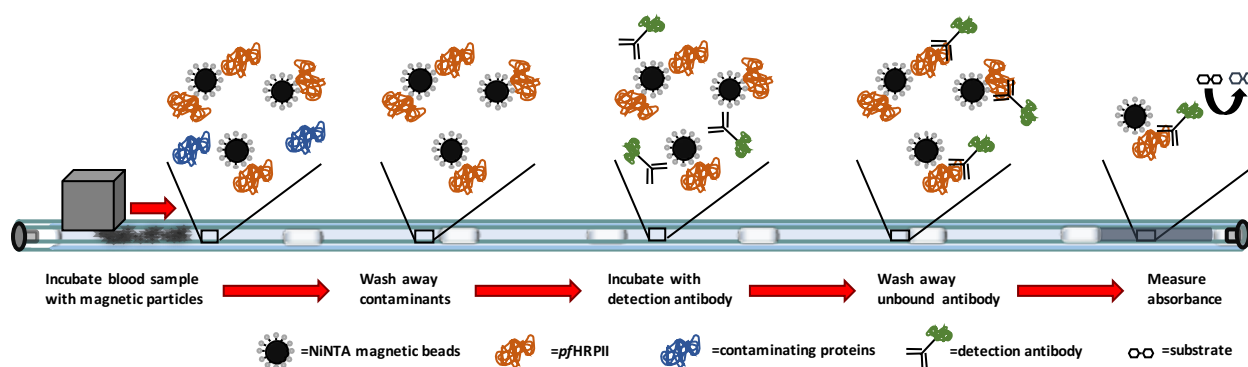
Supporting Information Figure IV. 2. PATH malaria panel samples and results.



Supporting Information Figure IV. 3. Comparison of manual and automated *pfHRPII* extraction efficiencies.

eluting *pf*HRPII from a blood sample, but the device was not yet equipped to be a complete sample processing and detection method.

In Phase 1.5 of the Gates POC Initiative, we were charged to fully develop our extraction method to include sample preparation and detection for whole cells, nucleic acids, small clinical chemistry molecules, and proteins. The OBE work detailed in Chapter IV outlines the chemistry behind getting the assay to work for detection of *pf*HRPII from a blood sample. The first iterations of the automated OBE were performed using the Co(II)NTA particles, as shown in Figure IV.4. Instead of using the HDR device, our colleagues in the Haselton laboratory designed a single axle device to automate the extraction. (Note: Extensive details of this device will not be discussed in this dissertation, aside from the final standard operating procedure included.)



Supporting Information Figure IV. 4. Layout of the *pf*HRPII on-bead ELISA.

When the Co(II)NTA based OBE was incorporated into the automated extraction format, the extraction took around 30 minutes total time. The biggest hurdle to reducing non-specific background noise was mixing of the particles in the tube. The original program only mixed the beads on one plane—that along the edge of the tube closest to the magnet. Thus there was no diffusion of the beads throughout the chambers to wash away

contaminants. With this motor motion, there was a great deal of non-specific binding of the detection antibody to the particles, which was evidenced by blue signal from a negative sample. When the extraction was performed by hand, in the tube, there was no signal from a negative sample. This suggests that if the automated device could be programmed to mimic the mixing mode from a manual extraction, non-specific turnover could be prevented.

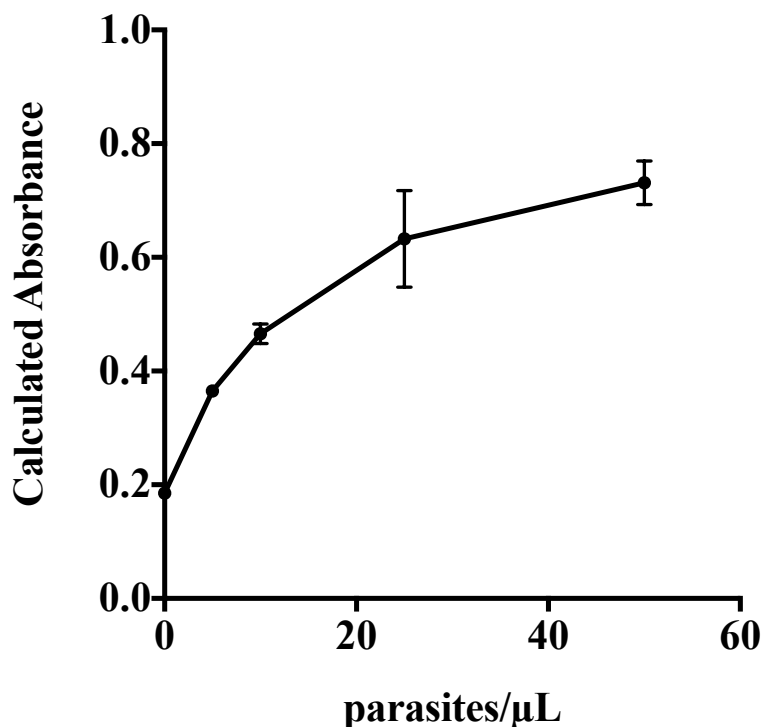
It was noticed from Chapter II experiments that placing the extraction tubes on a rotisserie was sufficient to mix the particles within a chamber. This type of gravitational mixing was incorporated into the automated device, as a form of “windshield wiper” motion. When the particles are pulled into a processing chamber, the motor wipes the extraction tube back and forth, with a pause in between each wipe. This pause allows for the particles to fall to the opposite end of the chamber in a “snowing” type of motion. After the programmed time in the chamber, the plastic disk holding the extraction tube



Supporting Information Figure IV. 5. Signal from 0, 400, and 4000 parasites/ μ L after automated extraction.

circles back around to the fixed magnet to process the particles into the next chamber. This modification of the mixing program served to reduce non-specific signal, as can be seen in Figure IV.5.

Around the time of figuring out the mixing motion on the automated device, the all in one OBE chemistry outlined in Chapter IV had been worked out. The issues with



Supporting Information Figure IV. 6. Results of automated OBE from parasite spiked blood samples.

fouled BSA in the detection antibody chamber causing false positives had plagued the manual extractions as well as the automated extractions. Switching to an all in one OBE format seemed to solve this problem for the manual assay, so it was incorporated into the tube. Upon working with our collaborators, we were able to create a “one-touch” platform to detect *p*fHRPII from a blood sample in 26 minutes. The calculated limit of

detection was determined to be around 1 parasite/ μL . The visual limit of detection, in the tube, appeared to be around 5 parasites/ μL (see graph below). This result fit nicely with the target product profile (TPP) set forth by the Gates Foundation at the onset of Phase 1.5.

In the future, the assay could potentially be improved upon by incorporating the optimization results outlined in Chapter IV. As the milestones were met for Phase 1.5, we did not pursue further optimization of the automated extraction. The standard operating procedure for the final automated *pf*HRP II ELISA is detailed below.

Part A: Extraction and Detection of *Plasmodium falciparum* Histidine Rich Protein 2 On-Bead ELISA

Purpose

Immunoassays are widely used to detect disease biomarkers, due to their sensitivity and specificity. However, lengthy time requirements and multiple reagent handling steps limit their use at the point-of-care. This standard operating procedure outlines the assembly of a self-contained immunoassay cartridge for the detection of PfHRP2 from a biological sample.

Scope

Intended for any operator wishing to detect PfHRP2 from a biological sample

1. Assay Preparation Procedure

A. Synthesis of anti-PfHRP2 streptavidin magnetic particles

1. Dissolve 2 aliquots (each aliquot is **15 μ L**) of 5.1mg/mL anti-HRP2 IgG (abcam Cat#ab9203) in **300 μ L** of 1x PBS (10mM phosphate buffer; 137mM NaCl).
2. Resuspend the EZ-link NHS-PEG₄-Biotin (Fisher Scientific Cat#21329) in **170 μ L** of water. To the **300 μ L** of antibody solution, add **2.6 μ L** of 20mM EZ-link NHS-PEG₄-Biotin and incubate for 30 minutes in a rotisserie.
3. During biotinylation incubation time:
 - a. Remove **500 μ L** of streptavidin Dynabeads from stock bottle (Dynabeads Myone streptavidin T1 Cat#65601) and wash 2x with 1x PBS. Resuspend in **500 μ L** of 1x PBS and save for later. Do not vortex, just pipette up and down to avoid beads getting stuck on the sides of the Eppendorf tube because of the absence of surfactant.
 - b. Prep two 0.5 mL 7MWCO desalting columns (Fisher Scientific Cat#89882)
 - i. Remove storage buffer (1 min, 1500 rcf) and wash 3x with **300 μ L** 1x PBS (1 min, 1500 rcf). Do the last wash right before desalting the antibody solution to avoid drying out the columns.
4. Desalt biotinylated antibody solution (to remove unconjugated biotin): Add **150 μ L** to each column and spin for 2 minutes at 1500 rcf.
5. Combine two fractions and add **300 μ L** of 1x PBS. Total volume: **600 μ L**.
6. Remove the buffer from the washed beads add antibody solution. Incubate for 30 minutes.
 - a. **Note:** Save a few microliters of the initial antibody solution to compare the supernatant after conjugation.
 - b. During conjugation:
 - i. Make up a 1mg/mL solution of D-biotin in 1x PBS. It is difficult to dissolve and usually requires heating.
7. After the 30 minute incubation, remove the supernatant from the beads and check the concentration of IgG remaining using the Take3 plate application on the BioTek SynergyH4 plate reader.
 - a. **Note:** Compare this to the concentration of IgG prior to conjugation using the reserve aliquot from 6a.
8. Wash the conjugated beads 2x with 1x PBS.

9. Re-suspend the beads in **500 μ L** of 1x PBS and add 20 μ L of the 1 mg/mL D-biotin solution to quench the unreacted streptavidin sites on the beads.
10. Incubate for 30 minutes.
11. Wash the beads 2x with 1x PBS and re-suspend in **500 μ L** of 1x PBS with 0.01% Tween-20.

B. Preparation of the surrogate malaria blood sample

1. Add **100 μ L** of lysis buffer (100mM phosphate, 600mM NaCl, pH 8.0, 2% Triton X-100) to **100 μ L** of blood containing lysed *P. falciparum* and allow the blood to fully lyse.
2. Lightly pack the bottom of a 1mL syringe (Norm-ject Cat# 4010-200V0) with glass wool and filter the lysed blood through this syringe (**Figure 1**). This step is necessary when using whole blood but may not be necessary with PATH samples.



3. To the filtered sample, add **0.5 μ L** of 1mg/mL anti-HRP2 HRPx (abcam Cat# ab30384) and **20 μ L** of the anti-*Pf*HRP2 magnetic particles prepared in section A.
4. Reserve the sample for addition to the assembled cassette in section C.

Figure 1. Lightly pack glass wool into a 1mL syringe to filter lysed whole blood samples before adding magnetic beads.

C. Assembly of the extraction cassette

1. Cut a 154mm piece of FEP tubing (McMaster Carr; Red FEP Tubing, .093" ID, 1/8" OD, .016" Wall Thickness; Cat# 9369T46)
2. Plug one end of the tube with Hemato-Seal Tube Sealing Compound (Fisher Scientific Cat# 02-678)
3. Thread the tube, sealed end first, into the labeled plastic tube holder as shown in **Figure 2**.

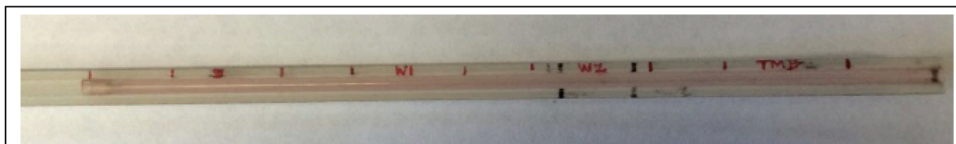


Figure 2. The labeled plastic tube holder simplifies loading of the tubing cassette with extraction and ELISA solutions.

4. Using a 1mL syringe fitted with a 22 x 6" septum needle (Cadence Science Cat# 4176), add **100 μ L** of wash buffer (50mM phosphate, 300mM NaCl, pH 8.0, 0.025% Tween 20) to the two regions on the tube holder labeled W1 and W2 (**Figure 3**).
 - a. **Note:** To do this, insert the needle into the open end of the tube and position the needle at the leftmost edge of the W1 region. Depress the syringe to deposit the buffer to fill the region. Repeat this for the W2 region.



Figure 3. A 1mL syringe fitted with a needle is used to load wash buffers 1 and 2 into the proper locations in the tubing cassette.

5. To the region labeled "TMB," add **100 μ L** of TMB One reagent (Promega Cat# G7431) using a gel pipette tip (**Figure 4**). Seal this end of the tube with the sealing compound.
 - a. **Note:** TMB One reagent is stable at room temperature and exposed to light during the duration of the cassette prep and assay (~30-45mins) however long term exposure to light is not recommended.
6. Using a razor blade, cut off the sealing compound plug from step C2 to open up the sample end of the cassette.

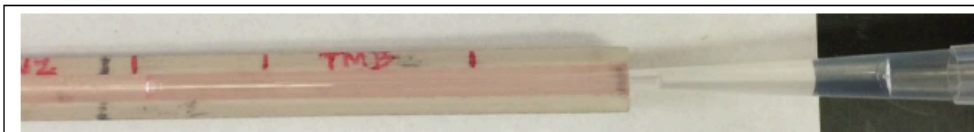


Figure 4. A gel loading pipette tip is used to load the TMB solution into the last chamber of the tubing.

7. Using a gel tip pipette tip, transfer the prepared sample from step B4 to the extraction cassette, leaving a 1cm air valve between the first wash chamber and the sample (**Figure 5**).



Figure 5. A gel loading pipette tip is also used to load the lysed blood and anit-PfHRP-2 magnetic bead sample into the tubing cassette.

8. Seal the sample end with sealing compound.

2. Preparation of the Rotary Drive and running ELISA

A. Hardware connectivity

1. Turn the Microsoft Surface on.
2. Turn on the hardware mounted on and under the platform; switch is in the back next to the power cord.
3. Confirm that the TDK-Lambda power supply is on. If not, turn on using the front panel power switch.
4. Confirm the USB cable is plugged into the back of the Qiagen fluorometer.
5. Three cables connect the Surface dock to the instrument, one purple network cable, and two USB cables. See **Figure 6**. These should be connected.
6. Confirm that the STR4 motor controller and motor are powered by toggling the switch on the right, under the platform. When power is on, the rotary cartridge will not turn easily.



Figure 6. The connectors from the instrument to the back of the Surface Dock.

B. Hardware alignment, tube mounting

1. Measure the chamber/valve locations in the assay tube. Also measure how long the entire tube is from one sealed end to the other sealed end. It should be about 150 ± 3 mm. Measurements are in millimeters.
Note: The “zero” point is the beginning of the sample chamber. All of the chamber lengths are measured from this point.
2. Use the motor switch to turn off the motor to allow mounting the tube onto the cartridge.
3. Place the assay tube onto the cartridge. Align the final chamber with the red colored fluorescent plastic in the rim of the cartridge; it is recessed into the spoke of the wheel assembly as shown in **Figure 7**.
4. Turn the motor and controller back on with the switch on the right, below the platform.
5. Check that the magnet is touching the assay tube or cartridge and that the spring force seems appropriate to maintain contact during rotation.

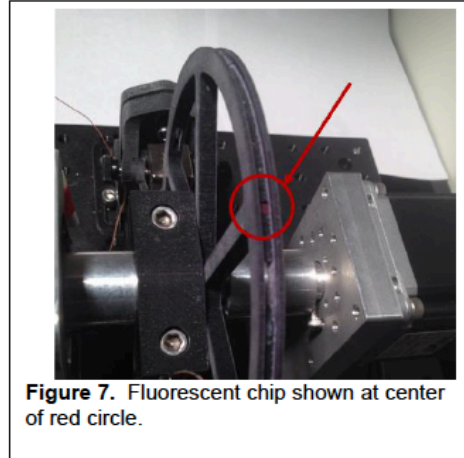


Figure 7. Fluorescent chip shown at center of red circle.

C. Software operation

1. Double click on the ELISA shortcut on the desktop shown in **Figure 8**. It points to `C:\Users\hasel_000\Documents\labview\black_beauty_control_v05\black_beauty_control_v05.lvproj`. This starts LabVIEW and shows the Project Explorer view of the software.
2. In the Project Explorer window, **Figure 9**, under the MotionControl Folder, double click on `MainControl_CellCount.vi`.
3. The Main Control will open (**Figure 10**) and you must click on the white arrow in the upper left corner to start the software.

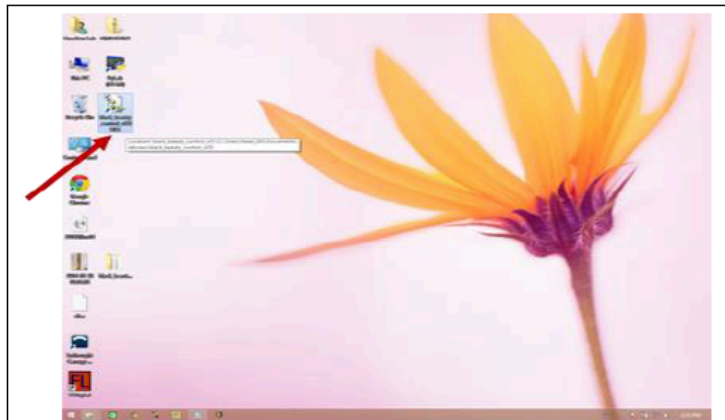


Figure 8. Desktop shortcut to start software.

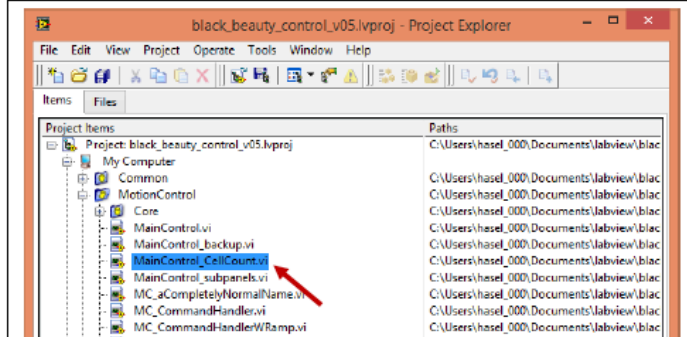
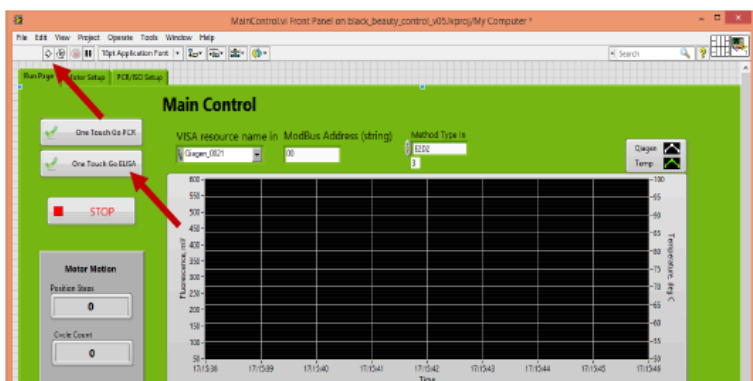


Figure 9. LabVIEW Project Explorer view of the software. Red arrow shows the MainControl software to click on.



4. **Figure 10** Select the Motor Setup tab shown in **Figure 11**. Use the Counter-Clockwise and Clockwise buttons to align the fluorescent chip and final chamber with the Qiagen flurometer. Use the Blink Qiagen button to turn it on to see the alignment. When aligned, press the “Set optics” button. Be sure to turn off the Qiagen when alignment is finished.
5. Again using the Motor controls, set the start of the first chamber at the magnet position. Click the “Set Start.”
6. Type in the tube measurements and mixing times in the fields on the lower left (**Figure 11**). For ELISA the “PCR Cycle Count” default is fine.
7. When this is correct, press the “Motor Setup Done?” button.

Select the PCR/ISO Setup tab. Select the Qiagen emission and detection wavelengths with the “Method Type Mirror” pulldown, and finally press the

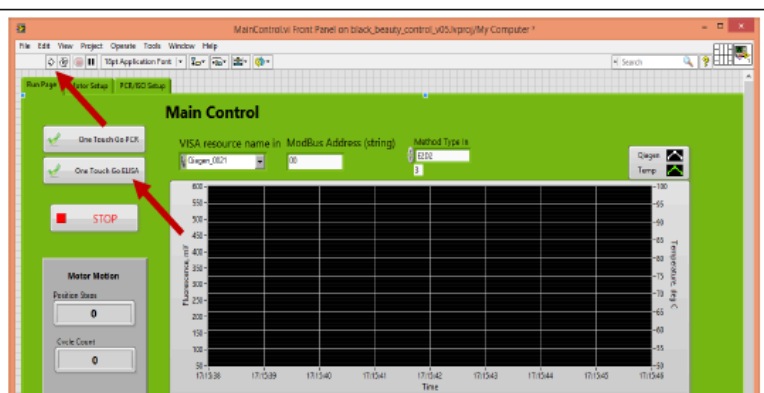
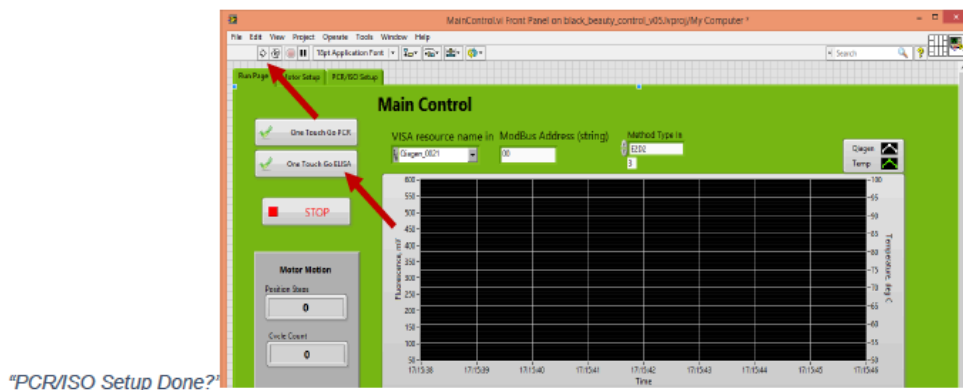


Figure 10. LabVIEW run button in the upper left corner starts the software. After entering the relevant data the “One Touch Go ELISA” button is pressed.



"PCR/ISO Setup Done?"

8. **Figure 10**The instrument will immediately move to the optics position and take a reference reading of the chip fluorescence passing through the final chamber (before any chemistry occurs in the tube). Write this value down. See below for the file it is save in.
9. The instrument then goes to the start, with the beginning of the first chamber at the magnet. The motion rotates in a way so the magnet holds the beads while the tube moves to the second chamber. There is a mixing step where the rotation is fast to pull the beads away from the magnet, and then mixes the beads with the chamber solution by moving to the one side, pausing and letting the beads fall and disperse.

10. When finished the rotation moves the beads out of the final chamber and then lines it and the flouroscent chip up with the Qiagen to take a final reading. The red fluorescence intensity is attenuated if the final cell has changed to blue, more attenuated the darker the blue.

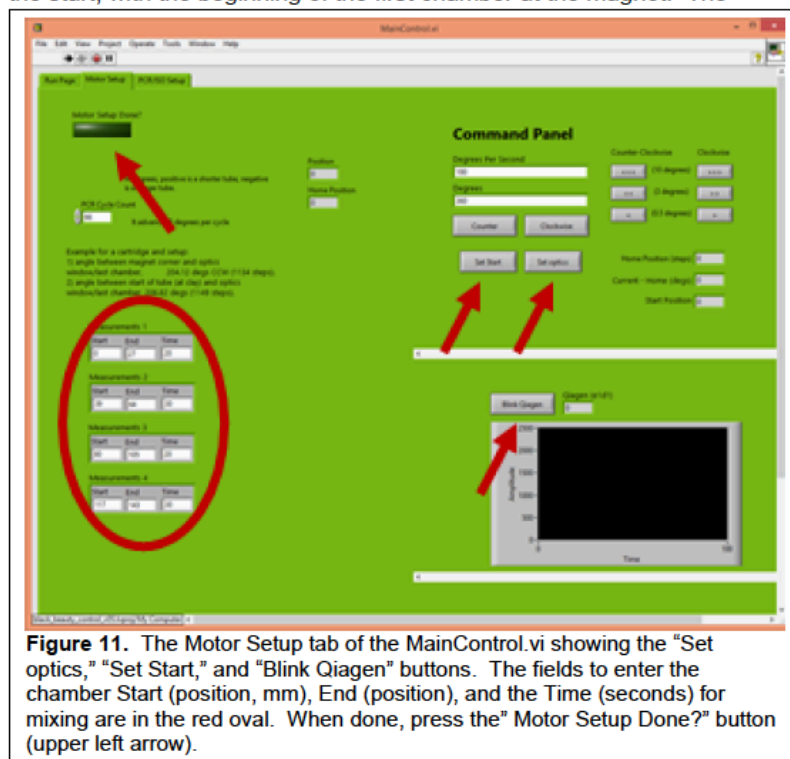


Figure 11. The Motor Setup tab of the MainControl.vi showing the "Set optics," "Set Start," and "Blink Qiagen" buttons. The fields to enter the chamber Start (position, mm), End (position), and the Time (seconds) for mixing are in the red oval. When done, press the" Motor Setup Done?" button (upper left arrow).

11. Data is saved in the backup file of all Qiagen fluorescent readings in C:\Users\hasel_000\Document\labview\black_beauty_control_v05\Vis with the name tempQiagenReadings.txt. It is a long format with 12 columns, with most recent data at the end of the file. The columns are relative time (seconds), E1D1 net (on minus off), E1D1 total (on value), E1D1 background (off value), same for E1D2, for E2D2, temperature of the Qiagen (degrees C), and finally the clock time in seconds since the Macintosh epoch (Mac timestamp).